TAMPEREEN TEKNILLINEN YLIOPISTO
TAMPERE UNIVERSITY OF TECHNOLOGY

SHINYA ABE

INFLUENCE OF EXERCISE HISTORY ON THE PROXIMAL FEMUR STRENGTH; FINITE ELEMENT ANALYSIS OF FEMALE ATHLETES

Master's thesis

Examiner: Professor Jari Hyttinen
Adjunct Professor Harri Sievänen
Examiner and topic approved by the Faculty Council of the Faculty of Natural Sciences on 7 March 2012.

PREFACE

This thesis project was conducted in the Master's Degree Programme of Biomedical Engineering at Department of Electronics and Communications Engineering in Tampere University of Technology. First, I would like to thank Dr. Harri Sievänen and Professor Jari Hyttinen to give me this fantastic opportunity to conduct a biomechanical research project as my MSc thesis.

I was very grateful to be involved in the research where I can combine and apply sports science background from my bachelor's degree and biomedical engineering from this Master's programme. Special thanks are due to Dr. Harri Sievänen for providing this thesis topic, data, and the general support and scientific guidance. I also like to appreciate great encourage from Professor Hyttinen toward the scientific research.

I am grateful to have supports and advices on statistical analysis, medical imaging processing techniques, and creation of the finite element models. Professor Jari Viik helped me to perform the statistical analysis. MSc. Nathaniel Narra Girish gave me great technical supports for the medical image processing. I would also like to give thanks to previous MSc. Degree student Daniel Oravec who conducted similar thesis project and created the basis for the creation of the finite element model using the data we have. It is undoubtedly that using some of the methods developed by him accelerated this project.

Moreover, I would like to give special thanks to Professor Randall Jensen from Northern Michigan University where I completed my BSc degrees in Sports Science. He has always motivated and inspired me toward conducting the research in biomechanics.

Lastly, I would like to thank my family for the great support for me to seek this academic success. I have planned to continue this research toward PhD degree and hope to find highly useful and practical information to the society.

May 21st, 2013
Tampere, Finland

Shinya Abe

ABSTRACT

TAMPERE UNIVERSITY OF TECHNOLOGY
International Master's Degree Programme in Biomedical Engineering
ABE, SHINYA: Influence of Exercise History On The Proximal Femur Strength; Finite Element Analysis of Female Athletes
Master of Science Thesis, 82 pages, 20 Appendix pages
June 2013
Major subject: Biomedical Engineering, Medical Instrumentation
Examiner: Professor Jari Hyttinen
Adjunct Professor Harri Sievänen
Keywords: Finite element modeling, hip fracture, proximal femur, ANSYS, lateral falling, magnetic resonance imaging.

Bone structure and material properties adapt to mechanical loading, and accordingly exercise highly influences bone's functional adaptation. Studying bones from various athletic subjects provides us a good opportunity to understand the mechanism of exercise-induced structural change in bone. Constructing 3D bone models has become available with current medical imaging techniques and is essential to investigate this mechanism. Finite element (FE) models of these bone models enable us to solve complicated numerical problems. In bone biomechanics, they provide an appropriate tool for assessing bone strength, detection of hip fracture prone regions and revealing the beneficial type of exercises to strengthen those regions. Hip fracture is a worldwide medical problem and majority of them are directly caused by falling. Cortical wall of the femoral neck get thinner with aging and some regions become more prone to the fracture. Impact loading exercises have positive effect on maintaining and/or increasing cortical thickness, increasing thus bone strength. This adaptation may be a key in preventing hip fractures. Therefore, the objective of this thesis was to investigate if the exercise history is associated with femoral neck bone strength in a lateral fall condition. To achieve this, MRI-based FE models of 36 young competitive female athletes' proximal femurs were created. These subjects were categorized into 5 different groups based on the exercise history; 1) High-Impact, 2) Odd-Impact, 3) High-Magnitude, 4) Repetitive Low-Impact, 5) Repetitive Non-Impact, and compared to a control group.

The proximal femur was modeled as the linear elastic, isotropic and homogenous material. Regional mean cortical and trabecular vonMises stresses were calculated for 8 anatomical sectors of the smallest cross-section of the femoral neck. Statistical analysis based on the nonparametric Mann-Whitney text was performed to investigate the difference in the sector-wise stress between each athlete's group and the control group.

At superior cortical region, ~17MPa stress was observed in the Odd-Impact group compared to ~20MPa stress in the control group. This result indicates that the proximal femur in the Odd-Impact groups has somewhat higher load bearing capacity in the lateral fall. Thus, Odd-Impact exercise performed in adulthood could be an optimal means to prevent bone fragility in older age. However, statistical power was very low and the findings from this study are preliminary and indicative only. Future study should include not only more subjects to obtain better statistical confidence, but also be based on more realistic the FE models and different loading conditions, including the dynamic situation.

LIST OF SYMBOLS

E	Young's modulus
F_{peak}	Peak force on the lateral aspect of the greater trochanter
I	Second moment of area
I_{MIN}	Minimum second moment of area
M	Bending moment
ρ	Apparent density
r_i	Inner radius of the cortical bone
r_o	Outer radius of the cortical bone
Z	Bending resistance defined as section modulus

LIST OF ABBREVIATIONS

3D	Three dimensional
BMD	Bone Mineral Density
BMU	Basic multicellular unit
CAD	Computer Aided Design
CT	Computed tomography
CSC	IT Center for Science Ltd
DXA	Dual-energy X-ray absorptiometry
FC	Falling Condition
FE	Finite element
FOS	Factor of safety
FRAX	Fracture Risk Assessment Tool
H-I	High-Impact
H-M	High-Magnitude
MRI	Magnetic Resonance Image
O-I	Odd-Impact
PCA	Principle Component Analysis
PCG	Preconditioned conjugate gradient
pQCT	Peripheral quantitative computed tomography
QCT	Quantitative computed tomography
R.L-I	Repetitive Low-Impact
R.N-I	Repetitive Non-Impact
SD	Standard deviation
VHP	Visual Human Project
VIBE	Volumetric interpolated breath-hold examination
WHO	World Health Organization

TABLE OF CONTENTS

1. INTRODUCTION

A large number of people suffer from hip fractures across the world. The number of annual incidents of the hip fractures in worldwide was increased from 1.3 million in 1990 to 1.6 million in 2000 (Johnell & Kanis 2004; 2006). There are over 340,000 (Kim et al. 2011), 120,000 (Yoshimura et al. 2005), 25,000 (Leslie et al. 2009), and 7,600 (Korhonen et al. 2013a) hip fractures reported annually in the United States, Japan, Canada, and Finland respectively. In the United States, estimated cost for the hip fracture treatment is approximately $10 billion annually (Cummings et al. 1990). By 2050, it is estimated that over 4.5~6.3 million hip fractures happen annually throughout the world (Cooper et al. 1992; Gullberg et al. 1997). Most of hip fractures occur at the femoral neck or trochanteric region of the proximal femur (Karagas et al. 2000). Although the osteoporosis diagnosed by low bone mineral density (BMD) measured with dual energy X-ray absorptiometry (DXA) is known to be highly related to the hip fracture, the low BMD causes the fracture directly very rarely (Stone et al. 2003). Therefore, the osteoporosis, as defined by BMD, is only a risk factor of fracture. (Silva, 2007.) Indeed, approximately over 90% of the hip fractures are directly caused by the fall (Hayes et al. 1993; Cumming & Klineberg 1994; Greenspan et al. 1994a; Parkkari et al. 1999). Keyak et al. (2001a) reported that the high impact on the lateral/posterolateral aspect of the greater trochanter from the falling can cause the fractures with very high chance.

Developing the accurate assessing methods for the hip fracture risk can help to manage prevention of the bone fragility by better identification of fracture-prone individuals. There are two major methods that have been developed over a few decades; 1) bone densitometry, and 2) finite element (FE) method. The BMD obtained from the imagine methods such as planar dual-energy X-ray absorptiometry (DXA) or volumetric quantitative computed tomography (QCT) is a moderate predictor for the hip fracture (Kanis 2002; Johnell et al. 2005; Kanis et al. 2005; Black et al. 2008). The low BMD indicates that patient has increased relative risk for the hip fracture (Cummings et al. 1993; Glueer et al. 1994; Greenspan et al. 1998; Alonso et al. 2000; Stone et al. 2003; Pulkkinen et al. 2004). However, Cody et al. (1999) and Langton et al. (2009) found that FE method is a more promising method to predict the hip fracture in their studies. While the coefficient of determination to predict failure load is 54.5% for the densitometry method, the coefficient for the FE method is 80.4% (Langton et al. 2009). Throughout the numerous FE modeling and experimental studies of the femur, it was reported that the hip fracture depends on various factors; loading conditions (for example, spontaneous/atraumatic, and lateral fall), material properties of the femur (for ex-

ample, Young's modulus), complex three dimensional geometry, internal muscle forces, gender difference, attenuation of the impact force due to soft tissues, osteoporotic condition and age (Robinovitch et al. 1995; Pinilla et al. 1996; Duda et al. 1998; Keyak et al. 2001a, 2001b, 2011; Bitsakos et al. 2005; Bouxsein et al. 2007; Cristofolini et al. 2007; Bessho et al., 2009). From the recent FE modeling study of Keyak et al., (2011), it was found that women have higher likelihood to experience the hip fracture especially if they fall laterally to cause high impact on the posterolateral aspect of the proximal femur than men.

Cortical thickness and the BMD of femoral neck decrease as aging except for the infero-anterior quadrant region of the femoral neck where the most of load transmission takes place during normal daily gait cycle. Especially, the cortical thickness of superoposterior region of the femoral neck declines from average of 1.63 mm at age of 25 years old to 0.33mm at the age of 85 years old in female (Mayhew et al. 2005; Poole et al. 2008). However, it is known that the bone strength can be maintained by the adequate amounts of exercises throughout the life (Forwood & Burr 1993; Pajamäki et al. 2003; Järvinen et al. 2003; Turner & Robling 2004; Ruff et al. 2006; Nikander et al. 2010b). It was recently revealed that exercise history of high impact (H-I) exercise loading (for example, triple jump and high jump) and odd impact (O-I) (for example soccer and squash) during young adulthood can increase the cortical thickness of the femoral neck. The H-I group had thicker cortex at inferior, anterior, and posterior region of the femoral neck while the O-I group had thicker cortex at superior, anterior, posterior part. (Nikander et al. 2009; Narra et al. 2013.) This indicates that those regions with thicker cortex may have higher load bearing capacity. Especially, thicker superior cortex has significant meaning in terms of reducing likelihood of femoral neck fracture. In engineering perspective, unusual high stress can be seen at this superior part in the lateral fall event. Thus, if the femoral neck has sufficiently thick superior cortex, it may have higher load bearing capacity in this region.

The exercise-induced bone thickening during the growth occurs through new bone formation below the periosteal surface of the bone while the age-related bone loss is mainly due to the bone loss on the endocortical surface of bone (Bass et al. 2002; Ruff et al.. 2006). This means the exercise-induced cortical thickness may be sustained throughout the life. In other words, the bone strength due to this exercise-induced cortical thickening in the femoral neck during growth phase may be sustained to the elderly. It highlights the meaning of the involvement in exercise in adolescence and young adulthood is highly important in terms of preventing the hip fracture in their future. However, to the author's knowledge, none of previous FE modeling studies investigated the influence of the exercise history on the female proximal femur to assess the hip fracture risk.

Thus, primary purpose of this thesis was to investigate the influence of different impact loading exercise history on the strength of the proximal femur using the FE method. Especially, it was focused if the H-I and O-I exercise groups had any advantages in terms of bone strength in the femoral neck. For the creation of the FE models, MRI-

based proximal femur geometries of 36 subjects, randomly selected 6 per each exercise loading group, were obtained from 111 subjects' data of Nikander et al. (2009). The proximal femurs were modeled as the linear elastic, isotropic and homogeneous materials in the FE models. A lateral falling condition which most likely causes femoral neck fracture was simulated. Stress distribution around the thinnest region of the femoral neck was analyzed in the post-simulation phase.

Previous MSc student, Mr.Daniel Oravec conducted a similar pilot study in his MSc thesis (Oravec, 2009). In his study, the FE method with the same MRI data was developed using the FE modeling software COMSOL MultiPhysics (COMSOL, Inc., Burlington, MA, USA). The objective in his study was to develop the FE method using the MRI data of three subjects. In spite of its advantage, COMSOL is not the common FE modeling software in the field of bone biomechanics. Instead, ANSYS (ANSYS Inc., Southpointe, PA, USA) has been often used in previous studies of others. Therefore, the secondary objective of this thesis was: 1) to increase the sample size from 3 to 36 (6 groups containing 6 subjects in each group), and 2) to switch the software from COMSOL to ANSYS. Some of the post-simulation analysis methods used in Oravec (2009) were adopted and modified in the present study.

This thesis consists of six chapters: Introduction, Theoretical Background, Materials and Methods, Results, Discussion, and Conclusion. In the Theoretical Background, basic background of bone and hip fracture, and literature review of proximal femur FE modeling studies are introduced to provide sufficient background to give rational for conducting this research. Especially, topics relating to mechanical aspect of long bone, bone functional adaptation for the exercise loading, mechanism of hip fracture, importance of superior part of the femoral neck are deeply discussed in this section. In addition to that, previous femur FE modeling studies are intensively explained to provide grounds why specific methods were adopted in the FE models in this study. In Materials and Methods, detailed processes from manual segmentation of the MRI data to the creation of the FE models using ANSYS and post processing methods are explained. In Results, visual images of created FE models and the comparison of the sector-wise regional mean stress values from the smallest cross-section of the femoral neck from all groups are shown as results. In Discussion, important features from the results are discussed in relation to the findings from previous studies. Furthermore, limitation and future study consideration are discussed in this section. In Conclusion, the merit of the research, summary and importance of the results, practical recommendations, limitation of the current study, and consideration for the future study are discussed.

2. THEORETICAL BACKGROUND

2.1. Bone

2.1.1. Anatomy and Physiology

Bone is a complex and dynamic living organ constituting the skeletal system together with other connective tissues such as ligaments, tendons, and cartilages. Its mechanical functions are providing the structural framework for the body, protection for the vital internal organs, and assistance in movement by acting as a lever system to transfer forces. It also performs important physiological functions: maintaining mineral homeostasis, and producing blood cells. (Tortora & Grabowski 2003; Nigg & Herzog 1999.) Throughout the life, bone tissue repeats a cycle of remodeling consisting of formation, resorption, and maintenance of bone. There are three different types of bone cells responsible for this remodeling: *osteoclasts*, *osteoblasts*, and *osteocytes*. Osteoclasts resorb bone and then release calcium into serum. On the other hand, osteoblasts form bones. The osteoblasts become osteocytes once they get surrounded by mineralized bone. (Nigg & Herzog 1999.)

Majority of bones can fall into five different bone types based on its shape: long (for example, humerus and femur), short (for example, wrist bone), flat (for example, cranial bones), irregular (for example, vertebra), and sesamoid bone (for example, patella). (Tortora & Grabowski 2003.) Its mechanical functions vary depending on this shape of bone. The function of the long bone, for example femur, is to act as a stiff lever and to transmit muscle generated-forces over joints. On the other hand, the function of flat bone, for example skull bones, is focused to provide protection for the internal organ such as brain. (Nigg & Herzog 1999.) The bone studied in this study, femur bone, falls into the long bone type. The femoral diaphysis comprises a long cylindrical shaft which is slightly curved anteriorly to direct mechanical stresses to make the stress pattern predictable. More details of this femur bone will be explained later. This long bone is illustrated in Figure 2.1.1.1.

Structurally, the bone consists of a number of components. The long bone consists of diaphysis, epiphyses, metaphyses, articular cartilage, periosteum, medullary cavity, and endosteum. This structure of the long bone is shown in Figure 2.1.1.1. A long cylindrical shaft in the middle part is called *diaphysis*. The distal and proximal ends of the bone are called *epiphyses* which are partly covered by the *articular cartilage*. (Nigg & Herzog 1999.) The mature bone regions where the diaphysis joins epiphyses are called *metaphyses*. Except for the surface of the epiphyses covered by the cartilage, the bone surface is surrounded by a tough sheath of dense irregular connective tissue called *pe-*

riosteum. It contains osteoblasts and plays an important role for growing in diameter of bone. The outer layer of the periosteum contains a number of blood vessels and nerves, some of which enter the bone. The space in the diaphysis containing the fatty yellow bone marrow is called *medullary cavity*. There is a thin membrane lining the medullary cavity called *endosteum*, which also contains the osteoblasts. (Tortora & Grabowski 2003.)

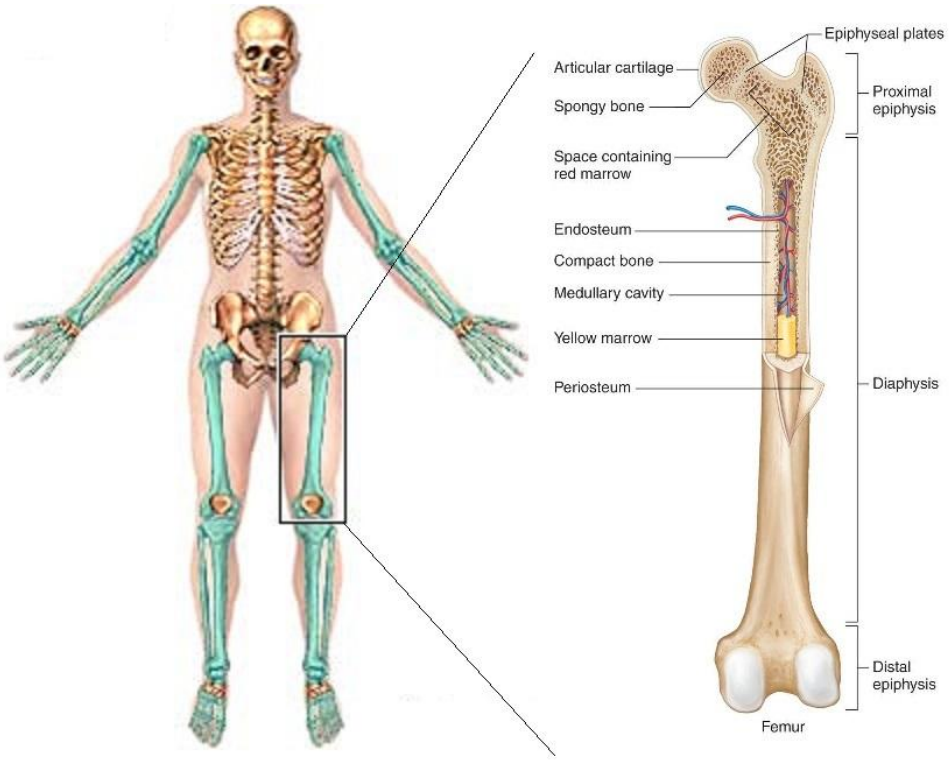

Figure 2.1.1.1. *Structure of the long bone. Light Green colored bones at left side of figure are long bones in the human skeletal system. The right figure shows the structure of a long bone, femur. Figures were obtained and modified from Shier & Lewis 2002.*

Rather being completely solid, bone has a large number of spaces between cells and matrix components. Density and size of these spaces varies from one region to another. Based on this, bone can be also categorized into either compact bone called *cortical bone* or spongy bone called *trabecular bone*, which are shown in Figure 2.1.1.1 and Figure 2.1.1.2. As the name indicates, the cortical bone contains fewer spaces in its matrix and provides rigid protection, support, and resistance for the mechanical stresses from weight and movements. The hard outer layer of bone is made of this cortical bone with porosity of 5-30% (Carter & Hayes 1977). The total mass of all cortical bone in our body accounts for 80% of the total bone mass of an adult skeleton. The basic unit of the compact bone is called *osteon* or *Haversian system*. (Tortora & Grabowski 2003.) The osteon is made by *lamellae*, which is the planar arrangement form of mineralized collagen fibers. It runs approximately parallel to the long axis of bone. (Rho et al. 1998.) In the osteon, blood, lymphatic, nervous vessels run longitudinally through a

canal called Haversian canal. Furthermore, these vessels run in perforating canal for the transversal communication between osteons. This histological structure of the long bone is shown in Figure 2.1.1.2 below.

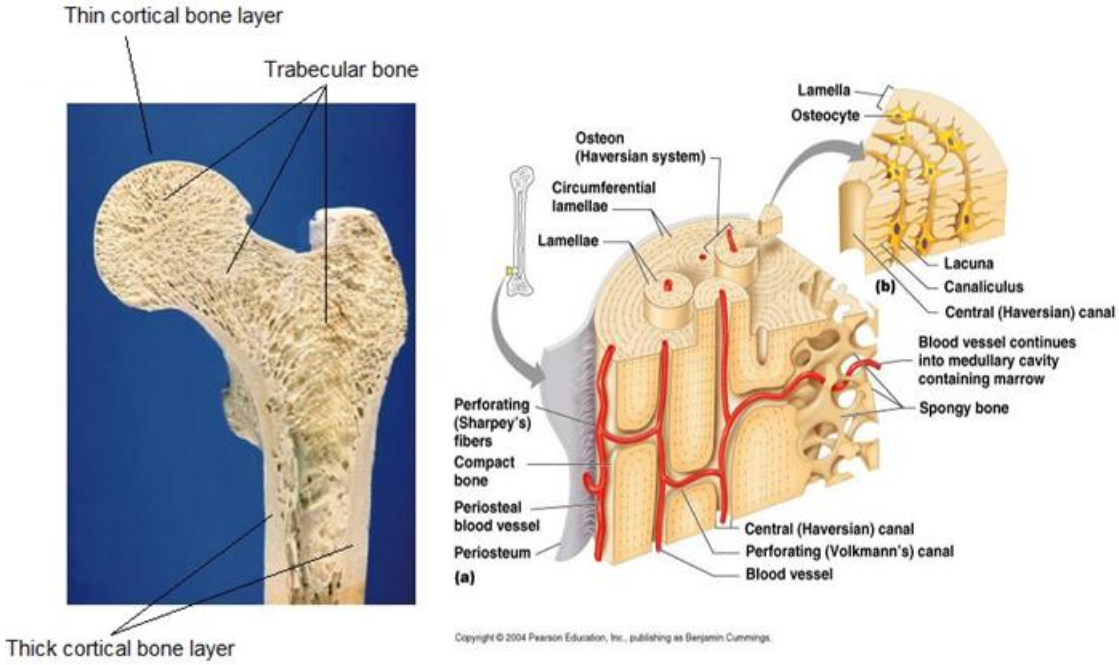

Figure 2.1.1.2. *Histological structure of the long bone (right), and cortical and trabecular bone in the proximal femur (left). The left figure shows thin and thick layer of the cortical bones, and the trabecular bone network in the proximal femur. Left Figure was obtained from Marieb 2009 and right figure was from Shea & Miller 2005.*

On the other hand, the trabecular bone contains much more spaces in its matrix. Inside of some of the bones are filled with this trabecular bone with porosity ranging from 30% up to 90% depending on the location of bone. This trabecular bone accounts for 20% of total bone mass. (Rho et al. 1998; Carter & Hayes 1977.) Differing from the cortical bone, the basic unit of the trabecular bone is called *trabeculae*, an irregular latticework of thin columns of bone. Various combinations of interconnecting framework of trabeculae constitute the trabecular bone (Rho et al. 1998). Trabecular bone also helps bones resisting mechanical stresses and transfer forces without breaking. Importantly, this trabecular bones contribute to reduce the overall weight of a bone. (Tortora & Grabowski 2003.) The femur bone studied in this thesis falls into the long bone type. Long bones are built of high amounts of compact bone tissues in their diaphyses. However, in their epiphyses, they contain large amount of trabecular bones while thickness of the cortical bone get thinner from the diaphyses to the epiphyses (See Figure 2.1.1.2). In this thesis, only proximal portion of the femur was modeled and used for simulation.

2.1.2. Material Properties of Bone

Bone is an *anisotropic* and *inhomogeneous* material. Its mechanical properties vary depending on the force direction applied and location in the bone. (Nigg & Herzog 1999.) According to Weiner and Wagner (1998), there is a structure-mechanical function relationship in bone. Bone is built up of a structural basic building block called *mineralized collagen fibril*. In parallel-fibered bone such as the long bone, the mineralized collagen fibrils align to form array in the direction parallel to the axis of long bone. This longitudinal orientation of the mineralized fibrils creates the high anisotropic material behavior. Material can fall into two categories based on the mechanical behavior in response to the direction of force applied: isotropic and anisotropic material. Isotropic material has identical material behavior in all directions while anisotropic material has different behavior in all directions. Due to its structure, bone has anisotropic material behavior. The parallel-fibered bone like the long bone has higher modulus in the direction parallel to the axis of the bone than the one in the direction perpendicular to the axis. (Keaveny & Hayes 1993; Weiner & Wagner 1998; Nigg & Herzog 1999.) A number of investigators measured the mechanical properties of bone. Table 2.1.2.1 summarizes the properties and includes longitudinal, transverse, and shear moduli, density, and Poisson's ratio (transverse modulus for the trabecular bone is not available). Since this study focused on the femur, the material properties of the femur were chosen.

Table 2.1.2.1. *Material properties of (femur) bone. Left column shows variables while the middle and the right columns show values in unit and comments respectively (bone location and cadaveric bone age). Data were obtained from: Burstein et al. 1976; Carter & Hayes 1977; Garnier et al. 1999; Goldstein 1987; Rho et al. 1998; Weiner & Wagner 1998; Wirtz et al. 2000; Morgan et al. 2003; Bayraktar et al. 2004.*

Human Cortical Bone		
Longitudinal Modulus	15.6-17.7 GPa 15.7-19.9 GPa	femur, age 20-89 femur, age 54-85
Transverse Modulus	11 GPa	not available
Shear Modulus	3.17-3.7 GPa	femur & tibia, age 20-89
Apparent Density	1.8 g/cm^3	not available
Poisson's ratio	0.2-0.5 (average 0.3)	not available
Human Trabecular Bone		
Longitudinal Modulus	1-20 GPa	various bones, n/a
Transverse Modulus	not available	
Shear Modulus	289 MPa	femur, age 47-81
Apparent Density	0.35-0.75 g/cm^3 (average0.56)	mean age 69
Poisson's ratio	0.01-0.35 (average 0.12)	not available

As shown in Table 2.1.2.1, there are great variations in the longitudinal (elastic) modulus of the trabecular bone. According to Goldstein et al (1983), the modulus of the

trabecular bone at the macrostructure level can vary from one location to another by factor of up to 100. This is because porosity of the trabecular bone varies in different locations and the degree of porosity determines the apparent density of the bone. The modulus changes depending on this density. (Carter & Hayes 1977.) This variation of density/porosity shows high *inhomogeneity* of the trabecular bone and affects the mechanical properties of bone. It is also well known that the material properties of the trabecular bones can vary due to loading directions, age, and relevant environmental and testing conditions in the studies, in which the mechanical properties of trabecular bones were measured (for example, sample shape, humidity, and size). (Goldstein 1987; Keaveny & Hayes 1993.) However, approximately a decade ago, several researchers investigated the mechanical properties of the trabecular bone at microstructure level using nanoindentation and acoustic microscopy techniques. Their finding was opposing to values at macrostructure level shown in Table 2.1.2.1. They found that the elastic modulus of the trabecular bone at microstructure level is similar to values of the cortical bones (Rho et al. 1997; Turner et al. 1999; Zysset et al. 1999).

One of the most significant features of the mechanical properties of bone is its strong relation to apparent density (Carter & Hayes 1976; Keaveny & Hayes 1993; Rho et a. 1995; Wirtz et al. 2000). Many researchers found the mathematical equations for the elasticity-density relationship based on their empirical studies. Table 2.1.2.2 shows selected equations from literature, which have high determination coefficient. In Table 2.1.2.2, the elastic modulus is expressed as *E (GPa* for the cortical bone and *MPa* for the trabecular bone*)* while the apparent density is shown as ρ_{app} *(g/cm^3).* Due to its high determination coefficient, two equations from Rho et al. (1995) were adopted and used to obtain values of Young's modulus in this thesis along with density values from Table 2.1.2.1.

Table 2.1.2.2 *Empirical mathematical relationship between the modulus (longitudinal) and apparent density of cortical and trabecular bone.*

Equation	Determination coefficient	Anatomical Location	Other relevant information
Human Cortical Bone			
$E = -13.43 + 14.261\rho_{app}$	0.67	Femoral Metaphysis	Lotz et al. 1991a
$E = 3.891\rho_{app}^{2.39}$	0.75	Tibial Diaphysis	Snyder & Schneider 1991
$\boldsymbol{E = -6.142 + 14\rho}$ [b]	**0.77**	**Femur**	**Rho et al. 1995**
Human trabecular bone			
$E = 1310\rho_{app}^{1.40}$	0.91	Femoral Neck	Lotz et al. 1990a
$E = 6850\rho_{app}^{1.49}$	0.85	Femoral Neck	Morgan et al. 2003
$\boldsymbol{E = 0.58\rho_{app}^{1.3}}$ [a. b]	**0.94**	**Femur**	**Rho et al. 1995**

[a] Unit of the apparent density only for this equation is kg/m^3.

[b] These equations were used to obtain Young's moduli for the cortical and trabecular bone in this thesis. The detail to calculate Young's modulus is explained in the subchapter 3.5.1.

2.1.3. Bone Functional Adaptation

Bone is known as a mechanosensitive tissue which adjusts its mass, structure, and mechanical properties based on the mechanical loading it is exposed to. This concept was first proposed by Julius Wolff in 1892, thus known as Wolff's law (Duncan & Turner 1995). He originally introduced this concept specifically for the development of the trabecular bone. He found that structure of trabecular bone in the proximal femur was highly associated with the principal direction of the mechanical loading. This theory is known as the trajectory theory. This was also observed in other bones such as vertebrae, tibia, and calcaneus. It is well known that not only the trabecular bone is influenced by the mechanical loading, but also the cortical bone is. (Turner 2007.) In order to avoid this confusion, the generalized Wolff's Law is now preferably called as *bone functional adaptation* (Ruff et al. 2006; Turner 2007).

Two different mechanisms are responsible for the construction of bone structure in our life: *modeling* and *remodeling*. In these two mechanisms, different types of bone cells such as osteoblast and osteoclast work as a team or individually to achieve skeletal formation and/or renewal. Bone modeling is a process taking place during bone growth before the skeletal maturity is reached. In the bone modeling, either osteoclast activation with following resorption of bone (A-R), or osteoblast activation with following formation of bone (A-F) is involved at any bone surface. In order to optimize the structure of bone, either resorption or formation of bone is selected in order to optimize the bone structure in response to the mechanical load. For example, adequate amounts of exercise and increase in body mass in growth increase formation of bone. On the other hand, lack of exercise can increase resorption. It is noteworthy to mention that, in bone modeling, resorption (A-R) and formation (A-F) cannot happen at a time at the same location of the bone surface. (Rubling et al. 2006; Turner 2007.)

Once skeleton reaches its maturity, a type of the mechanism shifts from modeling to remodeling. In the remodeling, osteoblasts and osteoclasts form a functional unit called *basic multicellular unit* (BMU), which perform remodeling together. Unlike the modeling process, remodeling always follows specific order of processes; an activation, and then resorption following formation (A-R-F). As shown in Figure 2.1.3.1, osteoclasts and osteoblasts perform a coupled activity. First, osteoclasts get active to resorb bone tissue and then osteoblasts start forming bone tissue. This takes place in Haversian canals in the cortical bone, and on the surface of trabeculae in the trabecular bone shown in Figure 2.1.3.1. (Hernandez et al. 2000; Turner 2007.) The net amount of bone resorption and new born formation in the remodeling cycle is called *bone balance*. If this balance is positive, the bone gets thicker. On the other hand, if it is negative, the bone gets thinner. (Eriksen et al. 1986.)

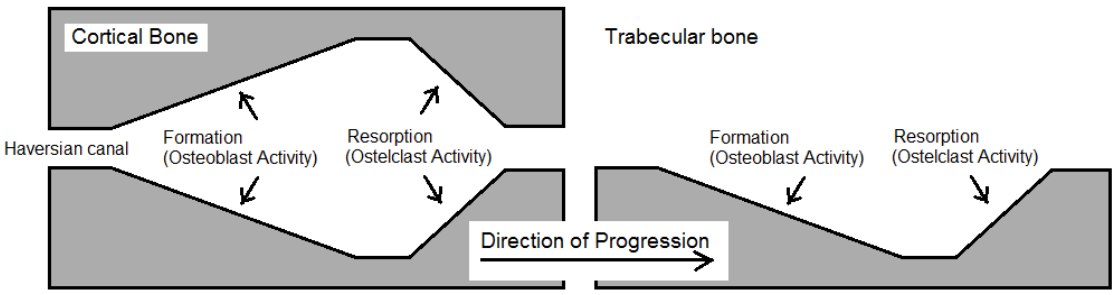

Figure 2.1.3.1. *Remodeling of cortical (left) and trabecular bone (right) by the BMUs. Figure was modified from Hernandez et al. 2000.*

The bone balance in the remodeling is highly affected by the quantity of the mechanical loading. If too less mechanical loading is applied to the bones over time (disuse), more resorption over formation occurs. On the other hand, if optimal amount of mechanical load is applied, more formation of bone happens over the resorption. This mechanism was well described by Harold Frost (1987) as Frost's *mechanostat* theory. He explained net amount of the formation and resorption of bone can be explained by a function of strain magnitude. As shown in Figure 2.1.3.2, if the strain magnitude is below 50 to 200 micro-strain, the status of remodeling falls into disuse and more resorption occurs. On the other hand, equal quantity of resorption and formation take place if strain magnitude range between 50~200 and 2000~3000 micro-strain. If the strain magnitude is over 2000~3000 micro-strain, the status can be considered as overload on bone and more formation of bone occurs. Furthermore, if the magnitude is over 4000 microstrain, the magnitude is large enough to cause permanent deformation considered as pathological overloading zone. (Duncun & Turner 1995; Robling et al. 2006.)

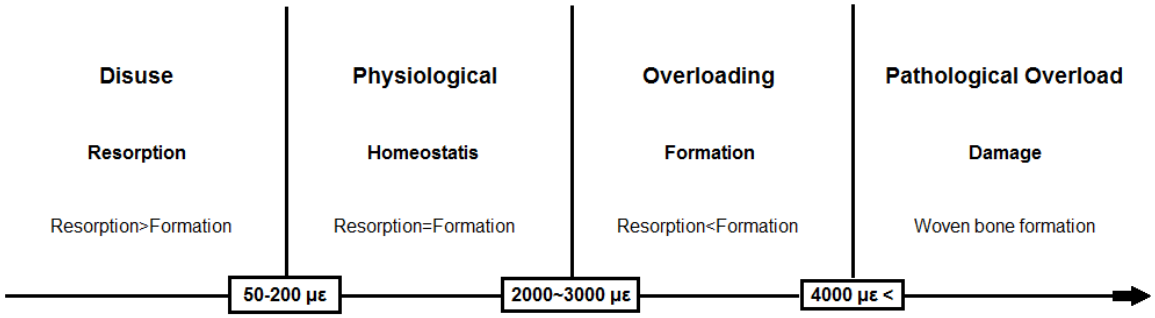

Figure 2.1.3.2. *Scheme of Frost Mechanostat theory. Microstrain is expressed as* με. *Figure was modified from Duncun & Tuner 1995.*

Obviously, the Frost's theory is simplified. Not only the strain magnitude affects the bone functional adaptation, but also other factors in the mechanical loading such as types of loading, loading frequency, and strain rate, duration of the mechanical loading do. (Robling et al. 2006.) Dynamic loading type has much greater effect on bone adaptation than the static loading type (Turner & Pavalko 1998; Tuner 1998; Robling et al. 2001a; Turner & Robling 2005; Ruff et al. 2006; Turner 2007; Robling et al. 2006). It

was found that both loading frequency and strain rate highly affect bone functional adaptation (Turner et al. 1994, 1995). From the experimental study of Turner and his colleagues (1994), it was found that loading frequency applied to bone has to be equal to or greater than 0.5 Hz to activate osteoblast's bone formation. Furthermore, minimum magnitude of loading for the osteogenesis can be decreased if the loading frequency is increased (Turner 1994). Extending duration of the mechanical loading does not contribute to further bone formation. Instead, bone tissue gets desensitized if it is exposed to long duration of the mechanical loading. 95% of mechanosensitivity can be lost after only 20 loading cycles. (Burr et al. 2002.) Certain resting period is necessary for bone tissue to resensitize itself prior to the next mechanical loading. According to Robling et al. (2001b), in their animal study, at least 4 hours is necessary for bones to resensitive itself for next effective bone formation. Furthermore, approximately 98% of bone mechanosensitivity was recovered within 24 hours. (Robling et al. 2006.)

Disuse and substantial overuse of bone have negative effect on bone strength. If low or too less quantity of stress is applied to bone, bone formation on the periosteal surface gets reduced while bone resorption is increased on endocortical and trabecular bone surface. The resorption dominates over bone formation in this disuse situation, which leads to rapid bone boss. (Robling et al. 2006; Turner 2007.) The decrease in the bone formation on the periosteal surface and increase in bone resorption on the endosteal surface was well presented through experimental animal studies. In growth phase, this negative effect of disuse has high impact on the periosteal surface of bone and normal bone growth is decreased. On the other hand, in mature bone, the effect is high on the endosteal surface of bone. This is illustrated in Figure 2.1.3.3 below. Furthermore, porosity of cortical bone is considerably increased. (Robling et al. 2006.)

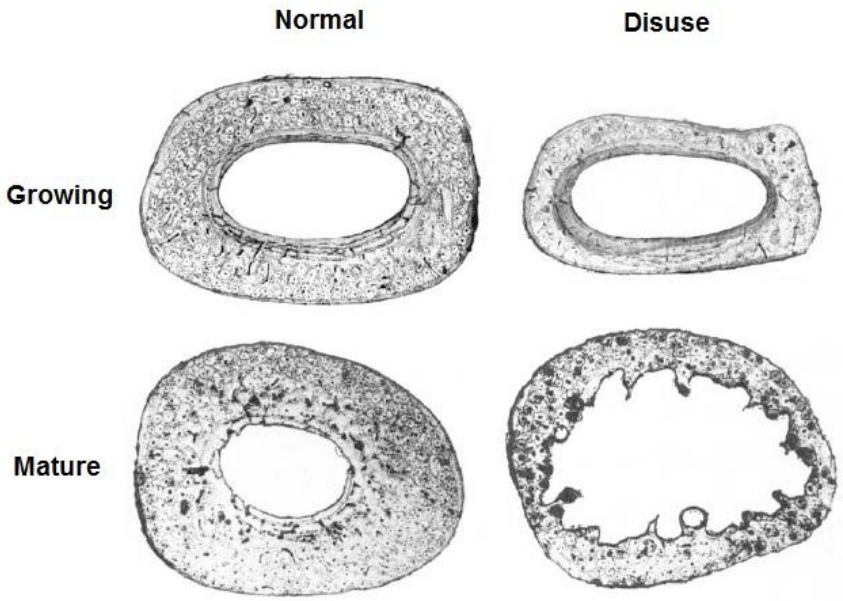

Figure 2.1.3.3. *Comparison of the cross sections of canine metacarpal bones between normal and disuse bone in growing and mature phase. Figure was modified from Robling et al. 2006.*

The consequence of disuse leads to the smaller cross sectional area, which leads to decrease in the bone strength. (Uhthoff and Jaworski 1978; Jaworski et al. 1980.) Overuse of bone can result in the creation of microscopic cracks and/or damages. This leads to resorption of the damaged part following the new bone formation, which combination is considered as the repairing of the damaged bone. This is the reason why the bone resorption increases in overuse of bone. If creation of damaged bone tissue is faster than this repairing rate, bone strength can be decreased substantially and can even result in a stress fracture. For example, overuse bone injuries due to accumulation of microscopic cracks are common in runners and ballet dancers (Matheson et al. 1987; Khan et al. 1995).

2.1.4. Bending Theory of Long Bone

In the engineering perspective, thickening cortical bone by formation of new bone on periosteal surface is significantly important in terms of strengthening bone. Long bones are mainly exposed to bending loading and have the shape of thick-walled tubes. Thus, following equation of deflection of a beam in bending can also be applied to the long bone;

$$\delta = \frac{ML^2}{8EI} \dots\dots (2.1.4.1)$$

where δ is the deflection of beam, M is the bending moment or the applied bending force, L is length of the long bone, E is the Young's modulus, and I is the second moment of area. For a given M, deflection of bean can be lessened by either increase Young's Modulus (E), decreasing the length (L), or increasing the second moment of area (I). This lowering beam deflection indicates the strengthening the bone. Furthermore, this second moment of area for the tube like long bone can be expressed as;

$$I = \frac{\pi}{4}(r_o^4 - r_i^4) \dots\dots (2.1.4.2)$$

where r_o is the outer radius while r_i is the inner radius of the cortical bone. Figure 2.1.4.1 describes these radiuses. Increasing I can be done by increase in r_o and/or decrease in r_i. This can be done by formation of bone on the periosteal or endosteal surface of cortical bone. On the other hand, the Young's modulus, E, can be raised by more mineralization of bone. However, it is known that increase in I is more efficient way from engineering perspective than increase in E. (Turner 2007.) Since the femoral neck also has the tube like shape despite of much shorter length and thinner cortical walls than those of the femoral shaft, this concept can still be applied to the femoral neck. Since whether the new bone formation takes place on either the periosteal or endosteal surface depends on the age, involving in the exercises in specific age range has significant meaning in terms of strengthening bone for life long period.

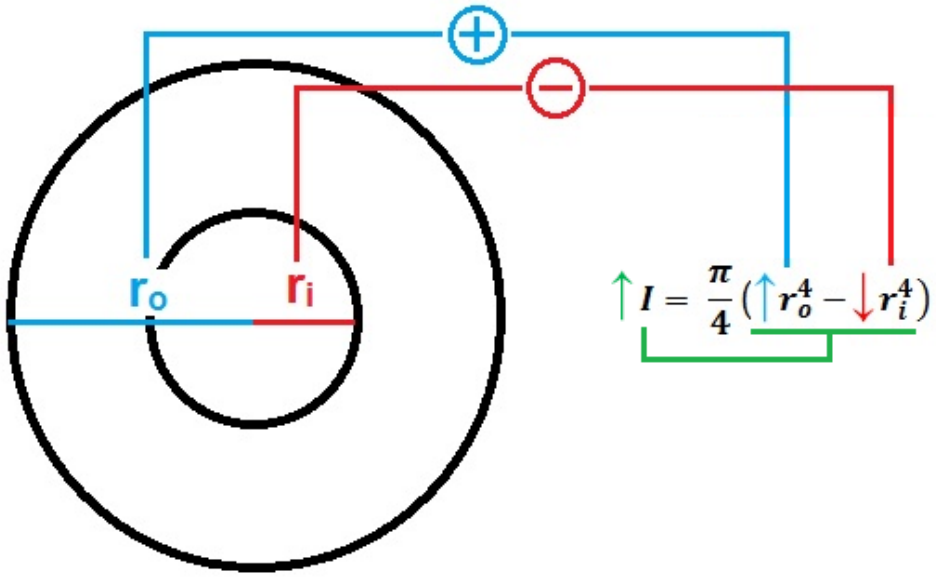

Figure 2.1.4.1. *The second moment of area and a scheme of the outer and inner radiuses of the tube like bone. Increase in the outer radius due to the periosteal expansion expressed as the positive sign in a circle and decrease in the inner radius caused by bone formation due to the endosteal contraction expressed as the negative sign in a circle lead to increase in the second moment of area expressed as I. This negative sign does not mean the endosteal contraction has the negative phenomenon in terms of bone strength. It means the negative sign can decrease* r_i.

2.1.5. Age-Dependent Surface-Specific Response

Bone response to the mechanical loading is also age dependent. Once skeletal maturity is reached, which usually occurs after age of 18 to 25 years old, the mechanosensitivity of bone to the mechanical loading starts declining. In adult, the response rate to the mechanical loading is slower than in juveniles. Although the main role of mechanical loading on the bone shifts to maintenance of the existing bone in adult, additional exercise is not totally meaningless in terms of strengthening the bone. Despite the slow rate of response to the mechanical loading, cumulatively significant changes in bone mass and structure can occur if the adequate amount of the mechanical loading is applied to bone in optimal frequency. This cumulative change of bone mass and structure is larger in younger adult than the elderly people. (Forwood & Burr 1993; Turner & Robling 2004; Ruff et al. 2006.) However, Kerr et al. (1996) reported that even postmenopausal women with mean age of 58 can increase their BMD at several skeletal sites (including hip) by small amount, but significantly (an average gain of 2.4%) over 1 year of weight-training. They also found that exercise with heavier weight and low number of repetition had more positive effect than with light weight and large number of repetition. Moreover, Leppänen et al (2008) reported an interesting and conflicting finding from their animal experimental study. They reported that significant exercise-induced increases in the mechanosensitivity were seen from old rats' bone after the experimental

training intervention. Their result indicates that mechanosensitivity to the loading may not decline with aging.

Not only the mechanosensitivity changes with aging, but also the location of the bone formation to the mechanical loading varies with aging. During early adolescence, subperiosteal surface responses to the mechanical loading; thus it expands the circumference of bone by the new born formation. On the other hand, after the adolescence, endosteal surface is more responsive to the mechanical loading and the circumference stays the same if adequate mechanical loading is applied. (Bass et al. 2002; Ruff et al. 2006.) Furthermore, according to Ducher et al. (2009), the periosteal expansion in response to the mechanical loading in the prepubertal boys was twice greater than in prepubertal girls. While exercise during or late in adolescence can still result in periosteal expansion in boys, it already starts resulting in endocortical contraction in girls (Daly 2007). Therefore, this surface-specific responses to the mechanical loading are gender-specific and age-dependent (Nikander et al. 2007). These subperiosteal and endosteal enlargement plays an important role in terms of strengthen the bone. Especially, increase in the outer radius due to subperiosteal expansion is significantly important because it directly contributes to increase the second moment of area, which increase can eventually decrease the beam deflection. As discussed earlier, this decrease in the beam deflection indicates the strengthening the bone. Therefore, subperiosteal expansion from the adolescence is very important in terms of increasing life-long bone strength.

The adequate mechanical loading has positive effects on the structure and the mineral contents of bone. These effects are most likely obtained throughout exercises or certain kinds of sports. Besides, as discussed already, the more positive effects happen to the bone, the earlier an athlete starts sports career. For example, several investigators found that the athletes who started their athletic career earlier had higher bone mineral contents and thicker cortex due to the periosteal expansion on their dominant upper extremity from the sports such as tennis, racket, and squash. (Ruff et al. 1994; Trinkaus et al. 1994; Kannus et al. 1995; Kontulainen et al. 2002). Furthermore, different loading type exercises have diverse effects on structuring the bone geometry. This is deeply discussed in the next subchapter.

2.1.6. Influence of Different Loading Exercises on Bone

Several variables affect the bone functional adaptation such as the frequency, magnitude, and loading rate (Ruff et al. 2006). Exercises involving high magnitude, high rate of load cycles, loading from unusual lateral directions are more advantageous in terms of osteogenic effect than those involving low magnitude, and slow rate of load cycles (Nikander et al. 2008). These exercises are not only effective in increasing the bone mass (osteogenic effect) (Heinonen et al. 1993, 1995), but also strongly associated with shaping a strong bone structure (Haapasalo, et al. 2000; Heinonen et al. 2001, 2002; Liu et al. 2003). Loading type varies depending on the nature of exercise or sports. Depending on this loading type, stress and/or strain distribution are altered considerably. Due to this, the response of new born formation to mechanical loading is site-specific.

(Lanyon 1996; Heinonen.2001.) Those exercises involving high-rate of load cycles, loading from unusual odd/lateral direction, high magnitude of loading are categorized as High-Impact (H-I), Odd-Impact (O-I), High-magnitude (H-M) loading exercises respectively. The osteogenic effects and its ability to shape strong bone structure from the different loading exercises have been well studied.

Heinonen and his colleagues (2001) studied the influence of the H-I loading on the mineral mass, size, and gross structural properties in triple jumpers' lower extremities. They found that areal BMD in the femoral neck and lumbar spine of the triple jumpers were much higher (31%) than the non-athlete control subjects. Also, it was reported that mean tibial cortical wall thickness, and bone strength of the tibia and femoral neck of the triple jumper were greater than those in the controls. The magnitude of the instant ground reaction force at the impact can be 20 times greater than the body weight onto a single leg. The great mechanical competence of triple jumpers' bone most likely permits this great ground reaction force. This study indicated that the exercise involving high impact loading can improve bone strength by increasing bone mass and increasing the size of bone in a site-specific response fashion. Thus, exercises engaging high impact loading have high osteogenic effect with site-specific fashion and can increase the strength of bone. This finding was also reported by Nikander et al. (2005, 2006). Heinonen and his colleagues (2001) also concluded that the enlargement of the strong cortex mainly contributes to increase the mechanical strength. Impact loading from unusual directions is also known to have similar osteogenic effect as the high impact loading. In the study conducted by Nikander and his colleagues (2008), it was found that the slalom ski skiers, which sport engages with the O-I loading, have thicker cortex at the anterior region of the femoral neck compared with nonathletic controls.

Furthermore, Nikander et al. (2005, 2010a) studied the influence of total of five different loading types, in addition to three mentioned earlier, on bone mass, bone size and structure in tibia and femoral neck; five different loading types are H-I (triple jump, high jump, volleyball, and hurdling), O-I (soccer, speed skating, step-aerobics, squash, tennis, and badminton), H-M (power lifting), repetitive low-impact (R.L-I) (endurance running, orienteering, and cross-country skiing), repetitive non-impact (R.N-I) (swimming and cycling). It was found that H-I, O-I, and R.L-I groups had thicker cortex at distal tibia. In the femoral neck, both H-I and O-I loading groups had higher aBMD, cross-sectional area, subperiosteal width, and greater bone strength.

These findings provide us clinically practical information in terms of strengthening bone to prevent bone fractures in older age. Despite the fact that the H-I loading exercise are highly osteogenic, the H-I exercise is clearly too risky for elderly people. The H-I loading may increase the risk of the damage of the articular cartilage and even the bone fracture. Since the O-I exercises involve less magnitude of loading, the risk of those are much less and there still osteogenic effect exists. Therefore, the O-I loading exercise can be attractive to strengthen bone. For example, this can be practically useful to strengthen the femoral neck to prevent fracture from lateral fall. (Nikander et al. 2008.)

So far, it has been discussed that some exercises involving H-I and O-I loadings are clearly advantage in term of strengthening bone. However, the question is if these positive effects are valid for all age groups. Studies of Nikander et al. (2006, 2010a), discussed so far, were conducted with over 200 young female subjects whose average age was around 20 years old. Also, Pettersson et al. (2000) found the similar results of positive effect of the H-I loading exercises from late adolescent female with average age 17.5 years old. Therefore, it is obvious that the H-I and O-I loading exercises have positive effects on bone strength of young adult. Although the degree of effect is less, it was also found that the H-I and O-I loading exercises can preserve and/or even increase BMD at lumbar spine, femoral neck in both premenopausal female with average age of around 35 (Martyn-St James & Carroll 2010) and postmenopausal female with average age of over 50 (Nikander et al. 2010b). Furthermore, the positive effects of the impact exercise training in the postmenopausal women are not only on BMD, but also on increasing cortical bone area (Adami et al. 1999; Uusi-Rasi et al. 2003). Therefore, the answer for the question is that the positive effects are valid for all age groups although the degree of the effect decreases with age.

Throughout these previous studies, recommended exercise protocols have been constructed. For children through young adult, exercise programs involving moderate to high-impact weight-bearing activities which are applied rapidly throughout multiple directions are recommended. For instance, skipping, dancing, jumping, and hopping should be involved in the programs. On the other hand, for middle-age and elderly people, low- to moderate-impact weight-bearing exercises combined with progressive resistance and/or agility training has been identified as the effective exercise program on bone health in terms of increasing and/or maintaining BMD. (Nikander et al. 2010b.) Again, it is noteworthy to mention that H-I loading is too risky for older people because it may cause articular damage or even bone fracture. Thus, movements engaging the H-I loading should be avoided in the exercise programs for elderly. However, the optimal impact type and dose of exercise for elderly are not well defined compared with the ones for younger people. Therefore, further long-term randomized controlled trials are necessary to investigate which specific exercise is the safest and the most effective on strengthening elderly bone, especially for hip and spine. (Nikander et al. 2010b.)

Recent study of Nikander and his colleagues (2009) investigated the influence of same 5 different impact types (H-I, O-I, H-M, R.L-I, and R.N-I) in young female athletes on femoral neck bone geometry and strength. Throughout this study, they found that H-I and O-I athletes have 20 to 30% higher BMD and mean cortical area at the femoral neck than the non-athletic controls. The most important findings of this study were that both H-I and O-I group had 20% thicker cortex at anterior and posterior regions of the femoral neck and the H-I group had up to 60% thicker cortex at the inferior region. Although its degree is less, superior region of the femoral neck was 15% thicker in the O-I group. The strength of the superior cortex of the femoral neck is significantly important in terms of preventing the fracture of femoral neck. In case of the lateral fall, the impact on the greater trochanter creates substantial compressive force at the

superior region of the neck. If its degree is excessive, it may end up with the fracture. (Lotz et al. 1995; Carpenter et al. 2005; Verhulp et al. 2008.) This suggested that the exercise programs involving odd-impact loading may have beneficial to strengthen the femoral neck against the lateral fall hip fracture (Nikander et al. 2009). This importance of the thickening of the superior cortex of the femoral neck is deeply discussed in the next chapter.

2.2. Hip Fracture

2.2.1. Morphology of Proximal Femur

The femur is the strongest, heaviest, and longest bone among all other bones in our body. The proximal end of femur consists of a rounded femoral head, neck, two trochanteric regions, and proximal side of the shaft as shown in the left picture in Figure 2.2.1.1 (Miller & Sanders 2012). The femoral head articulates with the acetabulum of the pelvic bone to form the hip joint. The neck connects the shaft to the head and keeps the proximal shaft of the femur away from the pelvic bone in a certain distance in order to avoid the impingement between bones. Two trochanters, the greater trochanter and lesser trochanter, are the projective places of the femur for the attachments of the muscles. At the junction of the femoral neck and the shaft, the greater trochanters projects laterally and posteriorly. On the other hand, the lesser trochanter locates and projects at the inferior end of the crest in a posterior-medical direction. Finally, the shaft of the femur runs to the knee joint. Interesting fact of this shaft is that it convexes slightly anteriorly (Right picture in Figure 2.2.1.1). This convexity enables the femur to bear a greater load than if it were perfectly straight.

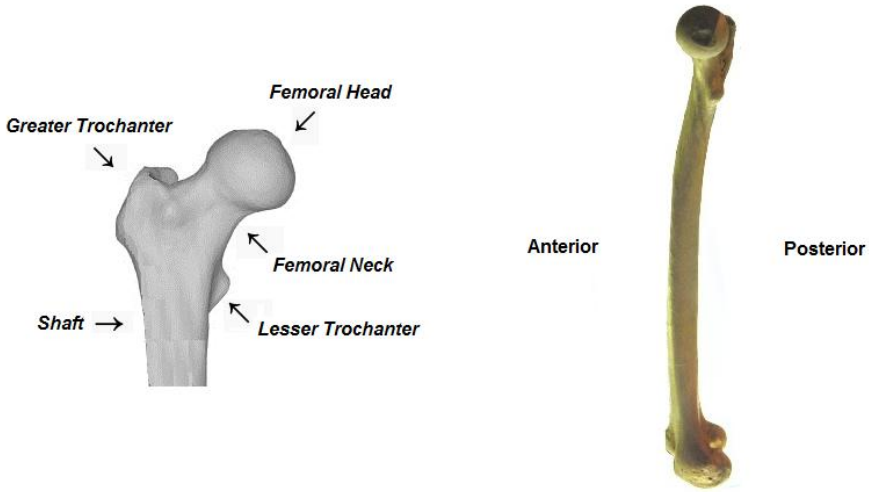

Figure 2.2.1.1. *Front view of the proximal femur (left) and side view of the femur (right) showing the slight convexity anteriorly. Left picture was modified from Cristofolini et al 2007. Right picture was taken at the exhibition of "Who am I" in the Science Museum, London, by the author of this thesis.*

Like any other bone, the femur bone mainly consists of two types of bones: cortical and trabecular bone. Throughout the gait, total of five different kinds of forces are applied on the proximal femur: tension, compression, bending, shear, and torsion forces. Depending on the type of the force, the proximal femur must withstand different kinds of stress. It needs to resist and absorb mechanical energy to stand repetitive stresses from the daily walking. In order to perform these two functions, the cortical bone has an important role at the femoral neck and its entire shaft to resist large shear and torsion forces. (Neumann 2002.) This cortical bone is not uniformly distributed throughout the femoral neck. The thickness of this cortical bone at the superior half of the neck is approximately 0.3 mm while the thickness at the inferior side is 6mm. There are much more trabecular bone at the femoral neck (22.7% as average) opposed to 12.5% of cortical bone. (Bagi et al. 1997.) This three-dimensional lattice network of the trabecular bone plays an important role to absorb mechanical energy. At the femoral neck, trabecular bone is not evenly distributed. They have a tendency to concentrate to the direction of the stress. Depending on the types of stress (compression or tension), the trabecular bone in the proximal femur forms an interesting structure. (Garden 1961; Robling et al. 2006.) Walking results in a large compressive stress at inferior side of the femoral neck. This creates the dense trabecular bands (shown as the blue line in Figure 2.2.1.2). While the superior side of the femoral neck is subjected to the tensile stress in walking, this leads to another dense trabecular band (shown as the red line in Figure 2.2.1.2). (Robling et al. 2006.)

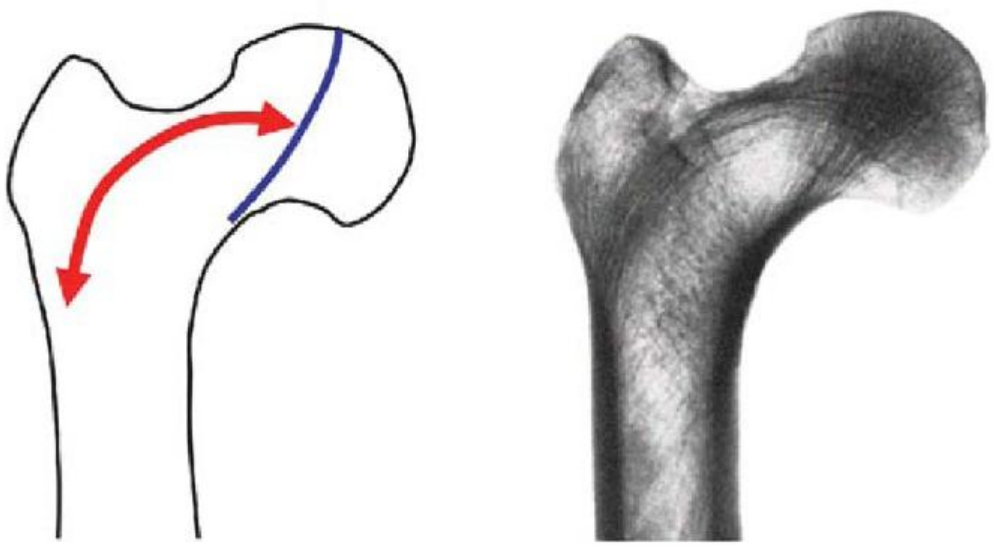

Figure 2.2.1.2. *Trabecular bone orientation in the femoral neck. Left picture shows the brief scheme of two dense trabecular bands: compressive band (blue) and tensile band (red). Right picture shows the X-tray image of the proximal femur, which shows the obvious dense trabecular structure in correspondence to the red and blue lines in the left picture. Figure was adapted from Robling et al 2006.*

2.2.2. Hip Fracture and Fracture Types

Hip fractures are defined as bone fractures at anywhere from the articular cartilage of the hip joint to 5cm below the distal point of the lesser trochanter (Abrahamsen et al. 2009). The hip fractures are more common in women over 50 years old and is known that it can result in high mortality and morbidity rates (Neumann 2002; Johnell & Kanis 2004; 2006). More details of the hip fracture such as the number of annual incidence, estimated increases of the fracture, medical cost and more will be discussed later in the subchapter 2.2.5 called "*Socio-Economic Impact of Hip Fracture*" in this thesis.

Hip fractures can be mainly categorized into two types based on the anatomical locations: femoral neck fractures and intertrochanteric fractures as shown in Figure 2.2.2.1. The intertrochantric fractures occur between the greater trochanter and the lesser trochanter. On the other hand, as name suggests, the femoral neck fractures take place at the femoral neck region proximal to the intertrochanteric fractures. Not only the location of the fracture differs, but also the etiology of each fracture type varies. It was found by several investigators that women with the intertrochanteric fractures have significantly lower BMD, indicating the osteoporosis, than those with the femoral neck fractures (Vega et al. 1991; Nakamura et al. 1992; Greenspan et al. 1994b). These women have low BMD especially due to large trabecular bone loss. On the other hand, the femoral neck fracture does not directly attribute to the bone loss and low BMD. (Mautalen et al. 1996.)

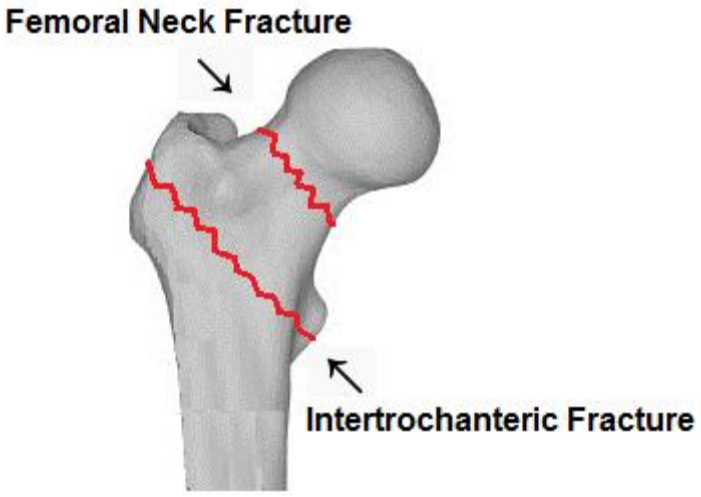

Figure 2.2.2.1. *Two major hip fracture types: femoral neck fracture and intertrochanteric fracture. Figure was modified from Cristofolini et al 2007.*

2.2.3. Fracture Mechanism

There are two major factors associated with the high incident rate of the hip fracture in the elderly: age-related osteoporosis and the falling (Neumann, 2002). According to Kannus et al. (2005), these two factors can cause the hip fracture alone or in combination. However, falling is much stronger single risk factor of hip fracture than any other.

Low BMD due to the osteoporosis is just a predominant risk factor, which leads to the bone fragility (Silva, 2007). Importantly, falling has caused the most of the hip fractures, and it was reported that over 90% of the hip fractures in elderly are caused by the fall (Hayes et al. 1996; Parkkari et al. 1999; Cumming et al. 2002). Due to this, Kannus et al. (2005) even suggested that the hip fractures in elder should be called *fall-induced high-impact injuries* instead of *osteoporotic hip fracture*. Indeed, while the fracture risk is increased by the factor of 2 to 2.5 if the BMD decreases by a one standard deviation, it is increased by the factor of 3 to 5 if elderly falls laterally. What is more, if the greater trochanter received the high impact from the lateral fall, the risk can be increased about 30 times. (Robinovitch et al. 2003; Järvinen et al. 2008.) Several age-related risk factors are increasing the likelihood of falling: neuromuscular and musculoskeletal impairments, balance impairment, impaired vision, cognitive impairment, decline in visual perception and proprioception, and impaired sensory function (Grisso et al. 1991; Silva 2007; Marks 2010.) It is important to understand the mechanism of fall-induced hip fracture to realize why it causes the most of the hip fractures.

It has been well investigated that the lateral or posterolateral aspect of the greater trocahnter receives high-impact force during the lateral fall. Often, the impact force applied on the greater trochanter is sufficient enough to cause hip fracture in the elderly. (Nankaku et al. 2005.) Sevaral researchers have investigated the fracture load using the cadaveric femoral bones and found that 2,000-4,000 N is large enough to cause hip fracture (Lotz & Hayes, 1990b; Courney et al. 1995; Okuizumi et al. 1998). In the study of Nankaku and his colleagues (2005), the subjects actually performed the actual lateral fall and landed on the ground with their greater trochanters. It was reported the measured ground reaction force (impact force) was large enough (over 2000N) to cause hip fracture in the elderly even though they landed on the 13cm thick mattress.

In the normal walking, inferior part of the femoral neck receives high compressive stresses while smaller tensile stresses occur at the superior part of the neck as introduced earlier. Conversely, during the lateral fall, the superior part of the neck receives much higher compressive stress while the lower tensile stresses are applied at the inferior part as shown in Figure 2.2.3.1. In the normal walking, the loading on the superior region is very light. (Lotz et al. 1995; Mayhew et al. 2005; de Bakker et al. 2009.) The peak magnitude of the stress during the lateral fall is approximately 4 times greater than that in normal gait (Lotz et al. 1995.) Due to this high compressive stresses at the superior part of the femoral neck, it has been suggested that the fracture initiates from this region (Carpenter et al. 2005; Mayhew et al. 2005). This has also been demonstrated by the finite element (FE) modeling study by Verhulp et al (2008). According to de Bakker et al. (2009), two steps are involved in the fracture; thus called *two-steps failure*. (Mayhew et al. 2005; de Bakker et al. 2009).

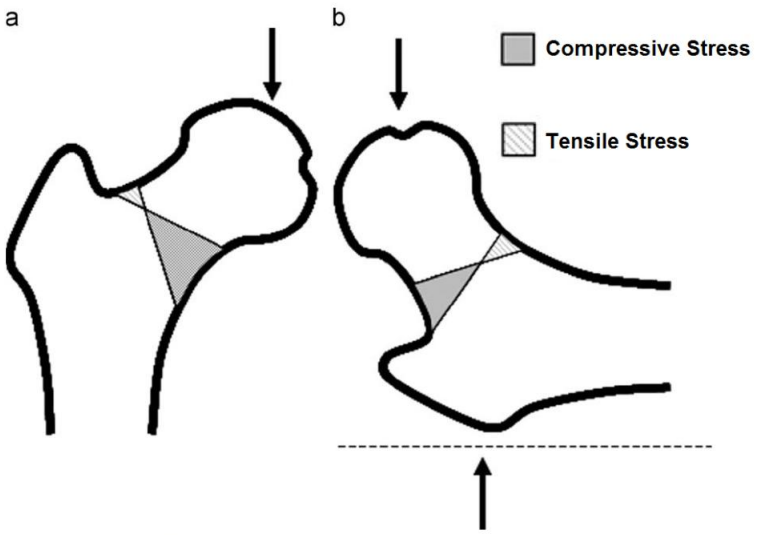

Figure 2.2.3.1. *Stress distribution of the proximal femur between the normal gait (left) and the lateral fall (right). Arrows indicate the impact forces acting on the proximal femur. Figure was modified from de Bakker et al. 2009.*

In the two-step failure, the crack initiates from the superior surface primarily due to high compressive stress. If the energy from the lateral fall is sufficient enough to drive the crack across the half the width of the femoral neck, the bending resistance measured as section modulus *Z* of the unfractured parts of the neck including the inferior part get reduced. This is due to that the bending resistance depends on the third power of the width. Then, the tensile stress in the inferior part of the neck is sufficient enough to initiate the 2nd crack from the inferior part of the femoral neck or medial intertrochanteric region. Importantly, this two-step failure was also seen both in intertrochanteric fracture. This suggests that the entire superior surface has higher risk of initiation of cracks than the inferior surface. (Mayhew et al. 2005; de Bakker et al. 2009.)

In the mechanical engineering perspective, two modes of failure are suspected as the responsible mechanism in this two-steps failure: 1) material or yield failure due to compression or tension, or 2) structural failure due to local buckling caused by compression. In the material or yield failure mode, shear failure takes place due to the accommodated stress or strain. In fact, the compressive failure is always induced by shear stress. On the other hand, in the structural failure mode, local buckling caused by the compressive stress is responsible for fracture in the superior cortical wall. It is well known that, under the high compressive stress, the buckling is the failure mechanism for thin-walled structure. (Mayhew et al. 2005; de Bakker et al. 2009.)

2.2.4. Importance of Exercise-Induced Bone Structural Change

Loading characteristics on the femoral neck changes as people age and plays an important role to increase the bone fragility. The amount of physical activity gets reduced while people age, and mechanical loading applied on the femoral neck is coming more solely from the daily walking. As mentioned earlier, the more mechanical load is ap-

plied on the inferior part of the neck while less mechanical load is applied on the superior part in the normal walking. This unbalanced loading causes asymmetric structure of the femoral neck; thicker inferior and thinner superior cortical walls in the femoral neck. The superior cortex loses ability to resist crushing in compression or in local buckling due to increased elastic instability. When the long bone is under bending stress, the fracture often occurs in the cortex under tension. However, if the cortical wall is thin enough, elastic instability increases and ends up with fracturing through local buckling due to compressing the cortex. The diameter of the femoral neck slowly enlarges with age. It is known that bone's resistance to bending measured as the section modulus, *Z*, is maintained by both BMD and the diameter of bone. The decrease in BMD has a negative effect on Z while the increase in diameter has a positive effect. The BMD can decrease due to the age-related osteoporosis while the femoral neck diameter increases with age. This combination can maintain the bending resistance Z. Beck et al. (2000) studied hip scan images obtained by DXA of U.S. adults aged from 20 through 99 years old, which data were acquired in the Third National Health and Nutrition Examination Survey (NHANES III). In this study, it was well reported that the section modulus was maintained by increase in the diameter of the femoral neck although BMD decreased. However, the cortical thinning can weaken the femoral neck strength alone, which can lead to the buckling alone. Normal walking has a beneficial effect on strengthening the inferior part of the femoral neck. In order to maintain balanced strength of the femoral neck, it is also necessary for the elderly to do specific exercises which can load the superior part of the femoral neck to avoid excessive thinning of the superior cortex. (Mayhew et al. 2005.) As mentioned earlier, exercises involving the O-I loading such as tennis, squash, and football/soccer may thicken the cortex at the superior region of the femoral neck in young female (Nikander et al. 2009). Therefore, this O-I loading exercise may have an important key to decrease the hip fracture risk. However, the question is if the thickened superior cortex can be sustained throughout the aging.

Several studies approached to answer this question. First, it was found that increase in the exercise-induced bone quantity during the years of skeletal development do not persist into adulthood throughout human and also experimental studies of rats (Pajamäki et al. 2003; Warden et al. 2005). Second, maintenance of the exercise-induced structural change of bone during growth is controversial. Pajamäki et al. (2003) and Järvinen et al. (2003) reported that the exercise-induced structural improvement such as increase in total cross sectional area (CSA) in the femoral neck were not maintained after a certain period of disuse throughout their experimental study. From their results, they suggested that continuation of the exercise is essential to maintain the positive effect of bone from youth exercise to adulthood. On the other hand, Warden et al. (2007) reported the contrasting result to those studies above. They found that exercise-induced bone structural improvement such as increase in the cortical area and increase in the minimum second moment of area (I_{MIN}) of rats' ulnas during growth were maintained after detraining phase. This finding indicates that bone strength due to the structural improvement can

be maintained even after detraining, which detraining means reducing the amount of physical activity in adulthood. There are some possible explanations of the controversial findings of these studies above. Anatomical locations (ulna versus femoral neck), gender (female versus male rats), mode of exercise (axial compression loading versus treadmill running) differed between the studies of Pajamäki et al. (2003) and Järvinen et al. (2003), and the study of Warden et al. (2007). Furthermore, Pajamäki et al. (2003) and Järvinen et al. (2003) compared the parameters between animals while Warden et al. (2007) compared the parameters within the same animal. These factors might have affected the results between those studies. Regardless of the results from studies above, the further studies are necessary to conclude if the exercise-induced change in bone structure from growth persists into the adulthood. If so, the studies should also focus on finding how much amount of exercise is needed to maintain the benefits of the exercise-induced gain after growth phase. (Pajamäki et al. 2003.) Depending on the answer of this, the possible positive effect of the O-I loading exercise during growth has more clinical significant importance.

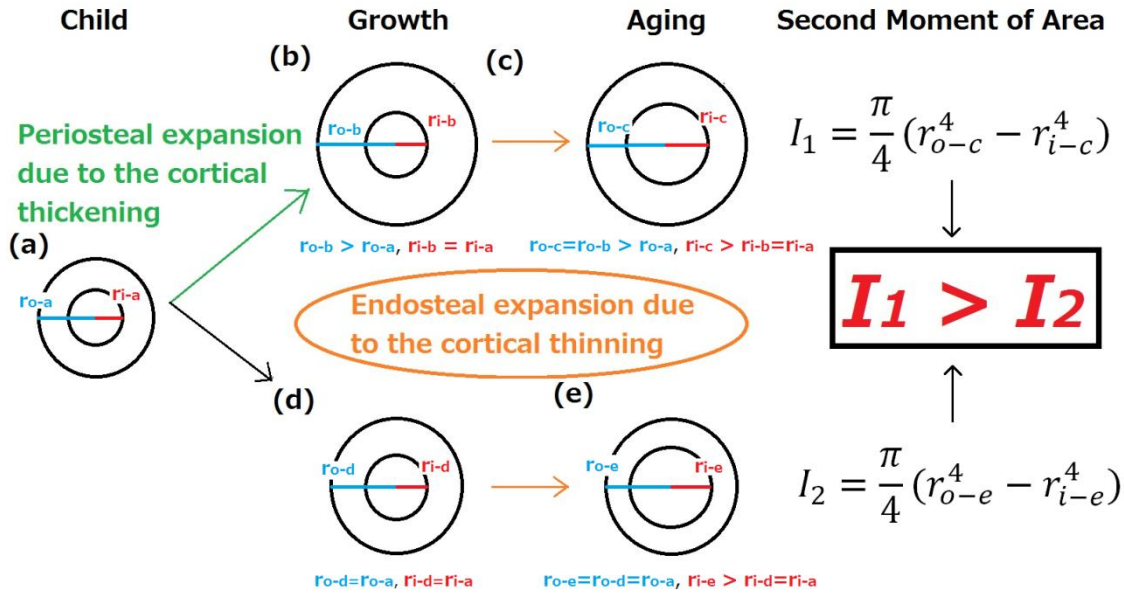

Figure 2.2.4.1. *Contribution of bone growth to the second moment of area of bone.*

The exercise-induced change in the bone structure during growth occurs through new bone formations below the periosteal surface while the age-related bone loss is mainly due to the bone loss on the endocortical surface as discussed previously. This points out that the amounts of new bone formation induced by exercise during growth plays an important role in terms of bone strength later in adulthood such as over 50 years old. (Warden et al. 2007.) This periosteal expansion during growth and endosteal expansion during adult plays important role to increase the second moment of area of bone, which ultimately contributes to increase bone strength to bending (See the subchapter 2.1.4). Figure 2.2.4.1 demonstrates this mechanism. Impact loading exercises during growth increases outer radius ($r_{o\text{-}a} \rightarrow r_{o\text{-}b}$) of the bone due to the periosteal ex-

pansion ((a) → (b)). However, if much less or none impact loading is done during growth, exercise-induced periosteal expansion is less ((a) → (d)). Inner radius gets increased slightly due to endosteal expansion ($r_{i\text{-}b/d} \rightarrow r_{i\text{-}c/e}$) ((b) → (c), (d) → (e)). Increase in the outer radius contributes to increase the second moment of area while slight increase in the inner radius works conversely. Therefore, the second moment area with the impact exercise during growth (I_1) is greater than the one without the impact exercise (I_2).

2.2.5. Socio-Economic Impact of Hip Fracture

Hip fracture causes major health care problems and leads to high rate of morbidity and even mortality in the elderly people. The number of annual incident of hip fracture in worldwide was increased from 1.3 million in 1990 to 1.6 million in 2000 (Johnell & Kanis 2004; 2006). There are over 340,000 (Kim et al. 2011), 120,000 (Yoshimura et al. 2005), 25,000 (Leslie et al. 2009), and 7,000 (Lönnroos et al. 2010) hip fractures reported annually in the United States, Japan, Canada, and Finland respectively. It is estimated that the annual incidents of the hip fracture in the world will increase to 2.6 million by 2025 and to 4.5 million by 2050 (Gullberg et al. 1997). In another study, Cooper et al. (1992) estimated that it may increase even up to 6.26 million by 2050.

Most of the hip fractures occur to the people who are over 50 years old with low BMD. It was reported that the peak number of the hip fracture occurs at age between 75 and 79 years old both in men and women. (Johnell & Kanis 2006.) The number of people who are older than 65 years old will increase to 133 million in Europe and 894 millioin in Asia by 2050. This large increase of the elderly population explains the drastic increase of the hip fracture by 2050. (Cooper et al. 1992; Cummings & Melton III 2002.) After the fracture, the patients have a high morbidity and lower their quality of life due to disability to walk. It was reported that only half of the hip fracture patients regained their pre-fracture mobility and independence (Sernbo & Johnell 1993). In the United States, it was estimated that about 10% of total hip fracture female patients remain to be disable to walk, and 19% of them require institutionalization, which account for almost 140,000 nursing home admissions annually (Poór et al. 1995; Ray et al. 1997). In addition, the high mortality rate has been reported in many studies. Approximately, 17 to 32% of hip fracture patients die within one year after the hip fracture incident (Kanis et al. 2003). Poór et al. (1995) reported in their study that the mortality rate was even 36% during the first year post-fracture in the United States. This high mortality rate is partially due to comorbidity. According to the recent study of Korhonen et al. (2013b), in 2009 in Finland, fall-induced death rate over 50 years old were 57.3% and 35.3% in men and women respectively and approximately 1000 people who were over 50 years old died due to the fall induced cases. Hip fracture patients usually have more other diseases than the general population. Moreover, it was estimated that only one forth of deaths after hip fracture were caused by the hip fracture itself. (Johnnell & Kanis 2005; Kanis et al. 2003.)

Hip fractures are not just disabling events for the elderly, but also leading to financial burdens for societies worldwide. The worldwide cost for the hip fracture is estimated to be US $34.8 billion in 1990 and to reach $131.5 billion in 2050. Cost for the immediate hospital care and total cost for the first year per patient are US $7,000 and $21,000 respectively. (Johnell 1997.) The mean total hospital expenditure per patient in different countries are, for example, £12,000 in United Kingdom (Lawrence et al. 2005), $20,000 in Japan (Kondo et al. 2009), €9,200 in Ireland (Azhar et al. 2008), €10,700 in Belgium (Haentjens et al. 2001). Khasaraghi et al. (2003) also reported that if the hip fracture patient has one medical complication, additional of approximately $6,000 can be added.

2.2.6. Hip Fracture Risk Assessment Methods

The current major hip fracture risk assessment method is to check for osteoporosis by measuring the BMD and then to provide these osteoporotic patients anti-bone resorptive drugs to maintain or increase the BMD as the preventive treatment. This BMD measurement is the standard diagnosis for osteoporosis and usually performed by dual-energy x-ray absorptiometry (DXA) (Unnanuntana et al. 2010; Baim & Leslie 2012). There are a number of advantages of the DXA: short examination times, and low radiation dose. Most importantly, the DXA is the non-invasive measurement available to evaluate osteopororis. (Kontulainen et al. 2002.) The BMD measured by the DXA is expressed as grams of mineral per square centimeter scanned (g/cm^2). When the patient's BMD value is diagnosed, it is usually compared with a reference value for young normal adults of the same sex using the special index called T-score. The T-score is the number of standard deviations showing how far the patient's BMD value is deviated compared with the BMD of a healthy 30 years old adult. According to the World Health Organization (WHO), T-score -2.5 is considered as threshold for the osteoporosis. (Unnanuntana et al. 2010.) To assess osteoporosis, the DXA-based BMD can be measured at several anatomical locations: lumbar spine, femoral neck, total hip, or radius (Baim & Leslie 2012).

It has been identified that not only low BMD is the risk factor for the bone fracture, but also there a number of other factors exist: age, history of maternal hip fracture, low body weight, height, poor health, previous hyperthyroidism, poor depth perception, tachycardia, previous bone fracture history, and benzodiazepine use. Recently, in order to include other risk factors in the assessment, the WHO developed the systematic assessment, the Fractrure Risk Assessment Tool, abbreviated as FRAX™. (Kanis et al. 2008; Unnanuntana et al. 2010.) FRAX can calculate the age-specific 10-year probability of 1) hip fractures and 2) major osteoporotic fractures (hip, spine, humerus, and foream) based on femoral neck BMD and clinical risk factors. Clinical factors included in FRAX calculation are age, sex, race, height, weight, body mass index, a history of fragility fracture, a parental history of hip fracture, use of oral glucocorticoids, rheumatoid arthritis, current tobacco smoking, excessive alcohol consumption, and other secondary etiologies for osteoporosis (Unnanuntana et al. 2010; Baim & Leslie 2012). FRAX can

be used without including BMD although of course FRAX with BMD gives much better prediction (Baim & Leslie 2012). According to several recommendations, treatments should be made for those who have a 10-year risk of hip fracture of ≥ 3% or a 10-year risk of major osteoporotic fractures of ≥ 20% from FRAX calculations (Unnanuntana et al. 2010).

The DXA-based BMD has a drawback although it has been used as the strong fracture risk indicator. The major problem is that the bone densitometry with DXA does not give reliable estimate of the true BMD value. Due to the DXA's planar scanning and the violation of the two-component DXA limitation, it can underestimate or overestimate the BMD by 20-50% (Bolotin & Sievänen, 2001; Bolotin 2007). This can mean that T-score of – 1.5 may have true value between 0 and – 3.0. Thus, the patient with T-score -1.5 can be diagnosed as osteoporosis if the true value lies on T-score -3.0 or normal if it lies on T-score 0. Therefore, this unreliable accuracy of the DXA obviously shows that the DXA-based BMD is a poor predictor for the bone fractures. Furthermore, an error in the measurement can vary between 6 and 15% if different scanners are used. (Järvinen et al. 2008.) In fact, over 80% of fractures happen to those who have T-score of ≥ -2.5, which means they do not have osteoporosis (Järvinen et al. 1999, 2005; Sievänen 2000; Stone et al. 2003; Siris et al. 2004; Unnanuntana et al. 2010). This does not mean the low BMD is not the risk factor for the bone fractures. The low BMD of course still increases the likelihood of the fracture.

The mechanical integrity of bone is determined by the interaction of both intrinsic material property such as the apparent density and the structural properties of bone such as size and shape of bone. The maximum stress the bone can bear measured as the ultimate strength is bone's intrinsic material property. On the other hand, fracture loads depend on the structure of bone. To evaluate the structure of bone, medical imaging methods such as the DXA and a peripheral quantitative computed tomography (pQCT) can be used. (Kontulainen et al. 2002; Warden et al. 2005.) As mentioned before, most of the hip fractures in the elderly are caused by the lateral fall (Hayes et al. 1996, Cumming et al. 2002). Therefore, non-skeletal and mechanical factors such as liability to fall, magnitude and direction of impact force should also be considered when the hip fracture risk is assessed. Each of these bone's material and structural properties, and non-skeletal and mechanical factors should not be assessed separately. Instead, there is a need for another method which can integrate all of these factors into single method in order to evaluate hip fracture risk more comprehensively. Finite element (FE) method has been studied for last two decades to develop it as more accurate hip fracture assessment tool. It was focused to study the structural analysis of the hip fracture both in the lateral fall hip fracture and atraumatic/single leg stance hip fractures. (Bessho et al. 2007.)

2.3. Finite Element Method

2.3.1. Principle of Finite Element Method

The *finite element* (FE) method is a universal and powerful numerical method to solve algebraic, differential, and integral equations. It was developed to solve the real world problem which involves complicated physics, geometry, and/or boundary conditions. In the mechanical engineering, the FE method allows non-destructive assessment of the material or structure in order to evaluate their mechanical behavior under the certain loading condition. Therefore, the FE method has the significant meaning in the field of bone biomechanics. With the FE method, it became possible to simulate/predict the hip fracture risk under such a dangerous event like the lateral fall. Experimental testing of such an event is possible only using the cadaveric bone, not a living human bone. (Reddy 2006.)

In the FE method, a given domain such as the entire proximal femur bone in this thesis is constructed by a collection of subdomains called *finite elements*. The process of this dividing the main domain into these finite elements is called *meshing* and each element consists of two components; *node* and *edge*. Figure 2.3.1.1 explains this meshing the domain (*a* to *b*) and each component of the element (*c* in the figure).

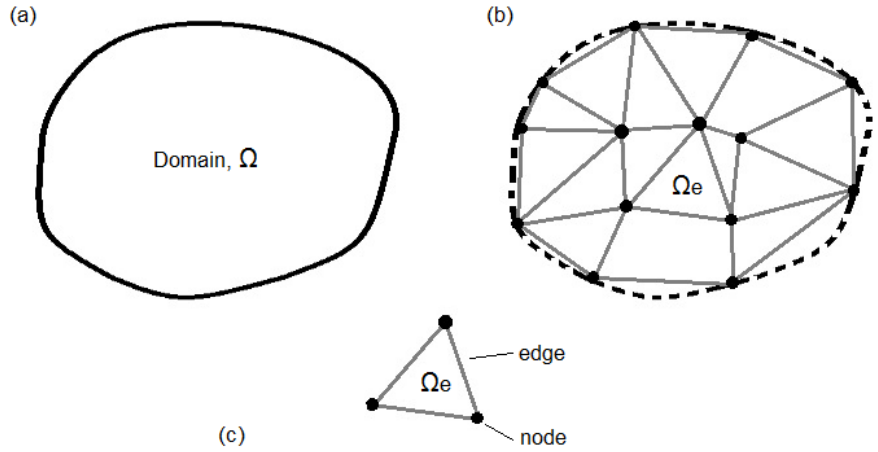

Figure 2.3.1.1. *Domain, meshing process, and finite element. Figure was obtained and modified from (Reddy 2006).*

To create the FE models of the bone, there are three required components: 1) geometry, 2) material properties, and 3) loading/boundary condition. First, this geometry can be obtained by medical imaging techniques such as the computed tomography (CT) and MRI methods. Second, the material properties of bone need to be applied to the given geometry. Since the bone contains two domains: the cortical and trabecular bone domain, the material properties of each domain need to be obtained and applied. These properties can be obtained from the literature review of the previous studies and are summarized in the subchapter 2.1.2. In this thesis, the bone was modeled as a linear elastic, isotropic and homogeneous material. For such a material, two material proper-

ties need to be specified for each domain: Young's modulus and Poisson's ratio. Lastly, the loading/boundary condition needs to be specified to simulate the lateral fall condition. To do so, two parameters need to be specified to boundaries of the domain: magnitude of the force and force direction. For next six subchapters, following contents of the FE method for the hip fracture study will be introduced: history of the development of the FE method, material property assigning techniques (homogeneous versus inhomogeneous technique and isotropic versus anisotropic method), lateral fall condition, impact force estimation technique, and the advanced FE modeling studies

2.3.2. History of Finite Element Modeling in Hip Fracture Study

Structural analysis of the proximal femur utilizing the FE method has been considered as a better assessment method to predict the hip fracture risk. (Lotz et al. 1991b; Keyak et al. 1998; Bessho et al. 2007). The FE modeling has a high potential to provide us more precise assessment due to its ability to integrate complex geometry/structure, material properties, and loading conditions. In fact, Cody and his colleagues (1999) compared the ability of hip fracture load prediction between the DXA, and the FE methods. They reported that FE modeling can explain at least 20% more accurate to predict the hip fracture load then the DXA can. Because of a number of advantages of the FE modeling, studies with the FE modeling have been performed for last two decades.

In the early 1990s, Keyak and his colleagues first introduced their subject-specific and automated CT-image based FE modeling of the proximal femur in series of three studies (Keyak et al. 1990, 1993; Keyak and Skinner 1992). The bone was modeled as the linear elastic, isotropic and inhomogeneous material in their studies. This inhomogeneous material mapping method became possible by obtaining the density value for each element from CT data, and utilizing the relationship between the density and the Young's modulus. The accuracy of their FE models was validated by comparing them with the mechanical testing of the cadaveric bones. This method enables one to estimate mechanical behavior such as stress, strain, and strain energy in the human proximal femur in vivo. However, only single-leg stance loading condition was modelled in their first three studies. (Keyak et al. 1990. 1993; Keyak and Skinner 1992.) The lateral falling condition in the FE method was first introduced by Lotz et al (1991b).

From the late 1990s to the early 2000s, Keyak and his colleagues studied if their method can precisely predict femoral fracture load, location, and types in both single-leg stance and lateral falling loading conditions in order to improve their method as clinically useful hip fracture risk assessment tool. Results from these studies showed that their method can estimate fracture load even slightly better than the densitometry (BMD measurement by DXA) and predict the fracture location and type with the accuracy of 70% in spite of the types of loading conditions. (Keyak et al. 1998, 2001a.) Furthermore, they reported that the lateral falling in which the impact force is applied on posterolateral aspect of the greater trochanter leads to the highest risk of fracture in the any falling loading conditions (Keyak et al. 2001b). Lately, they applied their FE method to

investigate the gender difference in proximal femoral strength and reported that women have higher risk of hip fracture when they fall laterally (Keyak et al. 2011).

It is noteworthy to mention two studies of Bessho et al. (2007, 2009) because their FE method is most likely the most sophisticated and accurate method today. Like any other CT-image based FE modeling studies, their proximal femur was modeled as the elastic isotropic inhomogeneous material. What differed from previous FE modeling studies were that their model was solved nonlinearly using Newton-Raphson method and two different element types were adopted. Tetrahedral element for the trabecular bone and the inner cortex, and 0.4mm thickness of triangular shell element for the outer cortex were used. Figure 2.3.2.1 illustrates these two elements shapes. In Keyak's studies and Lotz's studies, cubic and isoparametric solid elements were adopted respectively (Keyak et al. 1990. 1993; Lotz et al. 1991b; Keyak and Skinner 1992). FE models from Bessho et al. (2007, 2009) were also validated with the mechanical testing of the cadaveric bone. Most importantly, they reported the highest correlation between FE predicted values and measured values among any other proximal femur FE modeling studies, which correlation coefficient were r = 0.941, 0.979, 0.963 for yield loads, fracture loads, and principal strain respectively. This showed that their method has the most accurate prediction. (Lotz et al. 1991b, 1991b; Lengsfeld 1998; Cody et al. 1999; Ota et al. 1999; Keyak et al. 1990, 1993, 1998, 2001a, 2001b.)

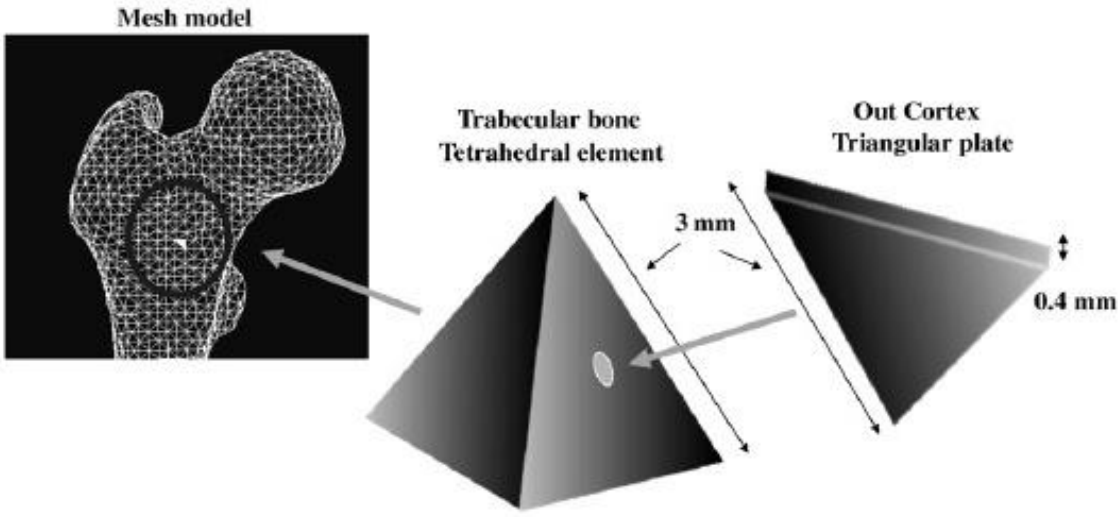

Figure 2.3.2.1. *Two different finite elements in Bessho's method. Figure was modified from de Bessho et al. 2007.*

In their second study (Bessho et al. 2009) like Keyak and his colleagues' study (2001b), they also investigated if their method can predict fracture load and site on the proximal femur precisely in five different loading conditions shown in Figure 2.3.2.2 (1 single-leg stance and 4 different lateral falling conditions). They employed data from 42 cadaveric female subjects (mean age, 82.4 years old) with previous hip fracture. The CT image data was obtained from the side of the proximal femur, which did not have

fracture, to construct the geometry of their FE models. Fracture loads and fracture sites were estimated by their FE models.

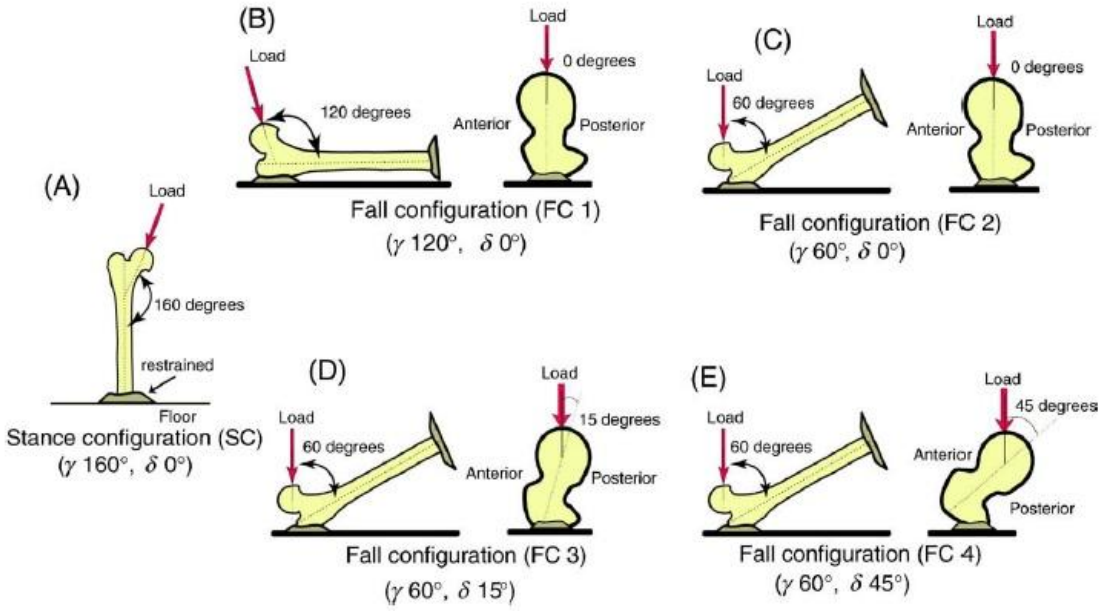

Figure 2.3.2.2. *Five different loading condition in Bessho et al. (2009): 1 single-leg stance, and 4 lateral falling conditions (FC). Force direction was altered by modifying two angles: γ and δ. The angle γ was defined as the angle between force direction and the long axis of the femur in the frontal plane. The angle δ was between force direction and femoral neck axis in the horizontal plane. Figure was adopted from Bessho et al. 2009.*

Two findings from this study are highly important. First, they found the likelihood of the hip fracture increases if people fall in the posterolateral direction. Secondly, in the falling configuration 1 (FC1 in Figure 2.3.2.2), a significant correlation was reported between real fracture type and predicted fracture type. In detail, 16 neck fractures were predicted by the FE method for the actual 20 femoral neck fractures while 18 trochanteric fractures were predicted for the actual 22 trochanteric fractures. Most importantly, this FC1 fall condition had the most neck fractures among others. Due to this high correlation between estimated and actual fractures, the lateral falling configuration FC1 in Figure 2.3.2.2 was also adopted in this thesis. Also because the aim of this thesis was to investigate the structural advantage of the femoral neck built through the history of the specific impact loading exercises, FC1 condition suits to study the aim of this thesis.

2.3.3. Inhomogeneous versus homogeneous material properties assignment techniques

There are two ways to assign material property such as Young's modulus into the geometry: homogeneously or inhomogeneously. Assigning homogeneous material property is an easier way and requires less computational power and time. However, it is unrea-

listic and can reduce the accuracy of the FE models if the material is indeed inhomogeneous material like bone, as evinced by ununiformly distributed apparent density. For the homogeneous material, two fixed value of Young's moduli are assigned into entire cortical and trabecular geometries. Modulus value can be obtained from previous studies in which mechanical testings were performed to measure the material properties (Reilly et al., 1974; Burstein et al. 1976; Carter & Hayes 1977; Goldstein 1987; Morgan et al. 2003; Bayraktar et al. 2004). The material properties of bone are summarized in Table 2.1.2.1. For example, in the previous FE modeling studies, Young's moduli of 15GPa, 17GPa, 19.3GPa or 20GPa, and 590 MPa, 1500MPa, or 2000MPa were assigned into the cortical and trabecular bone geometries respectively (Duda et al. 1998; Lengsfeld et al. 1998; Polgár et al. 2003a, 2003b; Taddei et al. 2006). This homogeneous material property assigning method is also called two-material model (Taddei et al. 2006). This method is typically used when the geometry is not obtained from the CT image. In this study, this two-material method was also used since the geometry was obtained from the MRI data.

Inhomogeneous material property assigning became possible and was first introduced by Keyak et al. (1990). In this method, each element in the FE model has own value of the Young's modulus. Because the density varies depending on the anatomical location, this inhomogeneous material property assigning is more realistic than homogeneous method. Due to this, this method has been used in many FE modeling-based proximal femur studies (Keyak et al. 1990, 1992, 1993, 1998, 2000, 2001a, 2001b, 2011; Lotz et al. 1991b, 1991c; Ota et al. 1999; Bitsakos et al. 2005; Taddei et al. 2006; Bessho et al. 2007, 2009). Using the linear relationship between Hounsfield unit values from the CT scan data and the bone apparent density, and the empirical relationship between the density and the Young's modulus, each finite element's modulus can be calculated. This empirical relationship (mathematical equations) is summarized in Table 2.1.2.2. Although predicted results from the FE models with this inhomogeneous material mapping method is more realistic and accurate, it requires larger computational efforts and time. Taddei et al. (2006) compared the FE models of the femur with this inhomogeneous material assigning method with the one with two-material method (homogeneous method). It was reported that the correlation with the predicted fracture load value from the FE models with inhomogeneous method (coefficient $r = 0.95$) was slightly better than the one with the two material method (homogeneous method) (coefficient $r = 0.94$). They concluded that the two-material method is still acceptable although the inhomogeneous method is slightly better. This validates that using two-material method in this thesis is rational.

2.3.4. Isotropic versus anisotropic material assignment techniques

Bone behaves mechanically differently depending on the direction of force and is mechanically anisotropic. However, in the all of previous FE modeling studies mentioned so far, their models were constructed as an isotropic material. This is because there is not enough mechanical properties information available as a function of the anisotropic

load directions. Therefore, further experimental studies are necessary in order to obtain sufficient mechanical property information for the development of the anisotropic FE models (Wirtz et al. 2000). Anisotropic material can often be approximated as *orthotropic* material. For orthotropic material, the mechanical properties vary in three orthogonal directions. (Nigg & Herzog 1999.) Briefly, in order to construct the anisotropic/orthotropic FE model, the material properties calculated by the bone apparent density and the direction of the orthotropic axes are required. Necessary mechanical properties to each element in the anisotropic FE model are the Young's modulus, tensile, compressive and torsional strengths, Poisson's ratio, and the shear modulus. These material properties can be derived from the CT data while the directions can be derived from the spatial orientation of trabeculae and the Haversian systems of the cortex. (Wirtz et al. 2000.) Despite this lack of the mechanical property information, Wirtz and his colleagues (2003) developed the first conceptional anisotropic FE models of the proximal femur. They obtained the geometry from the CT data and determined the direction of orthotropic axes based on the images of trabecular structure and Harvesian system. Although their method seems feasible, they concluded that further optimization is necessary before using in clinical and research areas. Therefore, the bone was also modeled as the isotropic material in this thesis. In this case, Young's moduli and Poisson's ratios for the cortical and trabecular bone domains are required.

2.3.5. Lateral Fall Loading/Boundary Condition

Effect of the lateral falling on the hip fracture has not only been studied by the FE model-based studies, but also been investigated through the experimental studies. The fracture loads obtained from the experimental studies are often useful to compare the predicted fracture load from the FE model studies.

Pinilla et al. (1996) measured fracture loads using the cadaveric proximal femur bones experimentally. Each cadaveric bone was tested in one of three lateral falling conditions: loading angle varies from 0°, 15°, to 30° in respect to the femoral neck axis in transverse plane while an angle between the horizontal and the axis of the femoral shaft in the frontal plane is fixed to 10° for all three conditions. These three conditions are shown in Figure 2.3.5.1. They found that the fracture load in the lateral falling decrease by 24% if the loading angle in the transverse plane increases from 0° to 30°. Courtney et al. (1995) also conducted similar experimental lateral falling study using the cadaveric femur bones from both older (mean age of 74 years old) and younger (mean age of 33 years old) individuals. Also, the specimens were tested only in the second loading condition of Pinilla et al. (1996). According to the comparison of the results between the young and old specimens, they concluded that the proximal femur bones from older adults were almost half weaker than those from the younger adults. (Courtney et al. 1995.)

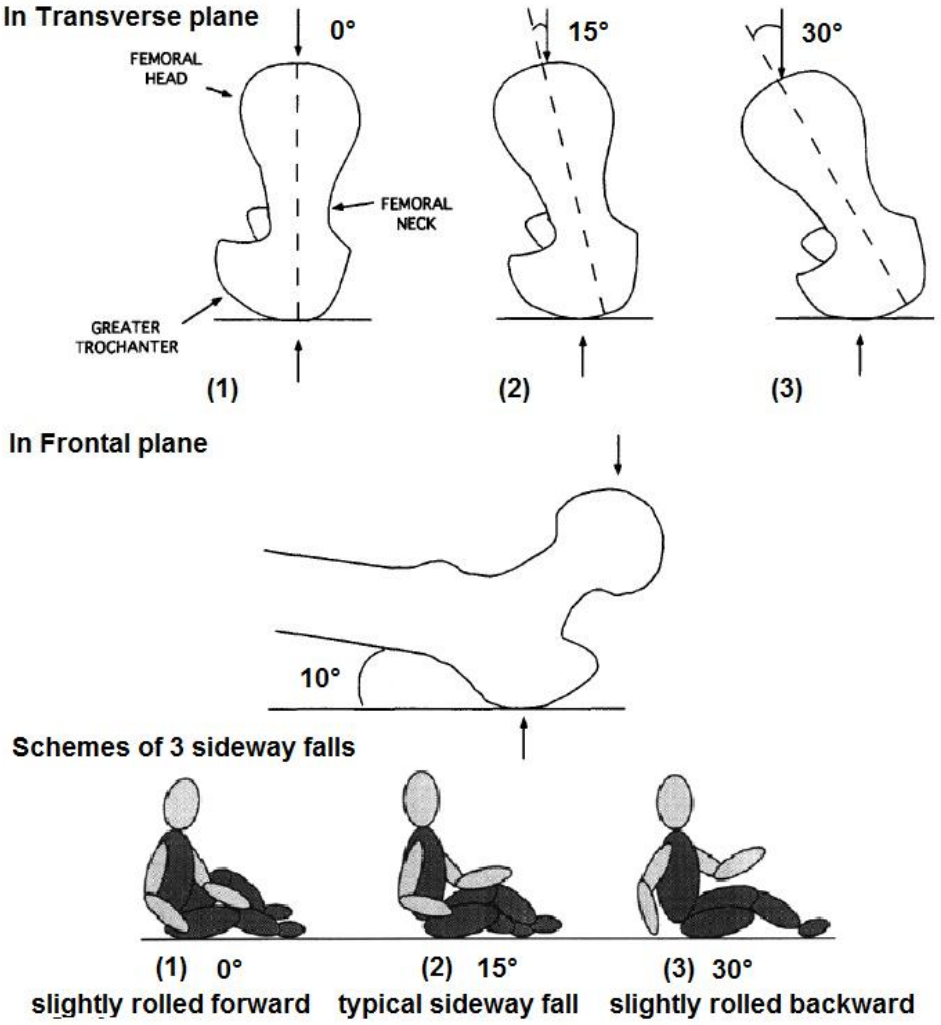

Figure 2.3.5.1. *Three different lateral falling conditions: (1) 0° in the transverse and 10° in the frontal plane, (2) 15° in the transverse and 10° in the frontal plane, and (3) 30° in the transverse and 10° in the frontal plane. Each scheme at the bottom corresponds to three loading conditions at the top. Figure was modified from Pinilla et al. 1996.*

Directions of the applied force in the lateral falls vary from one study to another in both FE modeling and experimental studies. Table 2.3.5.1 shows the summary of the different lateral falling conditions. High correlation was found between the predicted fracture sites from the FE models and the measured fracture site from the experiment in one of the lateral falling conditions (FC1 in Figure 2.3.2.2) of Bessho et al. (2009). Their FE model with this FC1 lateral falling condition could predict the neck fracture most accurately among other lateral falling conditions in their study. Therefore, this lateral falling condition was used in this thesis. Schemes and fracture loads in different studies are shown in Figure 2.3.2.2 and Table 2.3.5.2 respectively. Various loading conditions were tested in Keyak et al. (2001). However, only 4 cadaveric specimens were used to validate the predicted fracture sites in their study while total of 42 cadaveric specimens were used in Bessho et al. (2009).

Table 2.3.5.1 *Summary of the lateral falling conditions in both FE modelling and experimental studies.*

	Lateral Fall Loading Conditions		Type of study
Study	Angle α between the femoral neck axis and the load axis in transverse plane (°)	Angle β between the horizontal and the axis of the femoral shaft in frontal plane (°)	FE modeling or Experimental
Lotz et al. (1991b, 1991c),	30	30	FE modeling and experimental
Keyak et al. (1998, 2011)	20	30	FE modeling and experimental
Keyak et al (2001) *Total of 15 patterns	5, 15, 25, 35, 45	10, 20, 30	FE modeling and experimental
Bessho et al. (2009)	0, 15, 45.	See Figure 2.3.2.2 (B)γ = 120 with δ = 0, (C)γ = 60 with δ = 0, (D)γ = 60 with δ = 15, (E)γ = 60 with δ = 45,	FE modeling and experimental
Courtney et al (1995)	15	10	Experimental
Pinilla et al. (1996) *Shown in Figure 2.3.5.1.	0, 15, 30	10	Experimental

Fracture loads in the lateral falling conditions have been well investigated through both FE model-based and experimental studies. Table 2.3.5.2 shows the summary of the fracture loads from previous studies. Loads ranging from 2900 to 9990 N were also reported as the predicted peak *impact force* on the greater trochanter from the standing height in the lateral falls. Moreover, it was reported that the average of this peak impact force was 4260 N. These predicted peak force values were calculated mathematically using kinetic and kinematics models. (van den Kroonenberg et al. 1995.) In an experimental study conducted by Robinovitch et al. (1995), this predicted peak force ranged from 4050-6420 N. It is noteworthy to mention that the predicted fracture loads from the FE model studies in Table 2.3.5.2 were smaller than those from the experimental studies. This has been thought due to the assumption of isotropic material property in the models (Keyak et al. 2001, 2011; Bessho et al. 2009). Furthermore, the values from younger female cadaveric proximal femurs were larger than others. Therefore, in this thesis, similar loads were calculated and applied on the proximal femurs. More details how the loads were calculated are shown in the next subchapter 2.3.6. What is more, it was found that soft tissues over the hip such as muscles and adipose tissues can absorb the impact force for some degree. 1 mm thickness of this soft tissue can absorb maximum of 71N. (Robinovitch et al. 1991, 1995; Bouxsein et al. 2007.)

Table 2.3.5.2 *Summary of the fracture loads of proximal femurs from both FEmodelling and experimental studies*

Study	Fracture load (N) (mean ± SD)	Test condition
Lotz et al. (1991c)	1560~1780	FE modeling
Keyak et al. (2001)	1121-1797	FE modeling
Keyak et al. (2011)	Male: 276~4257 (average 1692) Female: 314-3071(average1088)	FE modeling
Bessho et al. (2009) *FC1~4 corresponds to those in Figure 2.3.2.2.	2270±600 (FC1) 1060±248 (FC2) 980±229 (FC3) 710±174 (FC4)	FE modeling
Courtney et al. (1995)	3440±1330 (older female) 7200±1090 (younger female)	Experimental
Pinilla et al. (1996)	4050±900 (α=0°) 3820±910 (α=15°) 3060±890 (α=30°)	Experimental

2.3.6. Lateral Fall Impact Force Estimation

The peak impact force applied to the lateral aspect of greater trochanter from the lateral fall can be estimated based on the previous studies describing the kinematics and dynamics of the falls from the standing height (van den Kroonenberg et al. 1995;1996) and impact forces in the falls (Robinovitch et al. 1991).

According to Robinovitch et al. (1991), this peak impact force is determined by the impact velocity of the hip, *V*, and the effective mass, *M*, the soft tissue stiffness, *K*, and damping coefficient of the body, *b*, at the moment of the contact from the lateral fall. They developed an experimental apparatus called the pelvis release-fall experiment to measure the stiffness and damping coefficient. Based on their experiments, they obtained the value of *K* equal to 71 kN/m and the value of *b* equal to 561 N-s/m. Then, van den Kroonenberg and his colleagues (1995) estimated the peak impact force based on their dynamic body models. From their best predicted model, the effective mass, *M*, is expressed as;

$$M = \frac{7}{20}m \text{.....(2.3.6.1)}$$

where *m* is the total body mass. Then, the approximated the peak force, F_{peak}, is expressed as;

$$F_{peak} = V\sqrt{KM} \text{.....(2.3.6.2)}$$

Since the impact velocity, *V*, at the moment of impact from the standing height (height of the center of gravity), the equation 2.3.6.2 can be further expressed as;

$$mgh_{cg} = \frac{1}{2}mV^2 \text{.....(2.3.6.3)}$$

$$V = \sqrt{2gh_{cg}} \text{.....(2.3.6.4)}$$

where h_{cg} is the height of an individual's center of gravity which is expressed as 0,51 × height (m). By substituting (2.3.6.4) into (2.3.6.2), the equation (2.3.6.2) becomes;

$$F_{peak} = \sqrt{2gh_{cg}KM} \text{.....(2.3.6.5)}$$

where g is the gravitational constant (9.81 m/s^2) and K is the soft tissue stiffness (71 kN/m). In this study, this equation (2.3.6.5) was used to estimate the peak impact force for each subject. Damping is not considered in this equation (2.3.6.5) since it was reported that damping ratio for the impact motion is small (damping ratio equal to 0.2) (Robinovitch et al. 1991).

2.3.7. Advanced FE Modeling Femur Studies

In order to obtain the most accurate results from the FE models, it is essential to simulate the models as realistic as possible. Several investigators included internal muscles forces in their models to approach this issue. Cristofolini et al. (2007) investigated if the involvement of the abductor muscles is important when femoral head and neck regions are evaluated through the FE models. They concluded that involvement of those muscle groups is not important when those regions are investigated for the single stance loading condition. However, in their study, the lateral falling was not investigated. Therefore, it is still unclear that if it is necessary to include those muscles in the lateral falls. However, the result of the study conducted by Robinovitch and colleagues (1991) indicated that activation of muscles around hip can increase the peak impact force in the lateral falls. From this consideration, activation of the abductor muscles possibly increases the compressive stress on the superior aspect of the femoral neck in the lateral falling condition. This mechanism is shown in Figure 2.3.6.1. Activating the hip abductor muscles attaching to the top of the greater trochanter can increase the compressive stress acting on the superior part of the femoral neck.

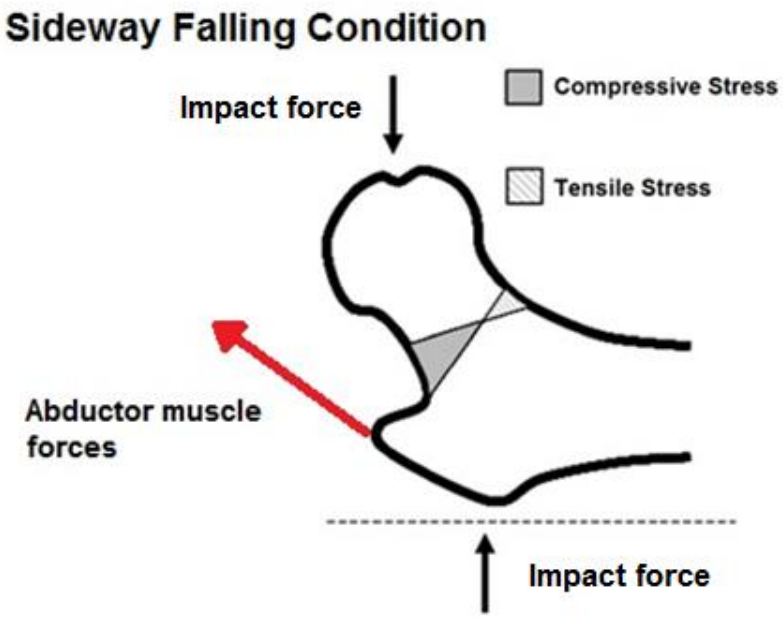

Figure 2.3.6.1 *Stress state of the proximal femur in the lateral fall with involvement of the hip abductor muscle forces. Figure was modified from de Bakker et al. 2009.*

The National Institute of Health conducted the project called the Visible Human Project (VHP), in which complete anatomical geometry of the male subject was constructed. Not only bone geometry from the CT data is available, but also muscle geometry and the direction of individual muscle paths from a set of cryosection colour photographs are available from this project. (NIH, 1996.) Several investigators utilized the data from this VHP. Bitsakos et al. (2005) constructed the FE models of the complete femur with involvement of a large number of muscles in the hip joint in order to simulate the bone remodeling after surgical operation of a hip implant stem. Polgár et al. (2003b) conducted the FE modeling study of the entire femur to make a comparison between concentrated muscle forces and distributed muscle forces on areas of insertions and origins on bone surface in the gait. Duda et al. (1998) also conducted similar FE modeling study to investigate the effect of involvement of muscle forces. Throughout these studies, it was concluded that omission of the muscles forces in the FE models of the femur can lead to the unrealistically high stress and strain values. Therefore, ideally the muscle forces should be included in the models. However, in this thesis, the muscle forces are not involved because only proximal part of the femur is available and the muscle geometry data is not available, yet.

3. MATERIALS AND METHODS

3.1. Subjects

Thirty six subjects with right dominant leg were selected from the previous study of Nikander et al (2009, and 2010a). In these studies, a total of ninety-one adult female athletes, who actively compete either at national or international level, and twenty non-athletic female as control subjects were recruited. This study was approved by the Ethics Committee of the Pirkanmaa Hospital District and a written informed consent was signed by each subject prior to the data measurement. These subjects were categorized into six different groups based on the types of impact loading involved in their sports: high-impact (H-I), odd-impact (O-I), high-magnitude (H-M), repetitive low-impact (R.L-I), repetitive non-impact (R.N-I), and the control group. In this thesis, each group contained six subjects. Descriptive data containing anthropometric data and physical performance of each subject measured previously are shown in Appendix 1.

3.2. Subject Specific Impact Force Calculation

In the subchapter 2.3.6, it was explained that the peak impact force caused by the lateral force can be estimated by the equations derived by previous studies. Using the equation 2.3.6.5 and the subject information such as height and weight from Appendix 1, the subject specific impact force was calculated. This subject specific impact forces are shown in Appendix 2. The actual force caused by the lateral force should be applied on the lateral side of the greater trochanter. However, to imitate one of the loading conditions (FC1) used in Bessho et al. (2009), which causes unusual high stress at superior part of the femoral neck, this calculated peak impact force was applied on the medial to superior aspect of the femoral head.

3.3. MRI Scanning and Manual Segmentation

The proximal femur geometry of each subject was obtained from the MRI measurement. A brief summary of this MRI measurement is introduced here. The details can be found in Nikander et al. (2009). A 1.5-T MRI system (Siemens, Avanto Syngo MR B15, Erlangen, Germany) was used to obtain the MRI data of the proximal femurs. With two haste localization series, sagittal, axial, and coronal images of the pelvic regions of subjects' dominant leg were obtained. The used imaging sequence was standardized axial T1-weighted gradient echo volumetric interpolated breath-hold (VIBE) examination. Slice thickness was 0.9 mm without gaps with a resolution of 0.9mm x

0.9mm. Cross section image aligned perpendicular to the femoral neck axis had matrix of 384 x 288. This image sequence covered the whole proximal femur from the femoral caput to the subtrochanteric level of the femoral diaphysis.

MRI data were ,then, manually segmented by delineating the periosteal and endocortical boundaries of the cortical bone using a touch panel Wacom Tablet Clintiq 12WX (Wacom Technology Corporation, Vancouver, WA, USA) with a medical image processing freely available software the ITK-SNAP 2.1.4-rcl (U.S: National Institute of Biomedical Imaging and BioEngineering and the NIH Blueprint for Neuroscience). Using this software, high quality manual segmentation became possible. Figure 3.3.1 shows the screen shot of ITK-SNAP software while the manual segmentation was being performed.

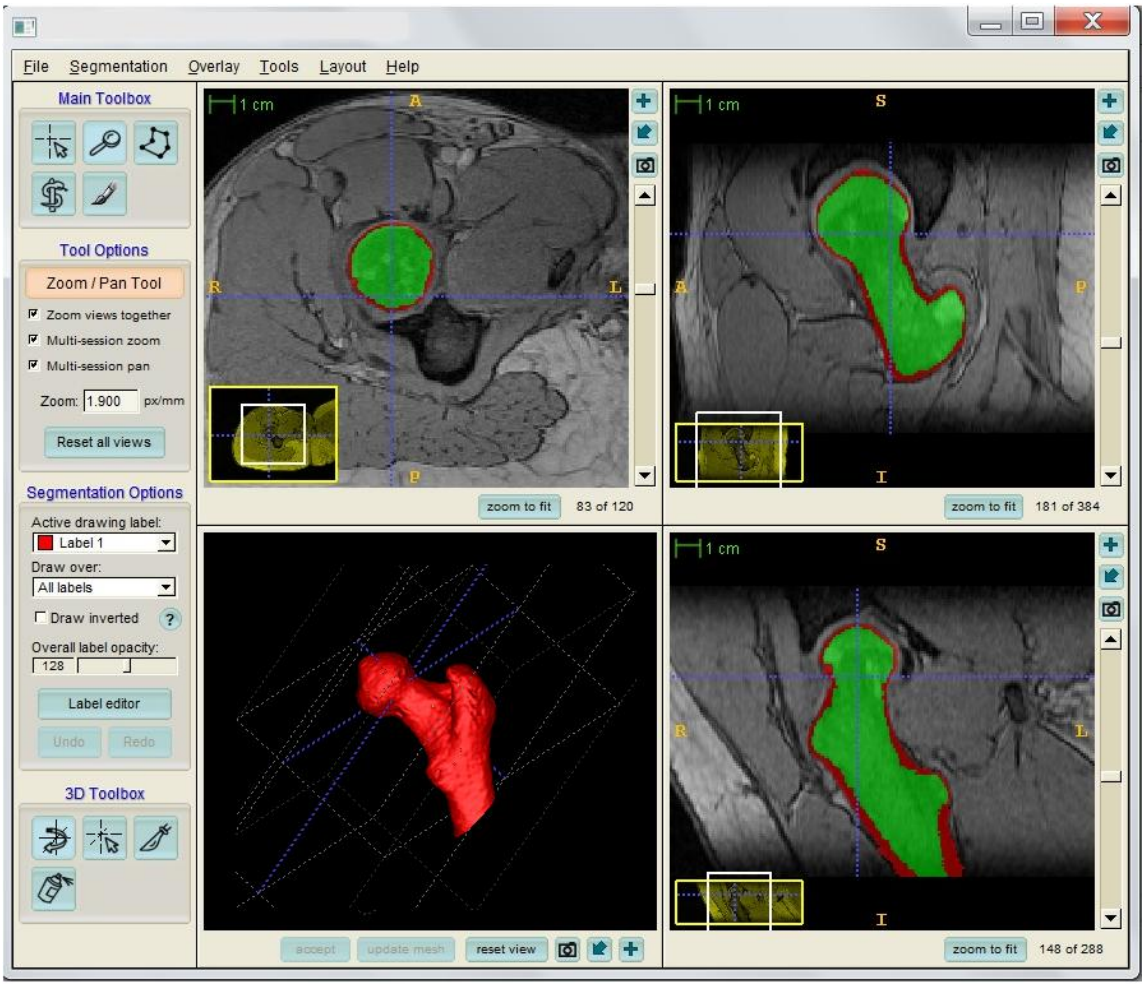

Figure 3.3.1 *Typical view of ITK-SNAP. Red represents the cortical bones while green represents the trabecular bones. An image at lower left corner shows the 3D image of segmented images. A figure at upper left hand corner shows the segmented femoral head in the transverse plane. The red-colored hollow and the green-colored circle represent the cortical and trabeculae bone respectively. Manual segmentation was performed by choosing each pixel box representing the cortical or trabecular bone.*

3.4. Conversion of MRI Data to solid file format

The segmented MRI data was converted from .vtk format created by the ITK-SNAP into the importable file format for the FE modeling software ANSYS Workbench 14.0 (ANSYS Inc., Southpointe, PA, USA). In the MSc thesis of Orabec (2009), the method of file format conversion was developed. In this thesis, his method was also adopted and modified slightly. First, the segmented data in .vtk format was converted into a 3D array (.mat) using MATLAB (MathWorks Inc., Natick, MA, USA). This 3D array contains numbers such as 0, 1, and 2 representing the air, trabecular, and cortical bones respectively. The MATLAB code used for this conversion is given in Appendix 5-A. Next, the open-source software iso2mesh for MATLAB was used to create a 3D tetrahedral FE mesh for each cortical and trabecular bone geometry (Fang, 2009). It is noteworthy to mention that this cortical geometry contained both cortical and trabecular bone inside of outer boundary of the segmented cortex. MATLAB code used in this operation is given in Appendix 5-B. As output file format, each geometry was saved as TetGen format: a list of nodes (.node), a list of tetrahedral (.ele), and a list of triangular faces (.faces).

Three other software such as winmeshview (Stanford University Haptics Lab, Stanford, CA, USA), Rhinoceros computer aided design (CAD) software 4.0 (Robert McNeel & Associates, Seattle, WA, USA), and Automesher (Automapki, Brussels, Belgium) were utilized to convert the files into the final importable file format. First, the TetGen files were converted to alias obj file format (.obj) by winmeshview, and then the alias obj files were converted into rhino 3D model file format (.3dm) by Rhinoceros CAD software 4.0. Finally, the files were converted into the final importable solid file format such as ACIS CAD format (.sat) by Automesher. Meshing the geometry by the iso2mesh was the necessary process only to enable the conversion of the file format to the final importable file format. Details of these file conversions are given in Appendix 6. However, the geometry in this final format was recognized again as single solid material constructed by meshed elements once it was imported into the ANSYS Workbench. Therefore, once the geometry was imported into the ANSYS, another meshing was necessary.

3.5. Creation of FE models with ANSYS

ANSYS Workbench 14.0 (ANSYS Inc., Southpointe, PA, USA) was used to create the FE models in this thesis rather than ANSYS Mechanical APDL 14.0. Although both softwares are technically same, ANSYS Workbench has more user friendly interface. Permission of using ANSYS Academic Research software including these two software sabove was obtained from IT Center for Science Ltd (CSC). CSC is administered by the Ministry of Education, Science and Culture in Finland. It is a non-profit company providing IT support and resources for academic, research institutes, and companies. Once ANSYS Workbench was opened, *Static Structural* was chosen as *Analysis Sys-*

tems (Figure 3.5.1). Once the Static Structural is chosen, the square box appears in the *Project Schematic*. Material properties, geometries, boundary/loading conditions were specified in the specific programs activated by clicking the rows such as *Engineering Data*, *Geometry*, and *Model* respectively.

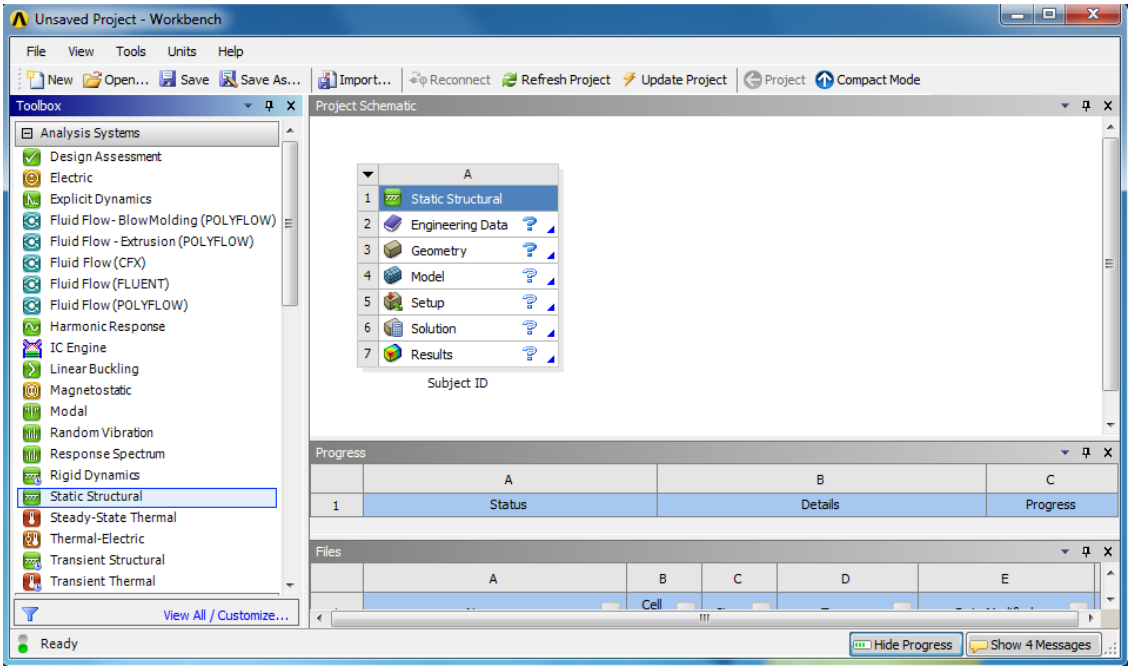

Figure 3.5.1 *Typical View of ANSYS Workbench. Static Structural can be chosen from the left column.*

3.5.1. Assigning Material Properties

Material properties for each cortical and trabecular bone can be specified in *Engineering Data* in shown in Figure 3.5.1.1. In this Engineering Data, homogeneous isotropic elastic material properties were specified into the cortical and trabecular bone separately. Two properties such as Young's modulus and Poisson's ratio were needed to be specified manually. Then, Bulk and Shear Modulus shown in Figure 3.5.1.1 were automatically calculated. Based on the literature review in the section 2.1.2, the densities of the cortical and trabecular bones were assumed to 1.8 g/cm^3 and 0.5 g/cm^3 respectively. Using these density values, Young's moduli were obtained from the following equations (also in Table 2.1.2.2): $E_{cortical} = -6.142 + 14\rho$ and $E_{trabecular} = 0.58\rho^{1.3}$, where ρ was the density (the unit of trabecular bone density was converted from g/cm^3 into kg/m^3 before putting it into the latter equation.) Throughout this process, the Young's modulus of 19GPa and 1871MPa were obtained and assigned into the cortical and trabecular bone respectively. Poisson's ratio of 0.3 and 0.12 were also adopted from the literature (Wirtz et al. 2000), and then assigned into cortical and trabecular bones respectively. These material properties were also adopted in the previous study of Oravec (2009). Figure 3.5.1.1 shows the view of the Engineering Data where material property assignment was performed. *Isotropic Elasticity* was chosen from *Liner*

Elastic from the left column, then two material properties (Young's modulus and Poisson's ratio) were specified separately for the cortical and trabecular bone.

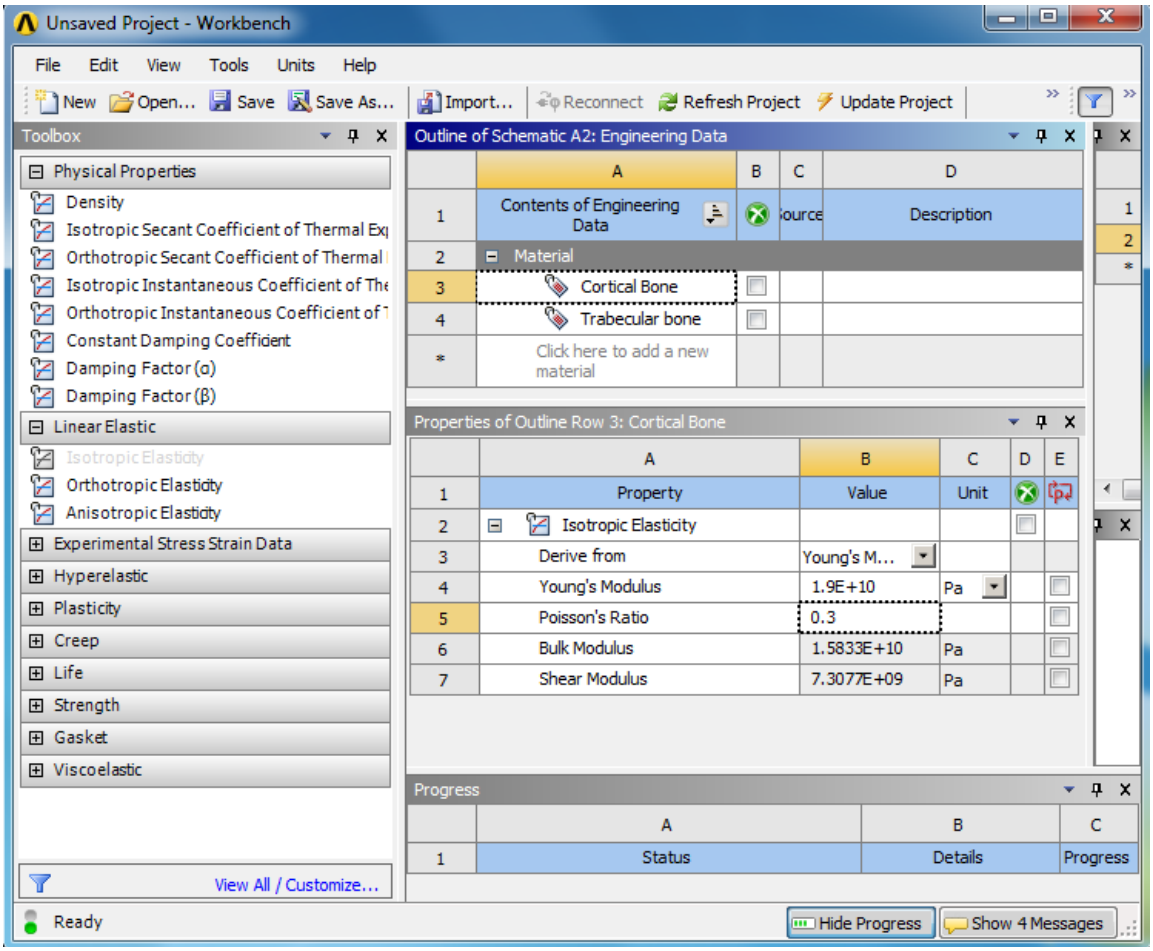

Figure 3.5.1.1 *Assignment of material properties in the Enginnering Data in the Workbench for cortical bone.*

3.5.2. Geometry

Geometry was then imported into the CAD program called *DesignModeler* in the ANSYS WorkBench. This DesignModeler was opened by right clicking the *Geometry* in the square box in Figure 3.5.1. In the Design Modeler, each geometry (.sat file format) was imported separately (Figure 3.5.2.1). The descriptive data of the geometry in the FE model is attached in Appendix 3.

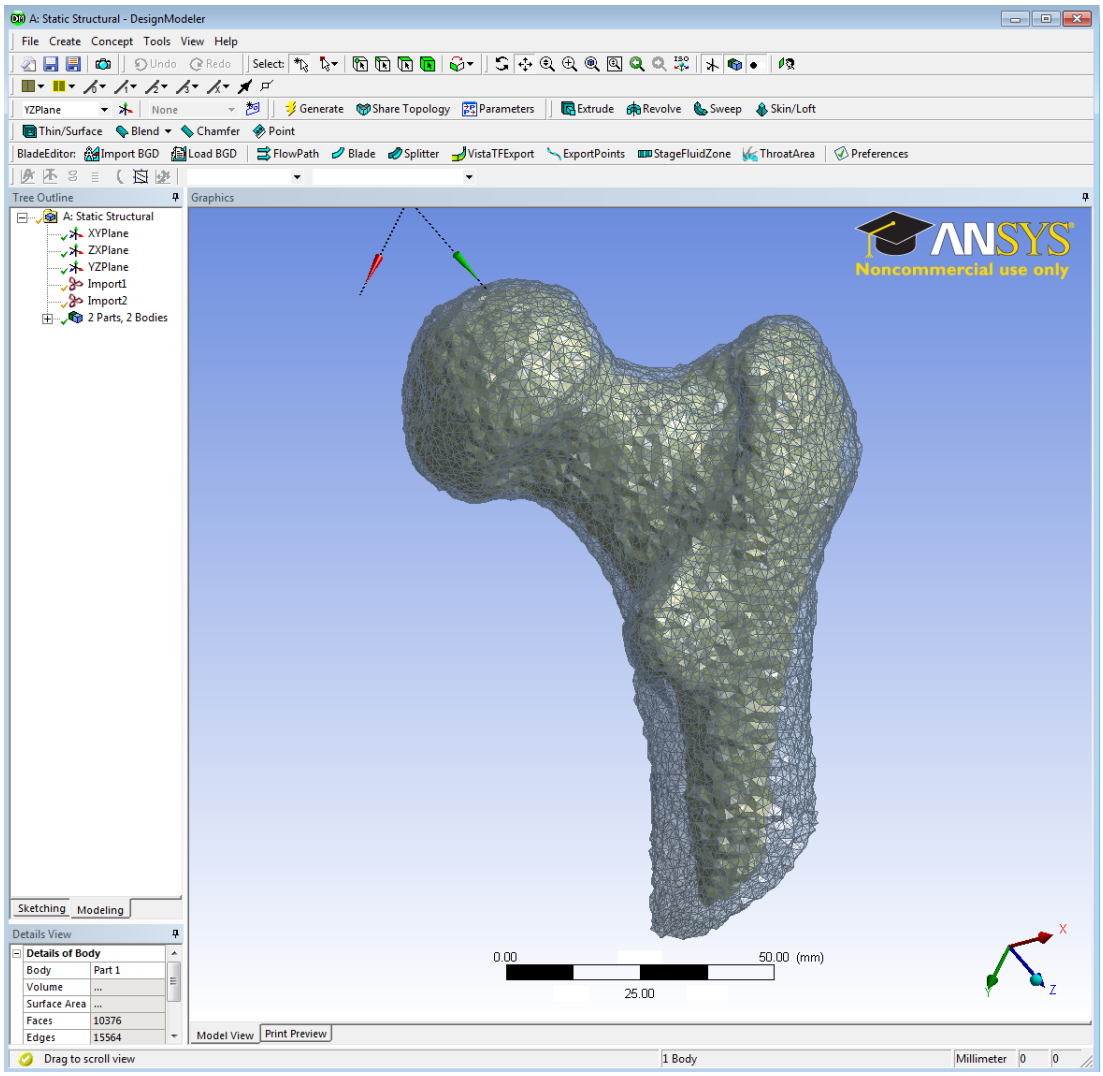

Figure 3.5.2.1 *Import of Geometries. Green geometry represents the trabecular bones while grey geometry represents the cortical bone.*

3.5.3. Meshing the geometry

Once the geometries were imported into the ANSYS Workbench, meshing was taken place again. Segmented image was already meshed earlier as described in the subchapter 3.4. This earlier meshing was necessary process only to convert MRI data based geometry into the importable file format to the ANSYS Workbench. However, once these meshed geometries were imported into the ANSYS Workbench, the geometries were recognized as unmeshed solids constructed by many tetrahedrons by the ANSYS Workbench. Therefore, additional meshing was required. In order to model complex geometry of the proximal femur, tetrahedron was chosen as the element shape again. *Patch Conforming* was selected as meshing algorithm. Element size was set to the default setting "coarse". Element growth rate and transition ratio were set to 1.2 and 0.272 respectively. If meshing geometries with these specifications was failed, another meshing algorithm called *Patch Independent* algorithm was selected. Also, in this case, minimum size limit and approximate number of elements per part were set to 4mm and

50000 respectively. This setting allowed meshing those geometries which could not be meshed by the Patch Conforming algorithm. Average of 367467 nodes and 240406 elements were created. The number of the node and element for each subject is shown in Appendix 4. Figure 3.5.3.1 shows one of the meshed FE model as an example.

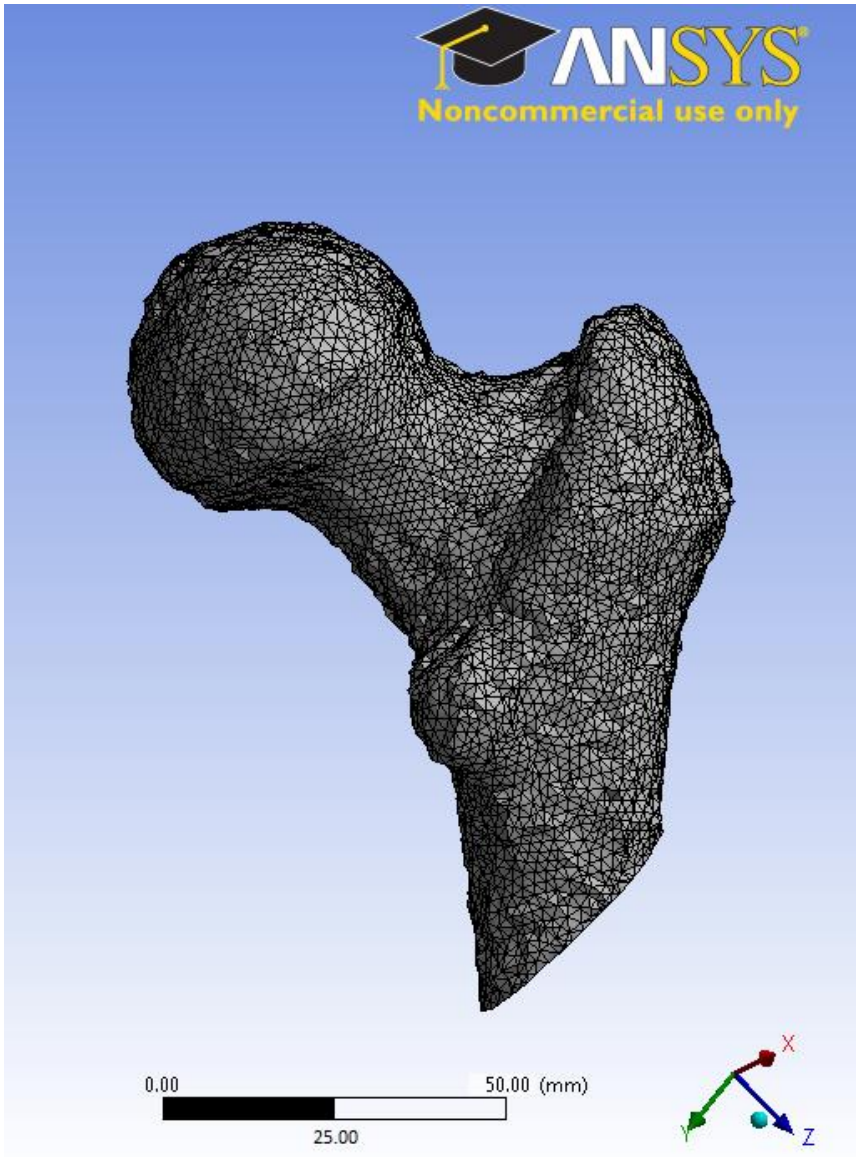

Figure 3.5.3.1 *Meshed FE model.*

3.5.4. Boundary Condition

Once meshing the geometry was completed, the boundary (loading) condition was specified in the software called *Mechanical* in the ANSYS Workbench. It can be opened by right clicking the *Model* in the square box shown in Figure 3.5.1. Based on the literature review in the subchapter 2.3.2 and 2.3.5, the loading condition with angle γ of 120° and angle δ of 0° (Figure 2.3.2.2) was adopted to simulate one of the lateral falling conditions (FC1) introduced by Bessho et al. (2009). This condition should cause unusual high stress at the superior part of the femoral neck. Boundary conditions needed

to be specified were following: 1) *force* (including magnitude, direction, and location), 2) *fixed supports*, 3) *free boundaries*, and 4) *contact* which specifies the boundary condition between the cortical and trabecular bone boundaries.

The subject specific impact force calculated in the subchapter 3.2 was applied on the medial-superior part of the femoral head. The location was identified, and approximately total surface area of 140 mm^2 was selected where the force was applied. This selected area is illustrated in Figure 3.5.4.1 below. Then, the direction of the force was specified so that angles γ and δ were 120° and 0° respectively (Figure 3.5.4.2).

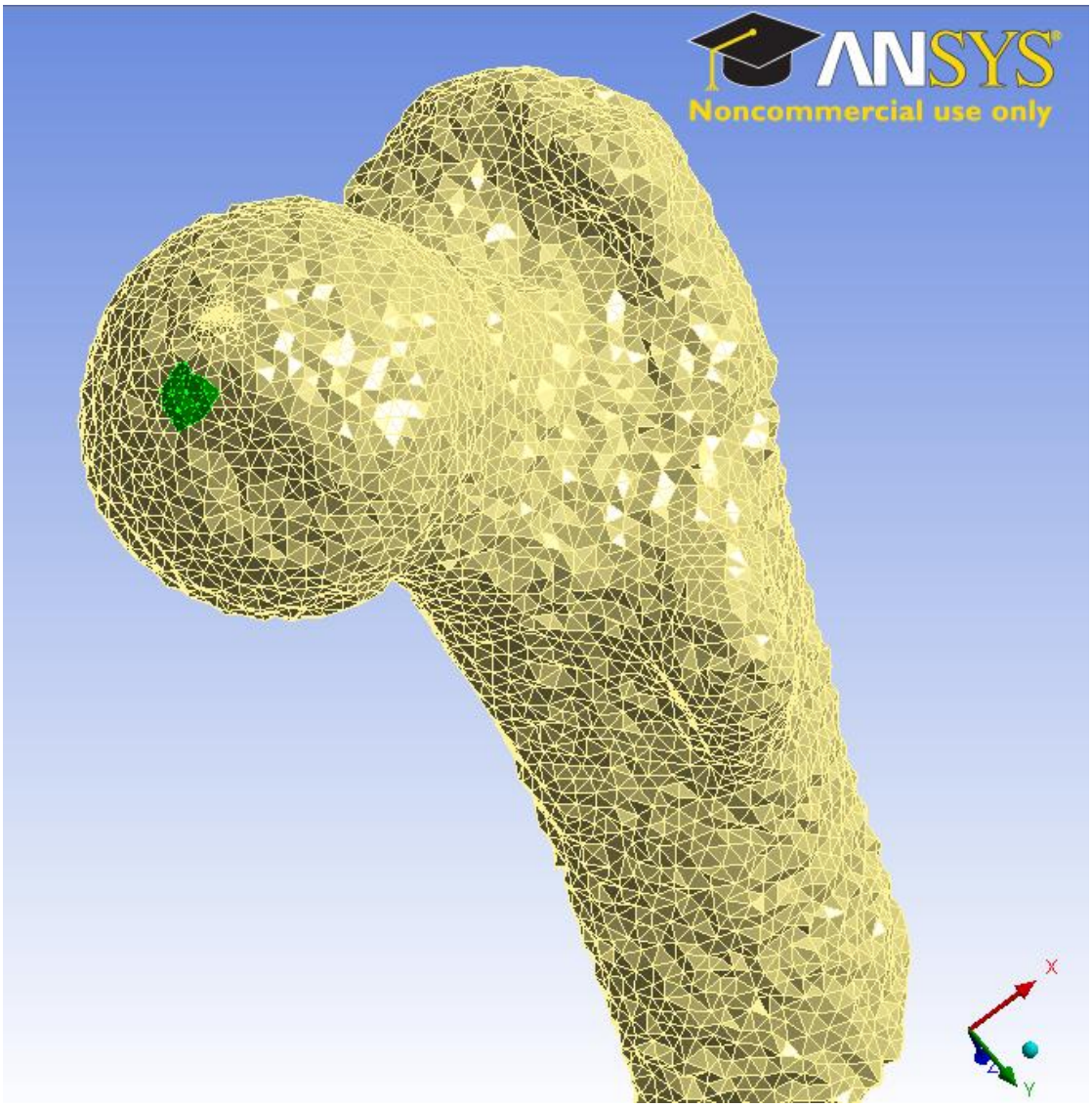

Figure 3.5.4.1. *Location of applied force in Mechanical view. Green area represents the selected surface where the force was applied.*

Next, the lateral surface of the greater trochanter and the distal end of the proximal femurs were selected as the fixed supports so that selected surfaces do not move or deform during the loading. Approximately the total surface area of 300 mm^2 at the lateral side of the greater trochanter and the distal end of the proximal femur were fixed (Fig-

ure 3.5.4.2). The location of this selected surface at the side of greater trochanter was recognized so that the angle δ became 0°. All other surfaces were free boundaries so that they could move freely.

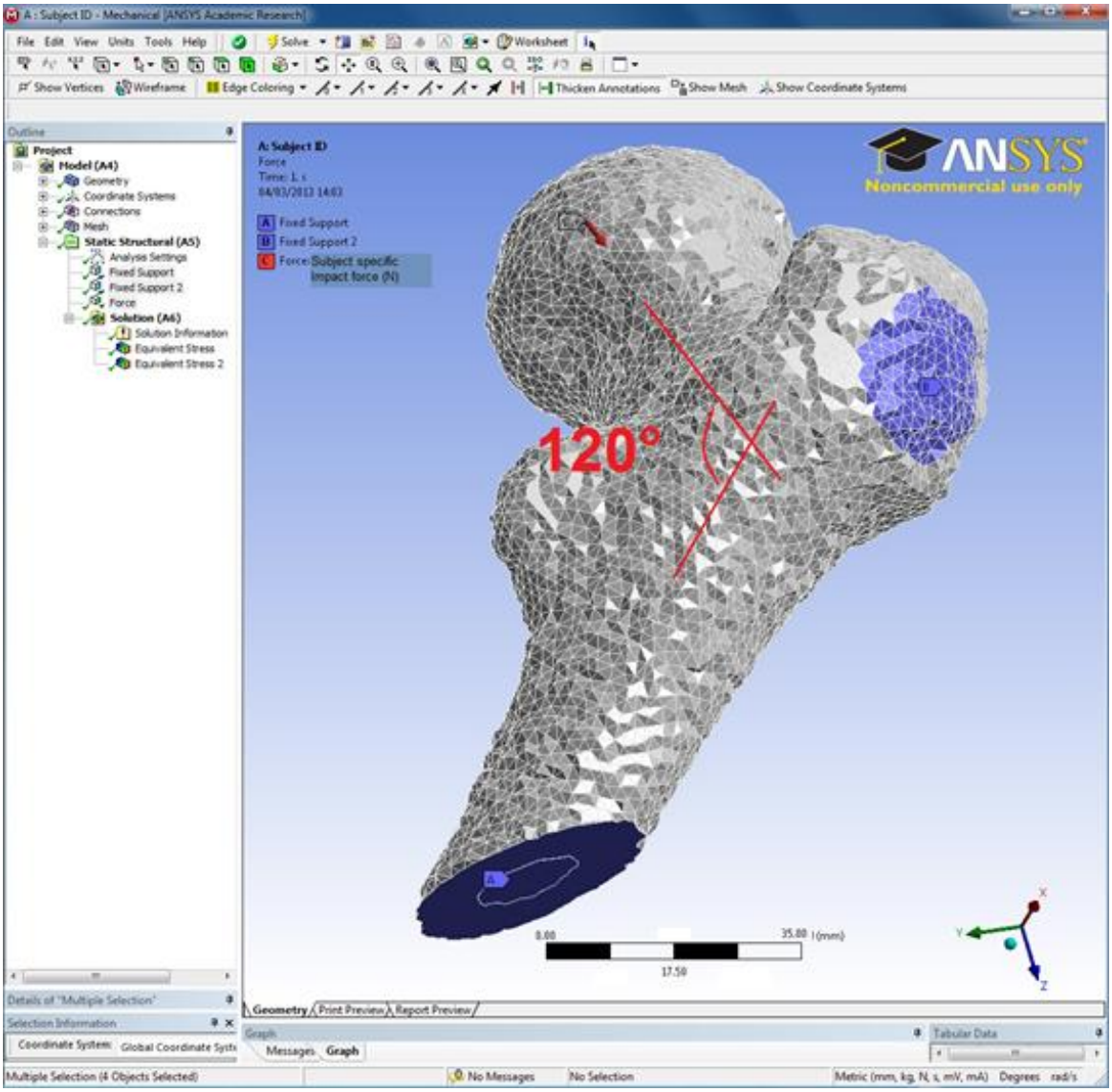

Figure 3.5.4.2. *Boundary/loading condition specification in Mechanical view. Blue—colored areas represent fixed supports while a red arrow represents a force applied on the femoral head. The angle in the frontal plane γ was set to 120°.*

Lastly, the boundary condition where the cortical bone contacts with the trabecular bone was specified so that the forces can be transferred between these two geometries. In order to do so, the connection type *Bonded – Solid to Solid* was chosen in the *Connection* (located in *Outline* on the left column in *Mechanical*). This connection type does not allow any sliding, or separation between the geometries. This connection specification is illustrated in Figure 3.5.4.3.

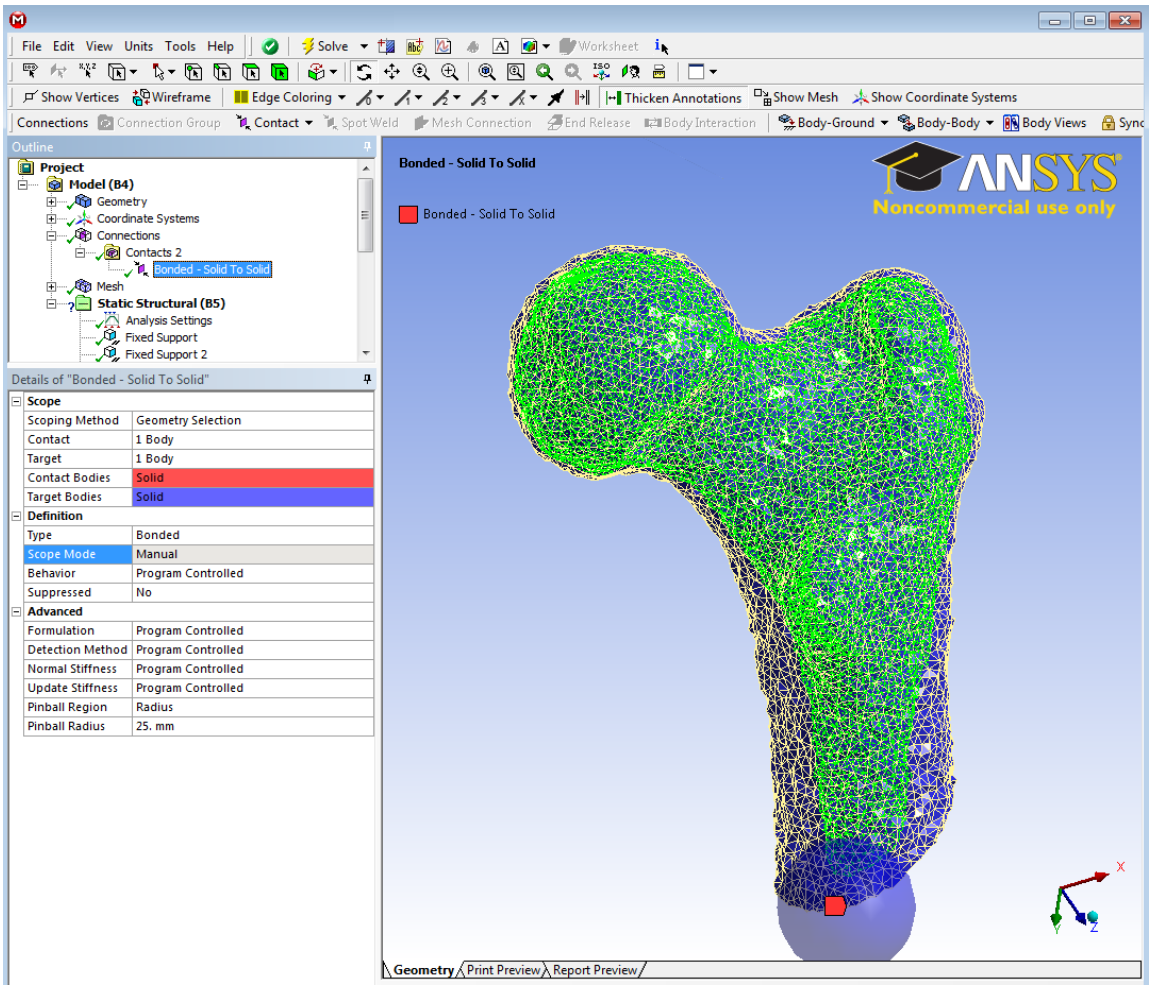

Figure 3.5.4.3. *Bonded connection for solid to solid. Green surface represents the contact surfaces between the cortical and trabecular bone. Bonded was chosen as the connection type.*

3.5.5. Solving the created FE model

Once material property setting, importing of the geometry, meshing, and loading condition specification were completed, the FE models were solved. Nonlinear analysis with the Newton-Raphson method was performed to solve the created FE models. Nonlinear analysis was chosen instead of the linear analysis due to the complexity of the geometries. From the choices of solvers available in ANSYS structural mechanical solutions, the preconditioned conjugate gradient iterative solver was chosen for the analysis. All FE models were solved in Lenovo ThinkCentre desktop computer (Lenovo Ltd., Morrisville, NC, USA) with a 2.83 gigahertz 64-bit Intel Core 2 Quad Q9500 processor (Intel Corp., Santa Clara, CA, USA). This desktop computer had system of 4 gigabytes of RAM. Average computation time of solving each FE models was approximately 15 minutes. Throughout the analysis, nodal vonMises stress in MPa and total deformation in mm for the cortical and trabecular bone geometry were calculated for each subject separately.

3.6. Post Processing

Result images of the vonMises stress distribution and the total deformation of the solved FE models are shown in the next chapter *Results*. The total deformation was chosen only to observe if the created model seems valid. On the other hand, in addition to the image, the vonMises stress was further processed in order to investigate the stress distribution at the femoral neck in the given lateral loading condition between each athlete group and the control group. The vonMises stress for the cortical and the trabecular bone were exported into the separated text files (vonMisesC.txt and vonMisesT.txt respectively). They contained the node number in the 1st column, xyz Cartesian coordination values (mm) of the node from the 2nd to 4th columns, and the vonMises stress (MPa) in the 5th column.

To study the differences in the stress distribution at the femoral neck, regional stress values were calculated for the narrowest region of the femoral neck (approximately 9mm). First, the smallest cross-section (slice) of the femoral neck was identified, and then the femoral neck was divided into 8 regions/sectors in the transverse/coronal plane; Inferior1, Inferior2, Anterior1, Anterior2, Superior1, Superior2, Posterior1, and Posterior2. After that, the stress values from total of 9 slices (±4 slices from the smallest slice) were obtained, and then the mean values from these 9 slices were calculated for each region/sector. The method of identification of the smallest neck cross-section was first developed by Nikander et al. (2009), adopted also in Oravec (2009), and then was further developed in this thesis. MATLAB was used for finding the smallest slice, dividing it to anatomical sector, and calculating the mean vonMises stress for each region/sector. Following sections explain these post processes in detail.

3.6.1. Finding the smallest femoral neck region

Exported cortical and trabecular vonMises stress files (.txt) were imported into MATLAB separately, and then combined into one array. This array contains node number, xyz coordination of each node, stress values (MPa), and material label (cortical or trabecular). Then, nodes were grouped by the z-coordination (the slice number of MRI data). Next, the average dimension of the bone in each slice number was calculated. The MATLAB code used for the process so far is given in the Appendix 5-C and the details are explained along with the code. The MATLAB code in the Appendix 5-C plots the Figure 3.6.1.1 showing this average dimension in y-axis and the slice number in x-axis. This code asks the user to click tops of two apexes, which represent the mid-femoral head at the smaller slice number and trochanteric region at the larger slice number in the x-axis. The slice number with the smallest y-value between these two apexes was identified as the smallest cross-section at the femoral neck.

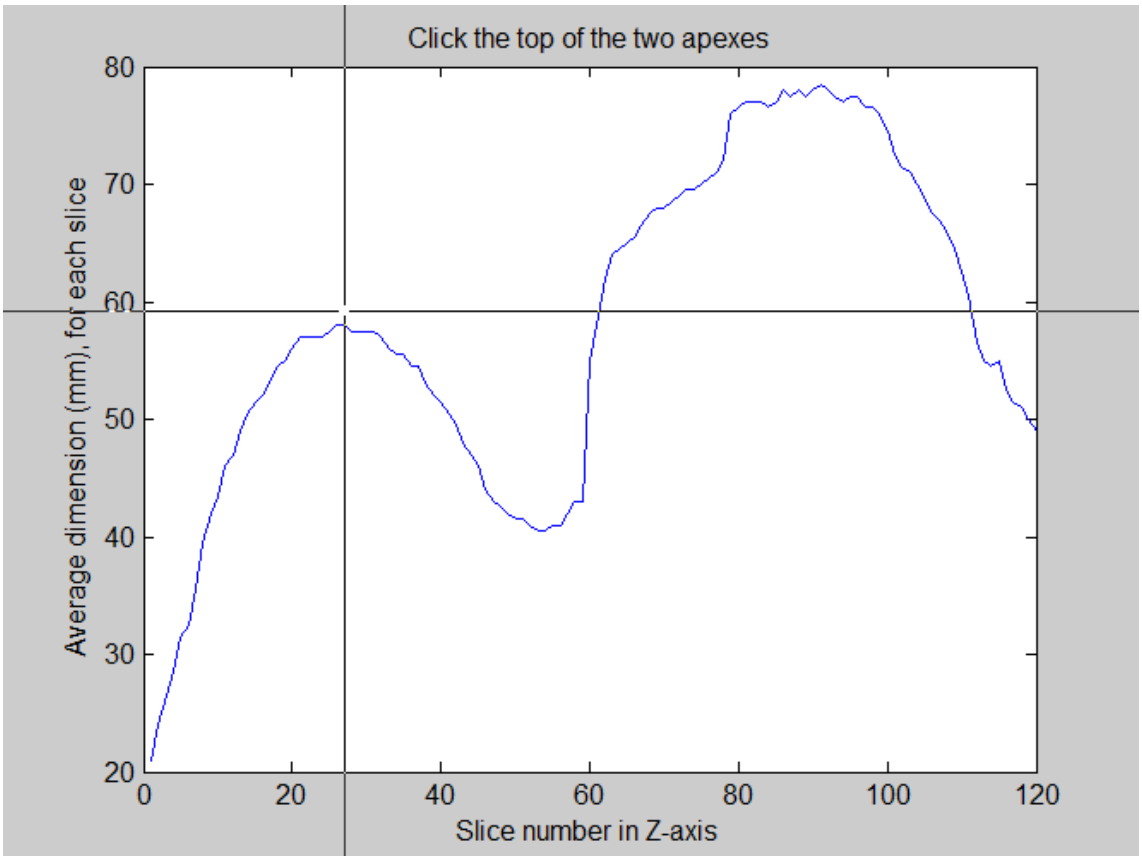

Figure 3.6.1.1. *Average dimension versus slice number of MRI. The code in the Appendix 5-C asks the user to click the tops of two apexes. Then, it finds the slice in the z-axis of the MRI data having the smallest average dimension, which means the smallest cross-section in the femoral neck. An apex at about 25 in x-axis represents the mid-femoral head while another apex around 95 in x-axis represents the trochanteric region. The smallest region of the femoral neck was identified as the one whose y-value is the smallest between two apexes.*

3.6.2. Division of the femoral neck cross-section

Once the narrowest femoral neck region was obtained, the femoral neck was divided into 8 regions/sectors in the transverse/coronal place. To do so, the centroid of the bone including the cortical and trabecular bone tissues in each slice was first calculated. Based on this calculated centroid, the slice was divided into 8 regions: Inferior1, Inferior2, Anterior1, Anterior2, Superior1, Superior2, Posterior1, and Posterior2 shown in Figure 3.6.2.1. The code used for this division is shown in Appendix 5-D. Oravec (2009) developed the code for dividing the slice into 4 quadrants based on the one developed from Nikander and his colleagues' study (2008). In this thesis, the code developed by Oravec (2009) was further modified so that the region can be divided into the 8 equal regions. The code in Appendix 5-D is the function file, which is used in another code in Appendix 5-E. This is explained in the next subchapter.

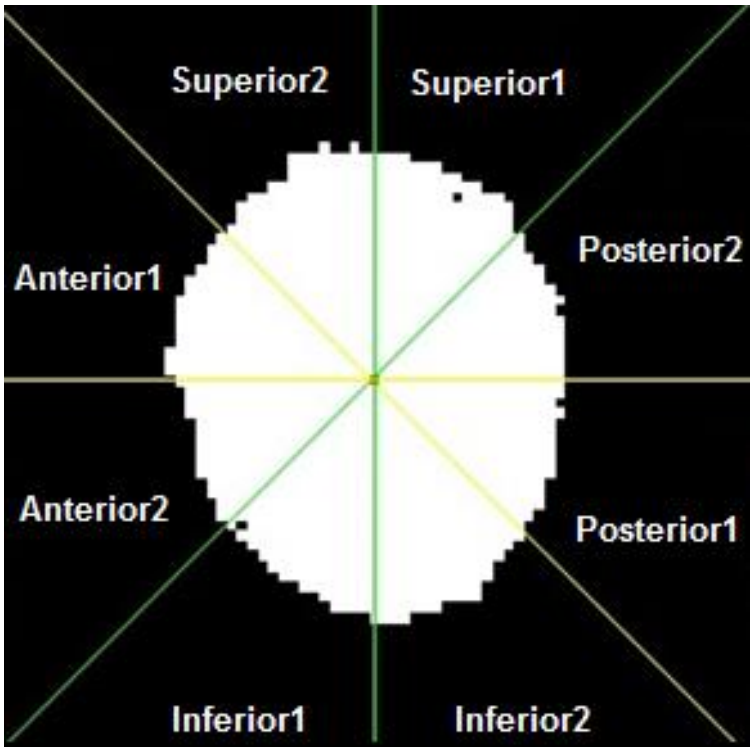

Figure 3.6.2.1. *Anatomical division of the femoral neck cross-section. The code in the Appendix 5-D divided the slice into 8 equal region: Inferior1, Inferior2, Anterior1, Anterior2, Superior1, Superior2, Posterior1, and Posterior2.*

3.6.3. Result Output

The vonMises stress values from total of 9 slices (±4 slices from the smallest cross-section slice number) were obtained. Then, mean vonMises stress value from 9 slices was calculated for each region for each subject. This regional mean value was calculated for cortical and the trabecular bone separately. The code in Appendix 5-E was used to obtain values from 9 slices and calculate the regional mean value. The code used to divide the femoral neck into 8 regions (Appendix 5-D) was the function file and it was called inside of the code in Appendix 5-E. The process from the manual segmentation of the MRI data to the calculation of this regional mean vonMises stress was summarized as Workflow in Appendix 6.

3.6.4. Statistical Analysis

Statistical analysis was performed with SPSS 21 (IBM Corporation., Chicago, IL, USA). Means regional vonMises stress at 8 different regions for each group and standard deviation (SD) were obtained as descriptive statistics. Due to the small number of subjects in each group, nonparametric test Mann-Whitney text was performed for evaluation of differences in the mean regional vonMises stress between each athlete group and the control group. A p value of less than 0.05 was considered statistically significant. Mean regional vonMises stress values from all six groups were ploted using Microsoft Excel 2010 (Microsoft Corp., Redmond, WA, USA).

4. RESULTS

4.1. vonMises Stress Distribution

Results of this thesis show that the stresses were highly concentrated at the femoral neck regions compared with stresses at other regions in all subjects in the simulated lateral falling condition. As an example, this is well illustrated in the Figure 4.1.1. The simulated lateral falling condition was supposed to create this high stress at the femoral neck region. Thus, this was well reproduced in the FE models in this thesis. Most importantly, the highest stresses were seen at the superior femoral neck region among other regions. This can be clearly seen in Figure 4.3.1 and Figure 4.3.2. The cortical and trabecular vonMises stress values from the whole 9mm slices of the neck region vary approximately from 2MPa to 25MPa and from 0.25MPa to 2.5MPa respectively. The vonMises stress distribution of the proximal femur of one subject from the H-M group is visualized in Figure 4.1.1 as the example.

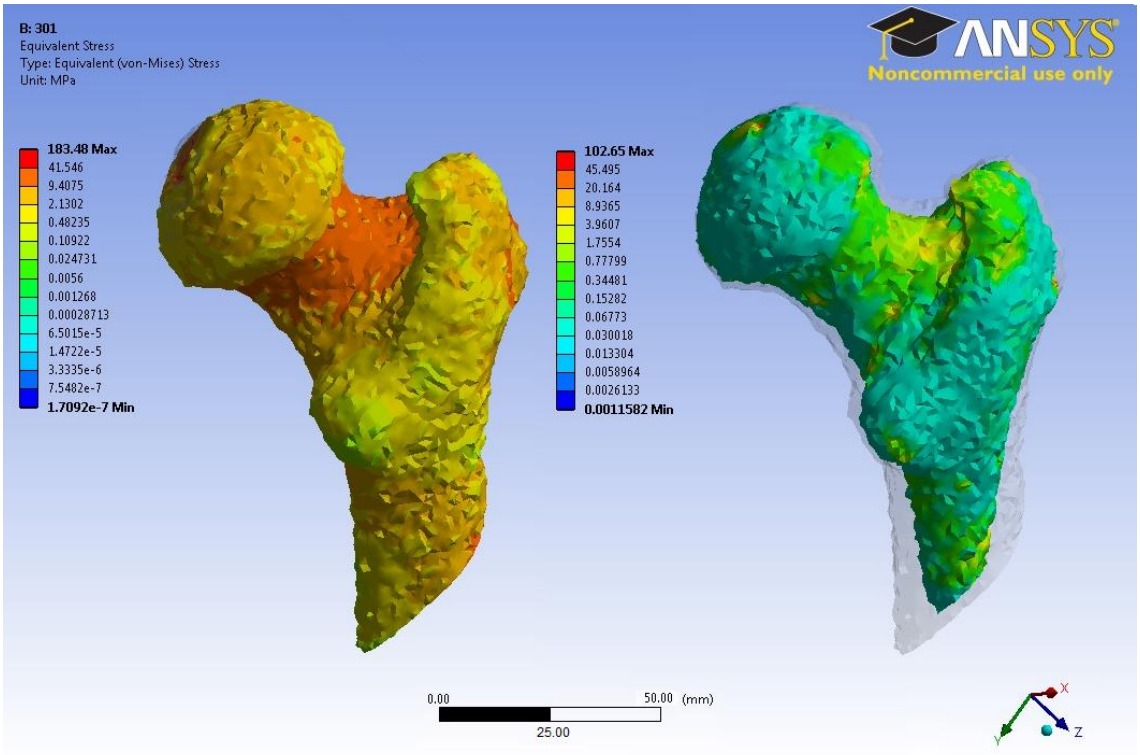

Figure 4.1.1. *The vonMises stress distribution (MPa) in the cortical bone (left) and the trabecular bone (right) in the lateral fall condition. Stress distribution image of the subject ID 301 from the H-M group was chosen as the example.*

4.2. Total Deformation

Total deformation was also calculated through the FE models. The results show that the cortical bone geometry deformed approximately from 0 to 0.2mm while the trabecular bone geometry deformed about from 0 to 0.15mm. At the femoral neck region, this total deformation for the cortical and trabecular bone ranged about from 0.03 to 0.07 mm and from 0.025 to 0.05 mm respectively. The largest deformations were seen at the location where the impact force was applied. The total deformation of one subject from the H-M group is illustrated in Figure 4.2.1.

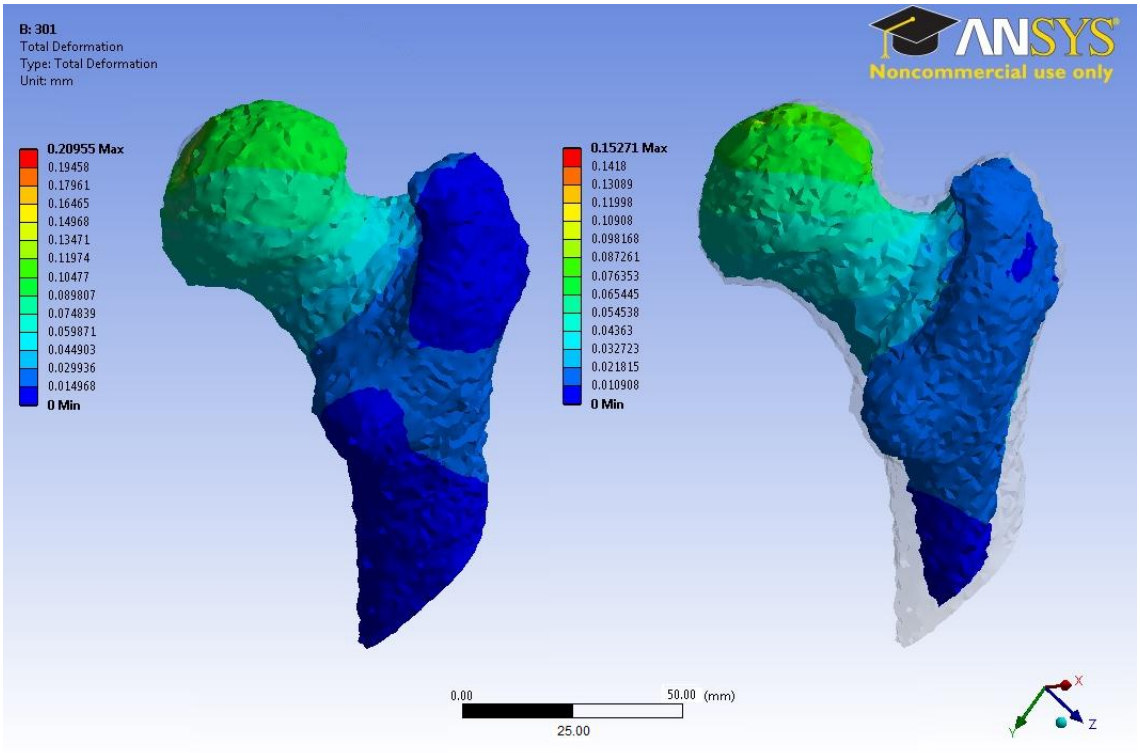

Figure 4.2.1. *Total deformation (mm) in the cortical bone (left) and the trabecular bone (right) in the lateral fall condition. Total deformation image of the subject ID 301 from the H-M group was chosen as the example.*

4.3. Comparison of vonMises Stresses Between Groups

Statistical analysis shows that the mean trabecular vonMises stress of the O-I group at the Posterior2 region was significantly different (p = 0.026). However, no other stress values were significantly different between each athlete group and the control group. Statistical results are shown in Table 4.3.1. Unfortunately, the stress value from the trabecular region in this region was not our interest. Mean regional vonMises stress values for the cortical and trabecular bone from all six groups are shown in Figure 4.3.1 and Figure 4.3.2 respectively. As shown in the Figure 4.3.1 and Figure 4.3.2, the highest stresses were clearly seen at superior regions in both cortical and trabecular bone (Superior1 & Superior2). As expected, the simulated lateral falling condition should

cause the highest stress at the superior cortex. This was well replicated in the created FE models. On the other hand, the lowest stress values were observed at the inferior regions (Inferior1 & 2) and the Anterior1 both in the cortical and the trabecular bone. Posterior regions also experienced relatively high stress in both bone types.

Table 4.3.1 *Between group differences in different anatomical regions. Comparisons were made between each exercise group and the control group. The p-values obtained from Mann-Whitney test are given.*

	Infe-rior1	Infe-rior2	Ante-rior1	Ante-rior2	Supe-rior1	Supe-rior2	Post-erior1	Post-erior2
Cortical bone								
H-I	0.24	1	0.937	0.818	0.589	0.699	0.818	0.485
O-I	0.31	0.394	0.589	0.589	0.485	0.24	0.818	0.485
H-M	0.24	0.699	0.589	0.485	0.132	0.24	0.818	0.589
R.L-I	0.699	0.699	0.818	0.31	0.24	0.31	0.132	0.937
R.N-I	0.065	0.24	0.589	0.937	0.31	0.394	0.589	0.485
Trabecular bone								
H-I	1	0.485	0.818	0.31	0.24	0.31	0.485	0.394
O-I	0.937	0.937	0.818	1	0.589	0.394	0.589	**0.026***
H-M	0.589	0.937	0.589	0.937	0.18	0.394	0.485	0.485
R.L-I	0.31	1	1	0.699	0.394	0.18	0.394	0.485
R.N-I	1	0.485	0.31	0.699	0.485	0.485	0.818	0.394

*significant difference since $p < 0.05$

It is noteworthy to mention about the stress values from all groups as well as the comparison of them with the control group in spite of the fact most of them were not significantly different according to the statistical analysis. Interestingly, the cortical stress values from the H-I group at the superior regions were the highest. On other hand, this group had the lowest cortical stress values at the inferior regions. This asymmetric stress distribution in the H-I group will be discussed in the Discussion chapter. As expected, the cortical stress values from the O-I group at the superior regions were relatively lower than that of the control group. Otherwise, the cortical stress values from the O-I group did not seem different at other regions from the control group. Surprisingly, the trabecular stress values from this group were high at almost all regions. Both cortical and trabecular stress values from the H-M group did not seem different from the control except for the stress values at superior regions. Interesting finding here is that both cortical and trabecular stress values from the R.L-I group were relatively low at all regions. Especially, this group had the lowest cortical stress values at Anterior2, Superior1, and Superior2. Cortical stress values from the R.N-I group seemed different at inferior regions; otherwise both cortical and trabecular bone stress seemed relatively same as those from the control group.

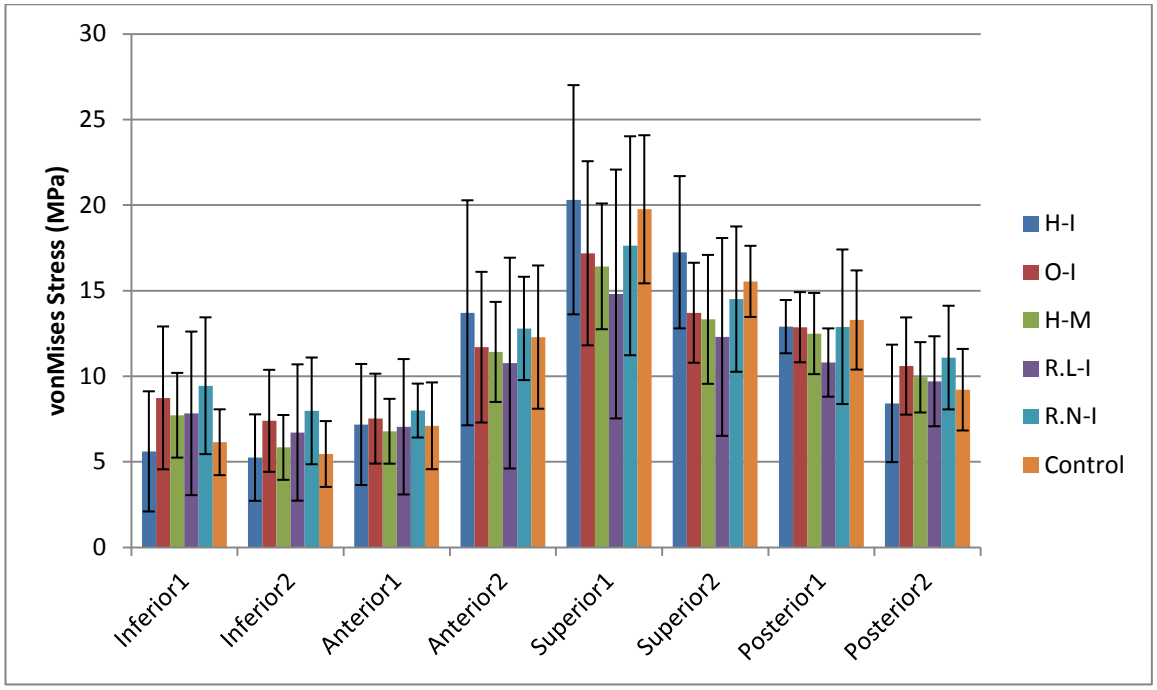

Figure 4.3.1. *Mean vonMises stress (MPa) in the lateral falling condition from the cortical bone at different regions from all groups. Error bars represent the standard deviation. * represents the significant difference if any.*

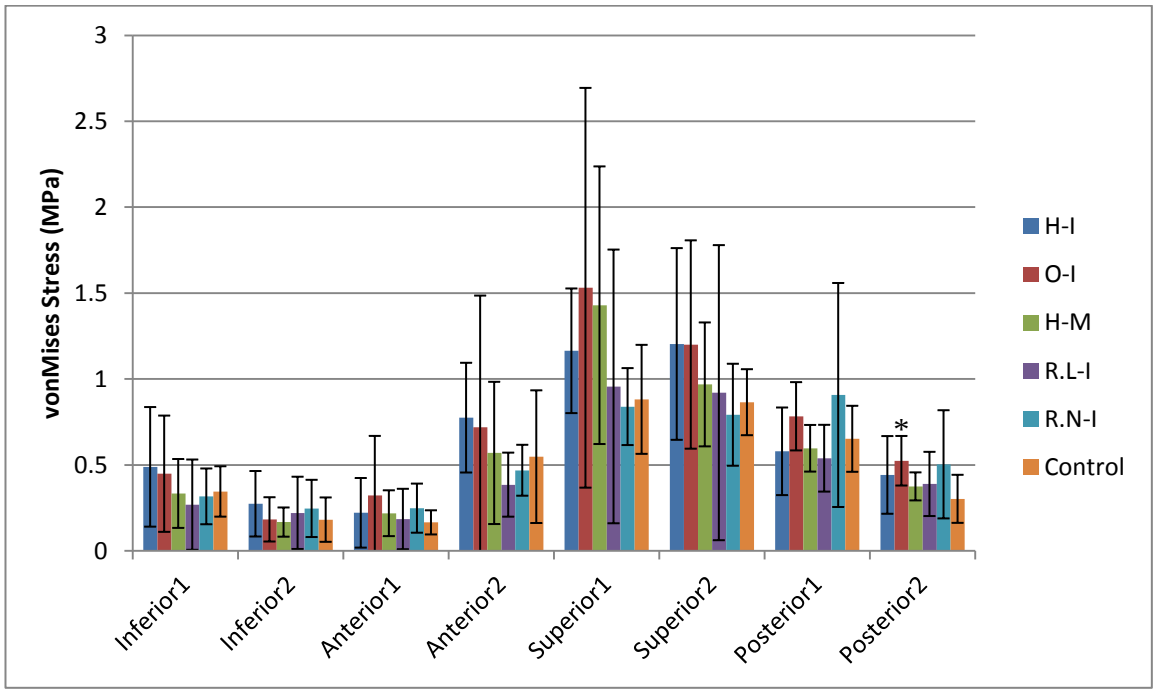

Figure 4.3.2 *Mean vonMises stress (MPa) in the lateral falling condition from the trabecularbone at different regions from all groups. Error bars represent the standard deviation. * represents the significant difference if any.*

5. DISCUSSION

5.1. Analysis of Results and Comparison with Previous Studies

The objective of this thesis study was to investigate whether the long term history of different exercise loading can modulate the femoral neck strength in the lateral fall condition. For this purpose FE models were constructed based on the MRI data of total of thirty six female subjects, which fell into six distinct exercise loading groups. From the FE models, the vonMises stress and the total deformation were simulated. The total deformation was used to observe the validity of the constructed FE models while the vonMises stresses were further analyzed. Regional mean vonMises stress values for eight equally divided anatomical regions from the smallest cross-section of the femoral neck was obtained and were used for the comparison of them between each exercise group and the control group.

Previous study on cortical geometry indicated that the history of some impact exercise may alter the strength of the femoral neck at some regions in the lateral falling condition. Specifically, Nikander et al. (2009) found that H-I and O-I groups had 20% thicker cortex at anterior and posterior regions and the H-I athletes had up to 60% thicker cortex at the inferior region. Most importantly, O-I athletes had 15% thicker cortex at the superior part of the femoral neck than other groups. Figure 4.3.1 shows that the mean cortical stress value at the anterior and posterior regions from the H-I and O-I groups did not seem different from other groups. Thus, the advantage of thicker cortex due to specific impact loading could not be seen at these regions in this study. On the other hand, the stress value at the inferior regions from the H-I groups were the lowest among the groups even though no significant difference was found between the H-I and the control groups. This indicates that thicker cortex due to the H-I exercise may contribute to lower stress value in the inferior part of the femoral neck. However, the low stress value at the inferior region is less important than the high value at the superior part in the lateral falling. Conversely, the H-I group had the highest stress values at the superior part. This high stress can increase the likelihood of the femoral neck fracture due to the lateral falling as discussed previously. Most importantly, the stress value at the superior regions from the O-I groups was lower than that from the control group. This indicates that thickened cortical bones from the O-I exercise may have an advantage to reduce the likelihood of the fracture. The H-M athletic groups such as power lifters had relatively low stress values in all regions. Also, R.L-I group such as long distance runners had very low values at most of the regions. These low stress values most likely attribute to the lower body weights of the subjects in the H-M and R.L-I

groups than those in other groups. Comparing the stress values at the superior regions between in the cortical bone and the trabecular bone, the O-I and the H-M groups had relatively lower values than the control group in the cortical bone while they had relatively higher values in the trabecular bone. This suggests that if the cortical bone carries more stresses, the trabecular bone may carry less stress or vice versa.

Cortical vonMises stress values in this study were approximately ten times larger than those in the trabecular bones. Most likely, this was due to the difference in the Young's modulus values assigned into each material. The modulus assigned into the trabecular bone was 1871MPa compared to 19GPa assigned to the cortical bone. The two moduli differed by a factor of 10, which made the difference in the stress value as the result. Magnitude of the vonMises stress in the femoral neck in this study was similar to those reported in the previous studies (Keyak et al. 1990; Crabtree et al. 2000; Voo et al. 2004; Mayhew et al. 2005; Cristofolini et al. 2007). The vonMises stress in the cortical bone of the femoral neck in this study ranged approximately from 5 to 25MPa. This result is very similar to ones from Cristofolini and his colleagues' study (2007) which loading condition was also very similar to the one used in this study. Therefore, based on the stress values under the simulated lateral falling condition, this result suggests that validation of the created FE models can be achieved for some degree.

Total deformation was also calculated from the FE models to verify the validity of the created FE models. Results showed the total deformation from this study was approximately one-tenth of the reported values from the experimental study of the cadaveric femur bones from Courtney et al. (1995). Courtney et al. (1995) reported the cadaveric femur bone from a woman who was thirty-one years old at the time of death deformed about 2mm in the experimental lateral falling condition with the impact force of 5000N. Average of 5046N was also applied to the FE models of the proximal femur bone in this thesis. Therefore, this result suggested that the constructed FE models were not validated by the total deformation values. However, this can attribute to several factors. The impact force in this thesis was applied nearly perpendicular to the axis of the femoral neck while the force in the study of Courtney et al. (1995) was applied far off from the axis. Since the bone has high load bearing capacity to the force on its axis, this could decrease the total deformation in this study. Besides, the force was applied on the surface of the femoral head although the actual force is applied on the lateral side of greater trochanter when the falling occurs. Second, the assumption was made that the trabecular bone was the isotropic material in the constructed FE models. Indeed, it has high anisotropy and the porosity varies greatly depending on the location even in the same bone. Due to this anisotropy, the bone behaves mechanically different depending on the direction of force applied. Therefore, this assumption might also contribute to the decrease in the deformation of the bone. Moreover, the material property of the trabecular bone might be overestimated and this might have contributed to small changes in the deformation. Third, the proximal femurs were modeled as the homogenous two-material. However, as discussed before, the bone is the inhomogeneous ma-

terial. Taddei et al. (2006) also reported that correlation between the FE model and experimental testing was reduced if the bone was modeled as the homogeneous material. Furthermore, internal muscle force was not included in the constructed FE models in this thesis. Especially, hip abductors can pull the greater trochanter, which may lead further bending of the femoral neck. In the future study, it should also be focused to find the error sources causing this too small deformation and fix them to improve the validity of the FE models.

Results showed that the simulated lateral fall condition successfully created the concentrated high stress distributions around the femoral neck area (Figure 4.1.1). This result was consistent with the study conducted by Bessho et al. (2009). According to Bessho et al. (2009), the simulated lateral loading condition used in this study was supposed to create more fracture at the femoral neck regions than the trochanteric regions. This means that higher stress distribution should be seen around the femoral neck regions. As discussed in the subchapter 2.2.3 (Fracture Mechanism), locally in the femoral neck region, there should be higher stress at the superior part than the inferior part when the lateral fall occurs. This higher stresses in the superior parts were clearly seen in Figure 4.3.1 and Figure 4.3.2. Therefore, the simulated lateral falling condition successfully created the preferred result in this thesis.

5.2. Limitations and For Further Studies

This study included only six subjects in each group making up a total of thirty six subjects. Although statistical analysis was performed, its statistical power was too low to make any conclusive indications out of this study. Therefore, this study only indicates the preliminary finding. Moreover, this poor statistical result could attribute to the high variability of the geometry. Depending on the body size, the size of bone varies. Besides, individual anatomical condition such as anteversion, retroversion, vargus, and valgus can increase this variability even higher.

To author's knowledge, in all of the previous femur FE modeling studies, their FE models were created based on the CT images of the cadaver femurs (Duda et al. 1998; Keyak et al. 1998, 2001a, 2001b, 2011; Wirtz et al. 2000, 2003; Polgár et al. 2003b; Taddei et al. 2004, 2007; Bitsakos et al. 2005; Cristofolini et al. 2007; Bessho et al. 2007, 2009; Helgason et al. 2008). It is well known that the CT images can provide very accurate bone geometric data due to high X-ray attenuation coefficient of bone while the MRI data can provide good geometric details of soft tissues such as muscle, tendons, and ligament. QCT can provide higher spatial resolution (around 0.5mm as opposed to 0.9 mm for the MRI data in this study). Therefore, this limitation does not only make our study be less comparable with previous CT-based femur FE modeling studies, but also make the geometry less accurate than others from the CT-based FE studies. However, using CT image device was not an option in this study because it is unethical to expose the fertile-aged young women to high dose of ionizing radiation for non-diagnostic purposes.

The FE models need to be validated with the mechanical testing of the bones. Our geometries were obtained from the MRI data of the young living subjects. Therefore, it is obviously out of consideration to perform the destructive mechanical test. However, it was also found that the MRI is a useful method for assessing the cortical bone structure at the femoral neck (McKay et al. 2004; Gomberg et al. 2005; Sievanen et al. 2007). In spite of this fact, to author's knowledge, the accuracy of the MRI-based FE models has not been validated, yet. Therefore, one of the further studies should include the MRI-based FE modeling using a cadaveric femur bones and the destructive mechanical testing to investigate the accuracy of the MRI-based FE models. It is also noteworthy to mention that segmentation of the MRI data was performed manually. This could contribute for the further error if reliability of the manual segmentation was low.

In this thesis, the homogeneous material property assigning method called two-material method was used, in which each cortical and trabecular bone material had fixed values for their Young's moduli throughout the entire geometries. However, as discussed previously, the bone is inhomogeneous material which density varies from one location to another even within the same bone such as femur. The material property assigned into the FE models in this study was Young's modulus and the Poisson's ratio. This Young's modulus varies depending on the bone apparent density. Inhomogeneous material FE models have already been introduced by some previous researchers and result shows better accuracy than the homogeneous material FE models. However, so far, CT image is the least requirement to build the FE model as inhomogeneous material. Therefore, inhomogeneous material FE models could not be created in our study because the geometry was derived from the MRI data. In spite of this drawback, the homogeneous FE models' accuracy is still acceptable. (Keyak et al. 1990; Taddei et al. 2006.) In addition, the FE models were created as the isotropic material. This means that created FE models in this thesis behave mechanically same in all directions. As discussed previously, however, the actual bone behaves mechanically different depending on the direction of force applied. This property is called anisotropic material behavior and the FE models should have this anisotropy instead of the isotropic material behavior. Researchers have worked on finding the true mechanical behavior of bone for all directions. Sufficient data to create accurate anisotropic FE femur models should be available from literatures in near future. (Wirtz et al. 2000, 2003.) Therefore, in our future studies, the FE models should also include the anisotropic material behavior.

In this study, the vonMises stress was obtained from the each FE model for the analysis. However, obtaining the stress values is not practical to assess the femoral neck strength. The fracture load should rather be computed from the models. To predict the fracture load, Keyak and his colleagues (1998, 2001a, 2001b, 2011) calculated a factor of safety (FOS) for each element using the distortion energy theory of failure. The FOS can be calculated by dividing element strength (obtained from the CT scan data) by element vonMises stress (computed from the FE models). They defined the fracture load as the load at which the FOS for 15 contiguous non-surface elements was less than 1.0. This method cannot be used in this study because our FE models were

based on the MRI data. However, in order to assess the femoral neck strength more precisely, a method to compute the fracture loads from the MRI-based FE models needs to be developed in the future studies.

Only one boundary condition was simulated in this study. Bessho et al., (2009) simulated four more lateral falling conditions by changing the directions and locations of the impact force (Figure 2.3.2.2). They reported the fracture loads and locations were varied when the loading direction was altered. Furthermore, the spontaneous fracture of the proximal femur caused by the atraumatic loading has also been well studied by numerous researchers. Spontaneous fracture of the proximal femur is caused by either physiological or sudden loadings and is typically simulated at 10% of the gait cycle (single-leg stance) (Duda et al. 1998; Keyak et al. 1998; Polgár et al. 2003b; Bitsakos et al. 2005). This spontaneous fracture usually occurs to the osteoporotic patients and is not common in the healthy adults. Stumbling or mis-stepping can create a high peak force on the femoral head during the gait, which can end up with the fracture. (Keyak et al. 2001a.) As discussed, the femoral neck structure varies depending on the history of types of the impact exercise. These different femoral neck structures may response in a different way depending on the lateral falling conditions. Relatively low stress values were found at the superior cortex in the O-I group. However, it is still not clear if O-I group's femoral neck behaves mechanically similar or differently if the force directions are altered. For example, the O-I group's femoral neck may behave mechanically weak to the specific lateral falling condition. Therefore, the future study needs to answer this question as well.

As discussed in the subchapter 2.3.7, the FE models did not include any internal muscle forces in the present study. It was found that the involvement of the internal muscle forces can alter the result of the FE models (Duda et al. 1998; Polgár et al. 2003b; Bitsakos et al. 2005). When people fall laterally and their lateral side of the greater trochanter receives the impact, the hip can be slightly adducted. In this case, the superior part of the greater trochanter, where muscles are attached, can experience high tension forces created by the hip abductor muscles; gluteus medius and minimus (Figure 2.3.7.1). Several researches reported the involvement of these internal muscles forces did not affect the stress state in the head-neck region under the single leg condition (Keyak et al. 2005; Cristofolini et al. 2007). However, they did not investigate the effect of those muscle forces in the lateral falling conditions. Therefore, it should also be considered to include the internal muscle forces in the FE models in the future studies.

In this thesis, the subject specific impact force (average ±SD: 5046.0 ±404.8 N) ranging from minimum of 4212.6N to maximum of 5984.1N was applied to the bones. In the study of Robinovitch et al. (195), in order to simulate more realistic falling condition, they studied if the trochanteric soft tissue could contribute to absorb the impact force in the falling condition. They found that the trochanteric soft tissue can decrease peak impact force by an average of 13±15% during falling and the peak impact force can decrease linearly with increasing soft tissue thickness at a rate of about 70N per 1mm thickness of the soft tissues. Fortunately, our femur bone geometry is based on

the MRI image, which shows soft tissue such as muscle and adipose tissue more precisely than the CT image data. Thus, thickness of the soft tissue can be easily obtained. By taking this into consideration, more realistic subject specific impact force can be obtained and this can be unique aspect from the data used in this study. Therefore, this should certainly be considered in our future studies.

In the future study, first the number of the subjects should be increased to acquire more conclusive results with the higher statistical power. It is planned for the next study that total of 111 subjects will be used to construct the FE models and each group contains approximately 18 subjects. This should provide us more accurate information on the question stated in this thesis. As discussed so far, in order to construct more accurate and realistic models, following should be included in the further studies: investigation of the correlation between the mechanical testing of the cadaveric bone and the FE model based on its MRI data for the validation of the FE model, the anisotropic material modeling of bone, simulating the fracture load, inclusion of the hip abductor muscles, and calculation the force attenuation due to the soft tissues. Although modeling all 111 subjects is the promising method to obtain the accurate result, it requires the large amounts of work load and especially time. Instead, it might be worth constructing one representative model for each group. It is feasible to create such model by obtaining the group-specific structural similarities of the proximal femurs. These similarities can be found by the mathematical procedure such as principle component analysis (PCA). Utilizing the PCA, the group representative model can be implemented. Then, this representative model needs to be validated by measuring its correlation with all FE models in a group for a loading condition. If the correlation is high, only 6 group representative models can be used for various loading conditions. To study the influence of the exercise history under other lateral falling conditions, reducing the number of required FE models can accelerate the research progress drastically.

The FE method is not only useful for the hip fracture study, but it can also be utilized to realize more about the exercise-induced bone functional adaptation. Instead of applying traumatic loading conditions such as the fallings, exercise specific loading conditions can be applied to the given proximal femur models. For example, the loading condition at the point when high jumpers take off can be applied to study if resultant stress distribution would match to the H-I exercise-induced structural advantage such as thicker cortex at some regions of the femoral neck. Those thicker cortex regions of the proximal femur should experience higher stresses than other regions because these cortical bones are ought to be induced by this H-I exercise. The proximal femurs from other exercise groups may behave mechanically differently under such loading condition. Applying the exercise specific loading condition may give us more understanding of mechanical behavior of the bone due to the structural differences. For example, the proximal femurs from some impact exercise athletes may not have good load bearing capacity in such loading condition. To simulate such loading condition, it is required to have force magnitude and direction, and the location where the force is applied on the femoral head. Such information can be obtained from either experiments or previous

researches, from which kinetic data with synchronous kinematic data are available. Throughout kinetic measurement, the force information is acquired while the force direction and the location can be calculated by the joint angles measured by the kinematic measurement. For example, Bergmann and his colleagues (2001) measured hip contact force during the gait cycles with the instrumented hip implant, the kinematic motion analysis of the gait, and kinetic measurement using the force platform. If similar kinds of data for some sports can be measured or obtained from the literature, this exercise specific loading becomes possible. Moreover, the hip contract force information during the complete gait cycle is available from Bergmann et al. (2001). This allows us to construct FE models not only for the static analysis, but also for dynamic analysis since the force data is available from the entire movement. Fortunately, ANSYS Academic Research license from CSC includes *ANSYS Autodyn* software, which allows us the dynamic simulation of the structure. In the further studies, both static and dynamic simulation of various loading conditions including both traumatic and exercise specific conditions should be simulated to understand more about the mechanical behavior of bone and the influences of the exercise history.

6. CONCLUSION

This thesis project was primarily aimed to investigate the association of different impact loading exercise history with the proximal femoral strength in the lateral falling condition using the FE method. As the proximal femur adapted to long-term multidirectional impact loading seemed to have somewhat better load bearing capacity in the same falling condition than proximal femurs in other exercise loading groups, a lower hip fracture risk is indicated. This leads us to provide a recommendation for both young and older people that these kinds of exercises should be included in their exercise regimen to strengthen their proximal femur to prevent the fracture from the falling

Results of this study showed that the history of impact loading exercise may affect the stress distribution at the femoral neck region in the falling condition. Athletes who have been involved in high impact loading exercises such as triple jump and high jump had lower stress values in the inferior regions of the femoral neck under the simulated lateral falling condition from the FE models in this thesis. These athletes have much thicker cortical wall at the inferior regions, which apparently contributed to the low stress values in these regions. However, regarding the hip fracture the strength at the superior region of the femoral neck is more important than the strength at the inferior part because unusual high stress occurs at the superior regions in the lateral fall. Athletes who have done odd impact loading exercises such as football and squash have slightly thicker cortex at the superior regions. Therefore, the focus was especially put on whether the stress values at the superior regions in these athletes were lower than those in the controls. It was observed the stress values at the superior regions in these athletes were relatively lower than those in the controls. This indicates that including the odd impact loading exercises may be advantageous in terms of strengthening the femoral neck in order to decrease the risk of femoral neck fractures. However, the results observed in this thesis did not reach any significance. This can be due to the low number of subjects studied in this project and very high variability of individual geometry. Therefore, the number of subjects needs to be increased in the future studies.

Developing the means for creating FE models of the proximal femur using the FE modeling software ANSYS was the secondary objective in this thesis. This was well accomplished; however, despite the consistent and logical results the validation of the created FE models is still not clear in the present study and needs to be ensured in the future study. Besides, accuracy of the FE models was lowered mainly by following: MRI data as the geometry source, manual segmentation, assuming isotropic and homogeneous material properties and exclusion of the internal muscle force and force attenuation effect of soft tissues. In the future study, not only the number of subjects should

be increased, but also the focus should be put on ensuring the validity of the FE models. Also, instead of measuring the stress value, a method of measuring the fracture load through the MRI-based FE model should be developed to enable to compare the result with previous FE modeling studies. Further, as only one lateral falling condition was simulated in the present study, the future study should include several lateral falling conditions to investigate if influence of the different impact loading history varies depending on the lateral falling conditions.

Although findings are preliminary, they indicate that exercise-induced structural advantages, such as thicker cortex at some regions in the femoral neck, can contribute to the lower stress values. This suggests that certain impact exercise may be advantageous to be included in the exercise regime to decrease the likelihood of the hip fracture especially femoral neck fractures. Especially so, because the O-I exercises are apparently less risky for older people, it should be considered to include these exercises to strengthen their femoral neck against the fractures.

REFERENCES

Alonso, C.G., Curiel, M.D., Carranza, F.H., Cano, R.P., Pérez, A.D. & the Multicenter Project for Research in Osteoporosis. 2000. Femoral Bone Mineral Density, Neck-Shaft Angle and Mean Femoral Neck Width as Predictors of Hip Fracture in Men and Women. Osteoporosis International 11, pp. 714-720.

Abrahamsen, B., van Staa, T., Ariely, R., Olson, M. & Cooper, C. 2009. Excess mortality following hip fracture: systematic epidemiological review. Osteoporosis International 20, pp. 1633-1650.

Adami, S., Gatti, D., Braga, V., BIanchini, D. & Rossini, M. 1999. Site-specific effects of strength training on bone structure and geometry of ultradistal radius in postmenopausal women. Journal of Bone and Mineral Research 14, pp. 120-124.

Azhar, A., Lim, C., Kelly, E., O'Rourke, K., Dudeney, S., Hurson, B. & Quinlan, W. 2008. Cost induced by hip fractures. Irish Medical Journal 101, 7, pp. 213-218.

Bagi, C.M., Wilkie, D., Georgelos, K., Williams, D. & Bertolini, D. 1997. Morphological and Structural Characterics of the Proximal Femur in Human and Rat. Bone 21, 3, pp. 261-267.

Baim, S. & Leslie, W.D. 2012. Assessment of Fracture Risk. Current Osteoporosis Reports 10, 1, pp. 28-41.

Bass, S.L., Saxon, L., Daly, R.M., Turner, C.H., Robling, A.G., Seeman, E. & Stuckey, S. 2002. The effect of mechanical loading on the size and shape of bone in pre-, peri- and postpubertal girls: a study in tennis players. Journal of Bone and Mineral Research 17, pp. 2274-2280.

Bayraktar, H.H., Morgan, E.F., Niebur, G.L., Morris, G.E., Wong, E.K. & Keaveny, T.M. 2004. Comparison of the elastic and yield properties of human femoral trabecular and cortical bone tissue. Journal of Biomechanics 37, pp. 27-35.

Beck, T.J., Looker, A.C., Ruff, C.B., Sievänen, H. & Wahner, H.W. 2000. Structural Trends in the Aging Femoral Neck and Proximal Shaft: Analysis of the Third National Health and Nutrition Examination Survey Dual-Energy X-Ray Absorptiometry Data. Journal of Bone and Mineral Research 15(12), pp. 2297-2304.

Bergmann, G., Deuretzbacher, G., Heller, M. Graichen, F., Rohlmann, A., Strauss, J. & Duda, G.N. 2001. Hip contact forces and gait patterns from routine activities. Journal of Biomechanics 34, pp. 859-871.

Bessho, M., Ohnishi, I., Matsuyama, J., Matsumoto, T., Imai, K. & Nakamura, K. 2007. Prediction of strength and strain of the proximal femur by a CT-based finite element method. Journal of Biomechanics 40, pp. 1745-1753.

Bessho, M., Ohnishi, I., Matsumoto, T., Ohashi, S., Matsuyama, J., Tobita, K., Kaneko, M. & Nakamura, K. 2009. Prediction of proximal femur strength using a CT-based nonlinear finite element method: Differences in predicted fracture laod and site with changing load and boundary conditions. Bone 45, pp. 226-231.

Bitsakos, C., Kerner, J., Fisher, I. & Amis, A.A. 2005. The effect of muscle loading on the simulation of bone remodelling in the proximal femur. Journal of Biomechanics 38, pp. 133-139.

Black, D.M., Bouxsein, M.L., Marshall, L.M., Cummings, S.R., Lang, T.F., Cauley, J.A., Ensrud, K.E., Neilson, C.M. & Orwoll, E.S. 2008. Proximal Femoral Structure and the Prediction of Hip Fracture in Men: A Large Prospective Study Using QCT. Journal of Bone and Mineral Research 23(8), pp. 1326-1333.

Bolotin, H.H. & Sievänen, H. 2001. Inaccuracies inherent in dual-energy X-ray absorptiometry in vivo bone mineral density can seriously mislead diagnostic/prognostic interpretations of patient-specific bone fragility. Journal of Bone and Mineral Research 16, 5, pp. 799-805.

Bolotin, H.H. 2007. DXA *in vivo* BMD methodology: An erroneous and misleading research and clinical gauge of bone mineral status, bone fragility, and bone remodelling. Bone 41, pp. 138-154.

Bouxsein, M.L., Szulc, P., Munoz, F., Thrall, E., Sornay-Rendu, E. & Delmas, P.D. 2007. Contribution of Trochanteric Soft Tissues to Fall Force Estimates, the Factor of Risk, and Prediction of Hip Fracture Risk. Journal of Bone and Mineral Research 22, 6, pp. 825-831.

Burr, D.B., Robling, A.G. & Turner, C.H. 2002. Effect of biomechanical stress on bone in animals. Bone 30, pp. 781-786.

Burstein, A.H., Reilly, D.T. & Martens, M. 1976. Aging of Bone Tissue: Mechanical Properties. Journal of Bone and Joint Surgery 58-A, 1, pp. 82-86.

Carpenter, R.D., Beaupre, G.S., Lang, T.F., Orwoll, E.S. & Carter, D.R. 2005. New QCT analysis approach shows the importance of fall orientation on femoral neck strength. Journal of Bone and Mineral Research 20, pp. 1533-1542.

Carter, D.R. & Hayes, W.C. 1976. Bone compressive strength: The influence of density and strain rate. Science(194), pp. 1174-1176.

Carter, D.R., Hayes, W.C. 1977. The compressive behavior of bone as a two-phase porous structure. Journal of Bone and Joint surgery 59, pp. 954-962.

Cody, D.D., Gross, G.J., Hou, F.J., Spencer, H.J., Goldstein, S.A. & Fyhrie, D.P. 1999. Femoral strength is better predicted by finite element models than QCT and DXA. Journal of Biomechanics 32, pp. 1013-1020.

Cooper, C., Campion, G. & Melton, L.J.III. 1992. Hip Fractures in the Elderly: A World-Wide Projection. Osteoporosis International 2, pp. 285-289.

Courtney, A.C., Wachtel, E.F., Myers, E.R. & Hayes, W.C. 1995. Age-related reductions in the strength of the femur tested in a fall-loading configuration. Journal of Bone and Joint Surgery, American Volume 77, 3, pp. 387-395.

Crabtree, N., Lunt, M., Holt, G., Kröger, H., Burger, H., Grazio, S., Khaw, K.-T., Lorenc, R.S., Nijs, J., Stepan, J., Falch, J.A., Miazgowski, T., Raptou, P., Pols, H.A.P., Dequeker, J., Havelka, S., Hosowski, K., Jajic, I., Czekalski, S., Lyritis, G., Silman, A.J. & Reeve, J. 2000. Hip Geometry, Bone Mineral Distribution, and Bone Strength in European Men and Women: The EPOS Study. Bone 27(1), pp. 151-159.

Cristofolini, L., Juszczyk, M., Martelli, S., Taddei, F. & Viceconti, M. 2007. In *vitro* replication of spontaneous fractures of the proximal femur. Journal of Biomechanics 40, pp. 2837-2845.

Cummings, S.R., Rubin, S.M. & Black, D. 1990. The future of hip fractures in the United State; numbers, costs, and potential effect of postmenopausal estrogen. Clinical orthopaedics and related research 252, pp. 163-166.

Cummings, S.R., Black, D.M., Nevitt, M.C., Browner, W., Cauley, J., Ensrud, K., Genant, H.K., Palermo, L., Scott, J. & Vogt, T.M. 1993. Bone density at various sites for prediction of hip fractures. The Lancet 341, pp. 72-75.

Cumming, R.G. & Klinegerg 1994. Fall frequency and characteristics and the risk of hip fracture. Journal of the American Geriatrics Society 42(7), pp. 774-778.

Cummings, S.R. & Melton, L.J.III. 2002. Epidemiology and outcomes of osteoporotic fractures. The Lancet359, pp. 1761-1767.

Daly, R.M. 2007. The effect of exercise on bone structural geometry during growth. Medicine and Sports Science 51, pp. 33-49.

de Bakker, P.M., Manske, S.L., Ebacher, V., Oxland, T.R., Cripton, P.A. & Pierre, G. 2009. During sideways falls proximal femur fractures initiate in the superolateral cortex: Evidence from high-speed video of simulated fracture. Journal of Biomechanics 42, pp. 1917-1925.

Ducher, G., Daly, R.M. & Bass, S.L. 2009. Effects of repetitive loading on bone mass and geometry in young male tennis players: a quantitative study using MRI. Journal of bone and Mineral Research 24, pp. 1686-1692.

Duda, G.N., Heller, M., Albinger, J., Schulz, O., Schneider, E. & Claes, L. 1998. Influence of muscle forces on femoral strain distribution. Journal of Biomechanics 31, pp. 841-846.

Duncan, R.L. & Turner, C.H. 1995. Mechanotransdution and the Functional Response to Bone to Mechanical Strain. Calcified Tissue International 57, pp. 344-358.

Eriksen, E.F., McKercher, S.R. & Melsen, F. 1986. Trabecular bone remodeling and balance in primary hyperparathyroidism. Bone 7, pp. 213-221.

Fang, Q. 2009. iso2mesh: a 3D surface and volumetric mesh generator for matlab/octave (version 0.7.9-1) [Computer software]. Boston, MA: Harvard University Photon Migration Lab, Martinos Center for Biomedical Engineering & Massacheusetts General Hospital (Harvard Medical School). Retrieved July 8, 2012. Available from http://iso2mesh.sourceforge.net/

Forwood, M.R. & Burr, D.B. 1993. Physical activity and bone mass: exercise in futility? Bone and Mineral 21, 2, pp. 89-112.

Frost, H.M. 1987. Bone “mass” and the “mechanostat”: a proposal. Anatomical Record, 219, 1, pp. 1-9.

Garden, R.S. 1961. The Structure and Function of the Proximal End of the Femur. The Journal of Bone and Joint Surgery 43B, 3, pp. 576-589.

Garnier, K.B., Dumas, R., Rumelhart, C. & Arlot, M.E. 1999. Mechanical characterization in shear of human femoral cancellous bone: torsion and shear tests. Medical Engineering & Physics 21, pp. 641-649.

Glueer, C.C., Cummings, S.R., Pressman, A., Li, J., Glueer, K., Faulkner, K.G., Grampp, S., Genant, H.K., & the Study of Osteoporotic Fractures Research Group. 1994. Precition of hip fractures from pelvic radiographs: the study of osteoporotic fractures. Journal of Bone and Mineral Research 9, pp. 671-677.

Goldstein, S.A., Wilson, D.L., SOnstegard, D.A., & Matthews, L.S. 1983. The Mechanical Properties of Human Tibial Trabecular Bone as a Function of Metaphyseal Location. Journal of Biomechanics 16, pp. 965-969.

Goldstein, S.A. 1987. The Mechanical Properties of Trabecular Bone: Dependence on Anatomic Location and Function. Journal of Biomechanics 20, 11-12, pp. 1055-61.

Gomberg, B.R., Saha, P.K. & Wehrli, F.W. 2005. Method for cortical bone structural analysis from magnetic resonance images. Academic Radiology 12, pp. 1320-1332.

Greenspan, S.L., Myers, E.R., Maitland, L.A., Resnicck, N.M. & Hayes, W.C. 1994a. Fall severity and bone mineral density as risk factors for hip fracture in ambulatory elderly. Journal of the American Medical Association 271(2), pp. 128-133.

Greenspan, S.L., Myers, E.R., Maitland, L.A., Kido, T.H., Krasnow, M.B. & Hayes, W.C. 1994b. Trochanteric bone mineral density is associated with type of hip fracture in the elderly. Journal of Bone and Mineral Research, 9, pp. 1889-1894.

Greenspan, S.L., Myers, E.R., Kiel, D.P., Parker, R.A., Hayes, W.C. & Resnickk, N.M. 1998. Fall Direction, Bone Mineral Density, and Function: Risk Factors for Hip Fracture in Frail Nursing Home Elderly. The American Journal of Medicine 104(6), pp. 539-545.

Grisso, J.A., Kelsey, J.L., Strom, B.L., Chiu, G.Y., Maislin, G., O’Brien, L., Hoffman, S., Kaplan, F. & The Northeast Hip Fracture Study Group. 1991. Risk factors for falls as a cause of hip fracture in women. The New England Journal of Medicine 324, 19, pp. 1326-1331.

Gullberg, B., Johnell, O. & Kanis, J.A. 1997. World-wide Projections for Hip Fractures. Osteoporosis International 7, pp. 407-413.

Haapasalo, H., Kontulainen, S., Sievänen, H., Kannus, P., Järvinen, M. & Vuori, I. 2000. Exercise-induced bone gain is due to enlargement in bone size without a cahgne in volumetric bone density: A peripheral quantitative computed tomography study of the upper arms of male tennis players. Bone 27, pp. 351-357.

Haentjens, P., Autier, P., Barette, M. & Boonen, S. 2001. The economic cost of hip fractures among elderly women. A one-year, prospective, observational cohort study with matched-pair analysis. Belgian Hip Fracture Study Group. Journal of Bone and Joint Surgery 83-A, 4, pp. 493-500.

Hayes, W.C., Myers, E.R., Morris, J.N., Gerhart, T.N., Yelt, H.S. & Lipsitz, L.A. 1993. Impact near the hip dominates fracture risk in elderly nursing home residents who fall. Calcified Tissue International 52(3), pp. 192-198.

Hayes, W.C., Myers, E.R., Robinovitch, S.N. & van den Kroonenberg, A. 1996. Etiology and prevention of age-related hip fracture. Bone 18(Suppl), pp. 77S-86S.

Heinonen, A., Oja, P., Kannus, P., Sievänen, H., Manttari, A. & Vuori, I. 1993. Bone mineral density of female athletes in different sports. Bone and Mineral 23, 1, pp. 1-14.

Heinonen, A., Oja, P., Kannus, P., Sievänen, H., Haapasalo, H., Manittari, A. & Vuori, I. 1995. Bone mineral density in female athletes representing sports with different loading characteristics of the skeleton. Bone 17, pp. 197-203.

Heinonen, A., Sievänen, H., Kyröläinen, H., Perttunen, J. & Kannus, P. 2001. Minera Mass, Size, and Estimated Mechanical Strength of Triple Jumpers' Lower Limb. Bone 29, pp. 279-285.

Heinonen, A., Sievänen, H., Kannus, P., Oja, P. & Vuori, I. 2002. Site-specific skeltal response to long-term weight training seems to be attributable to pricipal loadig modality: A pQCT study of female weightlifters. Calcified Tissue International 70, 6, pp. 469-474.

Helgason, B., Perilli, E., Schileo, E., Taddei, F., Brynjólfsson, S. & Viceconti, M. 2008. Mathematical relationships between bone density and mechanical properties: A literature review. Clinical Biomechanics 23, pp. 135-146.

Hernandez, C.J., Beaupré, G.S.& Carter, D.R. 2000. A model of mechanobiologic and metabolic influences on bone adaptation. Journal of Rehabilitation Research and Development 37, 2, pp. 235-244.

Jaworski, Z.F., Liskova-Kiar, M. & Uhthoff, H.K. 1980. Effect of long-term immobilisation on the pattern of bone loss in older dogs. Journal of Bone & Joint Surgery, British Volume 62B, pp. 104-110.

Johnell, O. 1997. The Socioeconomic Burden of Fractures: Today and in the 21st Century. The American Journal of Medicine 103(Suppl.1), pp. S20-S26.

Johnell, O. & Kanis, J.A. 2004. An estimate of the worldwide prevalence, mortality and disability associated with hip fractures. Osteoporosis International 15, pp. 897-902.

Johnell, O. & Kanis, J.A. 2005. Epidmiology of osteoporotic fractures. Osteoporosis International 16(Suppl.2), pp. S3-S7.

Johnell, O., Kanis, J.A., Oden, A., Johansson, H., Laet, C.D., Delmas, P., Eisman, J.A., Fujikawa, S., Kroger, H., Mellstrom, D., Meunier, P., Melton III, L.J., O'Neill, T., Pols, H., Reeve, J., Silman, A. & Tenenhouse, A. 2005. Predictive Value of BMD for Hip and Other Fractures. Journal of Bone and Mineral Research 20(7), pp. 1185-1194.

Johnell, O. & Kanis, J.A. 2006. An estimate of the worldwide prevalence and disability associated with osteoporotic fractures. Oseoporosis International 17, pp. 1726-1733.

Järvinen, T.L.N., Kannus, P. & Sievänen, H. 1999. Have the DXA-based exercise studies seriously underestimated the effects of mechanical loading on bone? Journal of Bone and Mineral Research 14, pp. 1634-1635.

Järvinen, T.L.N. Pajamäki, I., Sievänen, H., Vuohelainen, T., Tuukkanen, J., Järvinen, M. & Kannus, P. 2003. Femoral neck response to exercise and subsequent deconditioning in young and adult rats. Journal of Bone and Mineral Research 18, pp. 1292-1299.

Järvinen, T.L.N., Sievänen, H., Jokihaara, J. & Einhorn, T.A. 2005. Revival of bone strength: the bottom line. Journal of Bone and Mineral Research 20, pp. 717-720.

Järvinen, T.L.N., Sievänen, H., Khan, K.M., Heinonen, A. & Kannus, P. 2008. Shifting the focus in fracture prevention from osteoporosis to falls. BMJ 336, 7636, pp. 124-126. [accessed on 09.8.2012]. Available at: http://www.ncbi.nlm.nih.gov/pmc/articles/PMC2206310/pdf/bmj-336-7636-analysis-00124.pdf

Kanis, J.A. 2002. Diagnosis of osteoporosis and assessment of fracture risk. The Lancet 359, pp. 1929-1936.

Kanis, J.A., Oden, A., Johnell, O., De Laet, C., Jonsson, B. & Oglesby, A.K. 2003. The components of excess mortality after hip fracture. Bone 32, pp. 468-473.

Kanis, J.A., Borgstrom, F., Laet, C.D., Johansson, H., Johnell, O., Jonsson, B., Oden, A., Zethraeus, N., Pfleger, B. & Khaltaev, N. 2005. Assessment of fracture risk. Osteoporosis International 16, pp. 581-589.

Kanis, J.A., Johnell, O., Oden, A., Johansson, H. & McCloskey, E. 2008. FRAX and the assessment of fracture probability in men and women from the UK. Osteoporosis International 19(4), pp. 385-397.

Kanis, J.A., Odén, A., McCloskey, E.V., Johansson, H., Wahl, D.A. & Cooper, C. 2012. A systematic review of hip fracture incidence and probability of fracture worldwide. Osteoporosis International [electronic journal]. [accessed on 11.6.2012]. Available at: http://www.ncbi.nlm.nih.gov/pubmed/22419370

Kannus, P., Haapasalo, H., Sankelo, M., Sievänen, H., Pasanen, M., Heinonen, A., Oja, P. & Vuori, I. 1995. Effect of starting age of physical activity on bone mass in the dominant arm of tennis and squah players. Annals of Internal Medicine 123, 1, pp. 27.31.

Kannus, P., Uusi-Rasi, K., Palvanen, M. & Parkkari, J. 2005. Non-pharmacological means to prevent fractures among older adults. Annals of Medicine 37, 4, pp. 303-310.

Keaveny, T.M. & Hayes, W.C. 1993. A 20-Year Perspective on the Mechanical Properties of Trabecular Bone. Journal of Biomechanical Engineering 115, pp. 534-542.

Keller, T.S. 1994. Predicting the compressive mechanical behavior of bone. Journal of Biomechanics 27, pp. 1159-1168.

Kerr, D., Morton, A., Dick, I. & Prince, R. 1996. Exercise effects on bone mass in postmenopausal women are site-specific and load-dependent. Journal of Bone and Mineral Research 11, pp. 218-225.

Keyak, J.H., Meagher, J.M., Skinner, H.B. & Mote, C.D. Jr. 1990. Automated three-dimensional finite element modeling of bone: a new method. Journal of Biomedical Engineering 12, pp. 389-397.

Keyak, J.H. & Skinner, H.B. 1992. Three-dimensional finite element modeling of bone: effects of element size. Journal of Biomedical Engineering 14, pp. 483-509.

Keyak, J.H., Fourkas, M.G., Meagher, J.M. & Skinner, H.B. 1993. Validation of an automated method of three dimensional finite element modeling of bone. Jorunal of Biomedical Engineering 15, pp. 505-509.

Keyak, J.H., Rossi, S.A., Jones, K.A. & Skinner, H.B. 1998. Prediction of femoral fracture load using automated finite element modeling. Journal of Biomechanics 31, pp. 125-133.

Keyak, J.H., Rossi, S.A., Jones, K.A., Les, C.M. & Skinner, H.B. 2001a. Prediction of fracture location in the proximal femur using finite element models. Medical Engineering & Physics 23, pp. 657-664.

Keyak, J.H., Skinner, H.B. & Fleming, J.A. 2001b. Effect of force direction on femoral fracture load for two types of loading conditions. Journal of Orthopaedic Research 19, pp. 539-544.

Keyak, J.H., Kaneko, T.S., Tehranzadeh, J., & Skinner, H.B. 2005. Predicting proximal femoral strength using structural engineering models. Medical Engineering & Physics 23, pp.657-664.

Keyak, J.H., Sigurdsson, S., Karlsdottir, G., Oskarsdottir, D., Sigmarsdottir, A., Zhao, S., Kornak, J., Harris, T.B., Sigurdsson, G., Jonsson, B.Y., Siggeirsdottir, K., Eiriksdottir, G., Gudnason, V. & Lang, T.F. 2011. Male-female differences in the association between incident hip fracture and proximal femoral strength: A finite element analysis study. Bone 48, pp. 1239-1245.

Khan, K., Brown, J., Way, S., Vass, N., Crichton, K., Alexander, R., Baxter, A., Butler, M. & Wark, J. 1995. Overuse injuries in classical ballet. Sports Medicine 19, 5, pp. 341-357.

Khasraghi, F.A., Lee, E.J., Christmas, C. & Wenz, J.F. 2003. The economic impact of medical complications in geriatric patients with hip fracture. Orthopedics 26, 1, pp. 49-56.

Kim, S.H., Meehan, J.P., Blumenfeld, T. & Szabo, R.M. 2011. Hip Fractures in the United States: Nationwid Emergency Department Sample, 2008. Arthritis Care & Research 64, 5, pp. 751-758.

Kondo, A., Zierler, B.K., Isokawa, Y., Hagino, H. & Ito, Y. 2009. Comparison of outcomes and costs after hip fracture surgery in three hospitals that have different care systems in Japan. Health Policy 91, pp. 204-210.

Kontulainen, S., Sievänen, H., Kannus, P., Pasanen, M. & Vuori, I. 2002. Effect of long-term impact-loading on mass, size, and estimated strength of humerus and radius of female racquet-sports players: a peripheral quantitative computed tomogtraphy study between young and old starters and controls. Journal of Bone and Mineral Research 17, pp. 2281-2289.

Korhonen, N., Niemi, S., Parkkari, J., Sievänen, H., Palvanen, M. & Kannus, P. 2013a. Continuous decline in incidence of hip fracture: nationwide statistics from Finland between 1970 and 2010. Osteoporosis International 24, pp. 1599-1603.

Korhonen, Niina., Kannus, P., Niemi, S., Palvanen, M. & Parkkari, J. 2013b. Fall-induced deaths among older adults: nationwide statistics in Finland between 1971 and 2009 and prediction for the future. Injury. Article in Press. [accessed on 7.5.2013]. Available at: http://dx.doi.org/10.1016/j.injury.2013.03.004

Langton, C.M., Pisharody, S., & Keyak, J.H. 2009. Comparison of 3D finite element analysis derived stiffness and BME to determine the failure load of the excised proximal femur. Medical Engineering & Physics 31, pp. 668-672.

Lanyon, L.E. 1996. Using functional loading to influence bone mass and architecture: objectives, mechanisms, and relationship with estrogen of the mechanically adaptive process in bone. Bone 18,1 (Suppl 1), pp. S37-43

Lawrence, T.M., White, C.T., Wenn, R. & Moran, C.G. 2005. The current hospital costs of treating hip fractures. Injury 36, 1, pp. 88-91.

Lengsfeld, M., Schmitt, J., Alter, P., Kaminsky, J. & Leppek, R. 1998. Comparison of geometry-based and CT voxel-based finite element modeling and experimental validation. Medical Engineering and Physics 20, pp. 515-522.

Leppänen, O.V., Sievänen, H., Jokihaara, J., Pajamäki, I., Kannus, P. & Järvinen, T.L.N. 2008. PloS ONE 3(7), pp. 1-10.

Leslie, W.D., O'Donnel, S., Jean, S., Legacé, C., Walsh, P., Bancej, C., Morin, S., Hanley, D.A. & Papaioannou, A. 2009. Trends in Hip Fracture Rates in Canada. The Journal of the American Medical Association 302, 8, pp. 883-889.

Liu, L., Maruno, R., Mashimo, T., Sanka, K., Higuchi, T., Hayashi, K., Shirasaki, Y., Mukai, N., Saitoh, S. & Tokuyama, K. 2003. Effects of physical training on cortical bone at midtibia assesed by peripheral QCT. Journal of Applied Physiology 95, pp. 219-224.

Lotz, J.C., Gerhart, T.N. & Hayes, W.C. 1990a. Mechanical properties of trabecular bone from the proximal femur: a quantitative CT study. Journal of Computer Assisted Tomography 14, pp. 107-114.

Lotz, J.C. & Hayes, W.C. 1990b. The use of quantitative computed tomography to estimate risk of fracture of the hip from falls. Journal of Bone and Joint Surgery, American Volume 72, pp. 689-700.

Lotz, J.C., Gerhart, T.N. & Hayes, W.C. 1991a. Mechanical properties of metaphyseal bone in the proximal femur. Journal of Biomechanics 24, pp. 317-329.

Lotz, J.C., Cheal, E.J. & Hayes, W.C. 1991b. Fracture Prediction for the Proximal Femur Using Finite Element Models: Part I – Linear Analysis. Journal of Biomechanical Engineering 113, pp. 353-360.

Lotz, J.C., Cheal, E.J. & Hayes, W.C. 1991c. Fracture Prediction for the Proximal Femur Using Finite Element Models: Part II – Nonlinear Analysis. Journal of Biomechanical Engineering 113, pp. 361-365.

Lotz, J.C., Cheal, E.J. & Hayes, W.C. 1995. Stress distributions within the proximal femur during gait and falls: implications for osteoporotic fracture. Osteoporosis International 5, pp. 252-261.

Lönnroos, E., Kiviranta, I. & Hartikainen, S. 2010. Hip fracture management and outcomes. European Geriatric Medicine 1, pp. 101-103.

Matheson, G.O., Clement, D.B., McKenzie, D.C., Taunton, J.E., Lloyd-Smith, D.R. & MacIntyre, J.G. 1987. Stress fractures in athletes. A study of 320 cases. American Journal of Sports Medicine 15, pp. 46-58.

Marieb, E.N. 2009. Essential of Human Anatomy & Physiology. (9th ed.). Upper Saddle River, New Jersey, Pearson Benjamin Cummings. 592 p.

Marks, R. 2010. Hip fracture epidemiological trends, outcomes, and risk factors, 1970-2009. International Journal of General Medicine 3, pp. 1-17.

Martyn-St James, M. & Carroll, S. 2006. Progressive High-Intensity Resistance Training and Bone Mineral Density Changes Among Premenopausal Women. Sports Medicine 36, 8, pp. 683-704.

Mautalen, C.A., Vega, E.M. & Einhorn, T.A. 1996. Are the Etiologies of Cervical and Trochanteric Hip Fracture Different? Bone 18, 3(Suppl), pp. 133S-137S.

Mayhew, P.M., Thomas, C.D., Clement, J.G., Loveridge, N., Beck, T.J., Bonfield, W., Burgayne, C.J. & Reeve, J. 2005. Relation between age, femoral neck cortical stability, and hip fracture risk. The Lancet 366, 9480, pp. 129-135.

McKay, H.A., Sievänen, H., Petit, M.A., MacKelvie, K., Forkheim, K.A., Whittall, K.P., Forster, B.B., & MacDonald, H. 2004. Application of magnetic resonance imaging to evaluation of femoral neck structure in growing girls. Journal of Clinical Densitometry 7(2), pp. 161-168.

Miller, M.D. & Sanders, T.G. 2012. Presentation, Imaging and Treatment of Common Musculoskeletal Conditions. (1st ed.). Philadelphia, Pennsylvania, Saunders. 1568 p.

Morgan, E.F., Bayraktar, H.H. & Keaveny, T.M. 2003. Trabecular bone modulus-density relationships depend on anatomic site. Journal of Biomechanics 36, pp. 897-904.

Nakamura, N., Kyou, T., Takaoka, K., Ohzono, K. & Ono, K. 1992. Bone mineral density in the proximal femur and hip fracture type in the elderly. Journal of Bone and Mineral Research 7, pp. 755-759.

Nankaku, M., Kanzaki, H., Tsuboyama, T. & Nakamura, T. 2005. Evaluation of hip fracture risk in relation to fall direction. Osteoporosis International 16, pp. 1315-1320.

Narra, N., Nikander, R.,Viik, J., Hyttinen, J. & Sievänen, H. 2013. Femoral neck cross-sectional geometry and exercise loading. Clinical Physiology and Functional Imaging [electronic journal]. pp. 1-9. [Accessed on 5.5.2013]. Available at: http://onlinelibrary.wiley.com/doi/10.1111/cpf.12022/pdf

Neumann, D.A. 2002. Kinesiology of the Musculoskeletal System. Philadelphia, Pennsylvania, Elsevier – Health Sciences Division. 624 p.

Nigg, B.M. & Herzog, W. 1999. Biomechanics of the Musculo-skeletal System. (2nd ed.). West Sussex, England, John Wiley & Sons, Inc. 643 p.

NIH. 1996. An anatomical data set developed under a contract from the NLM by the Departments of Cellular and Structural Biology, and Radiology, University of Colorado School of Medicine. [accessed on 24.9.2012]. Available at: http://www.nlm.nih.gove/research/visible/visible_human.html

Nikander, R., Sievänen, H., Heinonen, A. & Kannus, P. 2005. Femoral neck structure in adult female athletes subjected to different loading modalities. Journal of Bone and Mineral Research 20, pp. 520-528.

Nikander, R., Sievänen, H., Heinonen, A. & Kannus, P. 2006. Loading modalities and bone structures at nonweight-bearing upper extremity and wight-bearing lower extremity – aQCT study of adult female athletes. Bone 39, 4, pp. 886-894.

Nikander, R., Sievänen, H., Heinonen, A., Karstila, T. & Kannus, P. 2008. Load-specific differences in the structure of femoral neck and tibia between world-class moguls skiers and slalom skiers. Scandinavian Journal of Medicine & Science in Sports 18, pp. 145-153.

Nikander, R., Kannus, P., Dastidar, P., Hannula, M., Harrison, L., Cevinka, T., Narra, N.G., Aktour, R., Arola, T., Eskola, H., Soimakallio, S., Heinonen, A., Hyttinen, J. & Sievänen, H. 2009. Targeted exercises against hip fragility. Osteoporosis International 20, pp. 1321-1328.

Nikander, R., Kannus, P., Rantalainen, T., Uusi-Rasi, K., Heinonen, A. & Sievänen, H. 2010a. Cross-sectional geometry of weight-bearing tibia in female athletes subjected to different exercises. Osteoporosis International 21, pp. 1687-1694.

Nikander, R., Sievänen, H., Heinonen, A., Daly, R.M., Uusi-Rasi, K. & Kannus, P. 2010b. Targeted exercise against osteoporosis: A systematic review and meta-analysis for optimising bone strength throughout life. BioMedCentral Medicine 8, 47, pp. 1-16. [accessed on 11.6.2012]. Available at: www.biomedcentral.com/1741-7015/8/47

Okuizumi, H., Harada, A., Iwata, H. & Konishi, N. 1998. Effect of the Femur of a New Hip Fracture Preventive System Using Dropped-Weight Impact Testing. Journal of Bone and Mineral Research 13, 12, pp. 1940-1945.

Ota, T., Yamamoto, I. & Morita, R. 1999. Fracture simulation of the femoral bone using the finite-element method: how a fracture initiats and proceeds. Journal of Bone and Mineral Metabolism 17, pp. 108-112.

Oravec, D. 2009. Proximal femur FEM representing Different Exercise loadign types. Tampere. Tampere University of Technology. Publication – Tampere University of Technology. 60 p.

Pajamäki, I., Kannus, P., Vuohelainen, T., Sievänen, H., Tuukkanen, J., Järvinen, M., Järvinen, T.L.N. 2003. The bone gain induced by exercise in puberty is not preserved through a virtually life-long deconditioning: a randomized controlled experimental study in male rats. Journal of Bone and Mineral Research 18, pp. 544-552.

Parkkari, J., Kannus, P., Palvanen, M., Natri, A., Vainio, J., Aho, H., Vuori, I. & Järvinen, M. 1999. Majority of hip fractures occur as a result of a fall and impact on the greater trochanter of the femur: a prospective controlled hip fracture study with 206 consecutive patients. Calcified Tissue International 65(3), pp. 183-187.

Pinilla, T.P., Boardman, K.C., Bouxsein, M.L., Myers, E.R. & Hayes, W.C. 1996. Impact direction from a fall influences the failure load of the proximal femur as much as age-related bone loss. Calcified Tissue International 58, pp. 231-235.

Polgár, K., Gill, H.S., Viceconti, M., Murray, D.W. & O'Connor, J.J. 2003a. Development and numerical validation of a finite element model of the muscle standardized femur. Proceedings of the Institution of Mechanical Engineers, Part H: Journal of Engineering in Medicine 217, 3, pp. 165-172.

Polgár, K., Gill, H.S., Viceconti, M., Murray, D.W. & O'Connor, J.J. 2003b. Strain distribution within the human femur due to physiological and simplified loading: finite element analysis using the muscle standardized femur model. Proceedings of the Institution of Mechanical Engineers, Part H: Journal of Engineering in Medicine 217, 3, pp. 173-189.

Poole, K.E.S., Mayhew, P.M., Rose, C.M., Brown, J.K., Bearcroft, P.J.,Loveridge, N. & Reeve, J. 2009. Changing Structure of the Femoral Neck Acroos the Adult Female Lifespan. Journal of Bone and Mineral Research 25(3), pp. 482-491.

Poór, G., Atkinson, E.J., O'Fallon, W.M. & Melton, L.J.III. 1995. Determinants of reduced survival following hip fractures in men. Clinical Orthopaedics and Related Research 319, pp. 260-265.

Pulkkinen, P., Partanen, J., Jalovaara, P. & Jämsä, T. 2004. Combination of bone mineral density and upper femur geometry improves the prediction of hip fracture. Osteoporosis International 15, pp. 274-280.

Sernbo, I. & Johnell, O. 1993. Consequences of ahip fracture: a prospective study over 1 year. Osteoporosis International 3, pp. 148-153

Shea, J.E. & Miller, S.C. 2005. Skeletal function and structure: Implications for tissue-targeted therapeutics. Advanced Drug Delivery Reviews 57, pp. 945-957.

Shier, D., Butler, J. & Lewis, R. 2002. Hole's human anatomy & physiology. (9th ed.) New York, McGraw-Hill. 1010 p.

Sievänen, H. 2000. A physical model of dual-energy X-ray absorptiometry-derived bone mineral density. Investigative Radiology 35, pp. 325-330.

Sievänen, H., Karstila, T., Apuli, P. & Kannus, P. 2007. Magnetic resonance imaging of the femoral neck cortex. Acta Radiology 48, pp. 308-314.

Silva, M.J. 2007. Biomechanics of Osteoporotic Fracture. Injury, International Journal of the Care of the Injured 38(Suppl3), pp. 69S-76S.

Siris, E.S., Chen, Y.T., Abbott, T.A., Barrett-Connor, E., Miller, P.D., Wehren, L.E. & Berger, M.L. 2004. Bone mineral density thresholds for pharmacological intervention to prevent fractures. Archives of internal medicine 164(10), pp. 1108-1112.

Snyder, S.M. & Schneider, E. 1991 Estimation of mechanical properties of cortical bone by computed tomography. Journal of Orthopaedic Research 9, pp. 422-431.

Stone, K.L., Seeley, D.G., Lui, L., Cauley, J.A., Ensrud, K., Browner, W.S., Nevitt, M. & Cummings, S.R. 2003. BMD at Multiple Sites and Risk of Fracture of Multiple Types: Long-Term Results From the Study of Osteoporotic Fractures. Journal of Bone and Mineral Research 18(11), pp. 1947-1954.

Taddei, F., Pancanti, A., & Viceconti, M. 2004. An improved method for the automatic mapping of computed tomography numbers onto finite element models. Medical Engineering & Physics 26, pp. 61-69.

Taddei, F., Cristofolini, L., Martelli, S., Gill, H.S. & Viceconti, M. 2006. Subject-specific finite element models of long bones: An in vitro evaluation of the overall accuracy. Journal of Biomechanics 39, pp. 2457-2467.

Taddei, F., Schileo, E., Helgason, B., Cristofolini, L., & Viceconti, M. 2007. The material mapping strategy influences the accuracy of CT-based finite element models of bones: An evaluation against experimental measurements. Medical Engineering & Physics 29, pp. 973-979.

Tortora, G. J. & Grabowski, S.R. 2003. Principle of Anatomy & Physiology. (10th ed.). Hoboken, New Jersey, John Wiley & Sons, Inc. 1104 p.

Trinkaus, E., Churchill, S.E. & Ruff, C.B. 1994. Postcranial robusticity in *Homo*,II: humeral bilateral asymmetry and bone plasticity. Americal Journal of Physical Anthropology 93, pp. 1-34.

Turner, C.H., Forwood, M.R. & Otter, M.W. 1994. Mechnotransduction in bone: do bone cells act as sensors of fluid flow? The Journal of the Federation of American Societies for Experimental Biology 8, 11, pp. 875-878.

Turner, C.H., Owan, I. & Takano, Y. 1995. Mechnotransduction in bone: role of strain rate. American Journal of Physiology Endocrinology and Metabolism 269, pp. 438-442.

Turner, C.H. & Pavalko, F.M. 1998. Mechnostranduction and functional response of the skeleton to physical stress: The mechanisms and mechanics of bone adaptation. Journal of Orthopaedic Science 3, pp. 346-355.

Turner, C.H. 1998. Three rules for bone adaptation to mechanical stimuli. Bone 23, pp. 399-407.

Turner, C.H, Rho, J., Takano, Y., Tsui, T.Y. & Pharr, G.M. 1999. The elastic properties of trabecular and cortical bone tissues are similar: results from two microscopic measurement techniques. Journal of Biomechanics 32, pp. 437-441.

Turner, C.H. & Robling, A.G. 2004. Exercise as An Anabolic Stimulus For Bone. Current Pharmaceutical Design 10, 21, pp. 2629 -2641.

Turner, C.H. & Robling, A.G. 2005. Mechanisms by which exercise improves bone strength 23(Suppl), pp. 16-22.

Turner, C.H. 2007. Skeletal Adaptation to Mechanical Loading. Clinical Reviews of Bone and Mineral Metabolism 5, pp. 181-194.

Ray, N.F., Chan, J.K., Thamer, M. & Melton, L.J.III. 1997. Medical expenditures for the treatment of osteoporotic fractures in the United States in 1995: Report from National Osteoporosis Foundation. Journal of Bone and Mineral Research 12, pp. 24-35.

Reddy, J.N. 2006. An Introduction to the Finite Element Method. (3rd ed.). New York. The McGraw-Hill Companies, Inc. 765p.

Reilly, D.T., Burstein, A.H., Frankel, V.H. 1974. The elastic modulus for bone. Journal of Biomechanics 7, pp. 271-275.

Reilly, D.T. & Burstein, A. 1975. The Elastic and Ultimate Properties of Compact Bone Tissue. Journal of Biomechanics 8, 6, pp. 393-406.

Rho, J.Y., Hobatho, M.C. & Ashman, R.B. 1995. Relations of mechanical properties to density and CT numbers in human bone. Medical Engineering & Physics 17, 5, pp. 347-355.

Rho, J.Y., Tsui, T.Y. & Pharr, G.M. 1997. Elastic properties of human cortical and trabecular lamellar bone measured by nanoindentation. Biomaterials 18, pp. 1325-1330.

Rho, J.Y., Kuhn-Spearing, L. & Zioupos, P. 1998. Mechanical properties and the hierarchical structure of bone. Medical Engineering & Physics 20, pp. 92-102.

Robinovitch, S.N., Hayes, W.C. & McMahon, T.A. 1991. Prediction of Femoral Impact Forces in Falls on the Hip. Journal of Biomechanical Engineering 113, pp. 366-374.

Robinovitch, S.N., McMahon, T.A. & Hayes, W.C. 1995. Force attenuation in trochanteric soft tissues during impact from a fall. Journal of Orthopaedic Research 13, pp. 956-962.

Robinovitch, S.N., Inkster, L., Maurer, J. & Warnick, B. 2003. Strategies for Avoiding Hip Impact During Sideways Falls. Journal of Bone and Mineral Research. Journal of Bone and Mineral Research 18, 7, pp. 1267-1273.

Robling, A.G., Duijvelaar, K.M., Geevers, J.V., Ohashi, N., & Turner, C.H. 2001a. Modulation of appositional and longitudinal bone growth in the rat ulna by applied static and dynamic force. Bone 29, pp. 105-113.

Robling, A.G., Burr, D.B. & Turner, C.H. 2001b. Recovery periods restore mechanosensitivty to dynamically loaded bone. Journal of Experimental Biology 204, pp. 3389-3399.

Robling, A.G., Castillo, A.B. & Turner, C.H. 2006. Biomechanical and Molecular Regulation of Bone Remodeling. Annual Reviews of Biomedical Engineering 8, pp. 455-498.

Ruff, C.B., Walker, A. & Trinkaus, E. 1994. Postcranial robusticity in *Homo*, III; ontogeny. American Journal of Physical Anthoropology 93, pp. 35-54.

Ruff, C., Holt, B. & Trinkaus, E. 2006. Who's Afraid of the Big Bad Wolff?: "Wolff's Law" and Bone Functional Adaptation. American Journal of Physical Anthropology 129, pp. 484-498.

Uhthoff, H.K. & Jaworski, Z.F. 1978. Bone loss in response to long-term immobilisation. Journal of Bone & Joint Surgery, British Volume 60B, pp. 420-429.

Unnanuntana, A., Gladnick, B.P., Donnelly, B.A.E. & Lane, J.M. 2010. Current Concepts Review; The Assessment of Fracture Risk. Journal of Bone and Joint Surgery, 92A, 3, pp.743-753.

Uusi-Rasi, K., Kannus, P., Cheng, S., Sievänen, H., Pasanen, M., Heinonen, A., Nenonen, A., Halleen, J., Fuerst, T., Genant, H. & Vuori, I. 2003. Effect of alendronate and exercise on bone and physical performance of postmenopausal women: a randomized controlled trial. Bone 33, pp. 132-143.

van den Kroonenberg, A.J., Hayes, W.C. & McMahon, T.A. 1995. Dynamic models for sideways falls from standing height. Journal of Biomechanical Engineering 117, pp. 309-318.

van den Kroonenberg, A.J., Hayes, W.C. & McMahon, T.A. 1996. Hip impact velocities and body configurations for experimental falls from standing height. Journal of Biomechanics 29, pp. 807-811.

Vega, E., Mautalen, C., Gomez, H., Garrido, A., Melo, L. & Sahores, A.O. 1991. Bone mineral density in patients with cervical and trachanteric fractures of the proximal femur. Osteoporosis International 1, pp.81-86.

Verhulp, E., van Rietbergen, B., & Huiskes, R. 2008. Load distribution in the healthy and osteoporotic human proximal femur during a fall to the side. Bone 42, pp. 30-35.

Voo, L., Armand, M. & Kleinberger, M. 2004. Stress Fracture Risk Analysis of the Human Femur Based on Computational Biomechanics. Johns Hopkins APL Technical Digest 25(3), pp. 223-230.

Warden, S.J., Fuchs, R.K., Castillo, A.B. & Turner, C.H. 2005. Does exercise durig growth influence osteoporotic fracture risk later in life? Journal of Musculoskeletal & Neuronal Interactions 5, 4, pp. 344-346.

Warden, S.J., Fuchs, R.K., Castillo, A.B., Nelson, I.R. & Turner, C.H. 2007. Exercise when young provides lifelong benefits to bone structure and strength. Journal of Bone and Mineral Research 22, pp. 251-259.

Weiner, S. & Wagner, H.D. 1998. The Material Bone: Structure-Mechanical Function Relations. Annual Review of Materials Science 28, pp. 271-298.

Wirtz, D.C., Schiffers, N., Pandorf, T., Radermacher, K., Weichert, D. & Forst, R. 2000. Critical evaluation of known bone material properties to realize anisotropic FE-simulation of the proximal femur. Journal of Biomechanics 33, pp. 1325-1330.

Wirtz, D.C., Pandorf, T., Portheine, F., Radermacher, K., Schiffers, N., Prescher, A., Weichert, D. & Niethard, F.U. 2003. Concept of development of an orthotropic FE model of the proximal femur. Journal of Biomechanics 36, pp. 289-293.

Yoshimura, N., Suzuki, T., Hosoi, T. & Orimo, H. 2005. Epidemiology of hip fracture in Japan: incidence and risk factors. Journal of Bone and Mineral Metabolism 23, pp. 78-80.

Zysset, P.K., Guo, X.E., Hoffler, E., Moore, K.E. & Goldstein, S.A. 1999. Elastic modulus and hardness of cortical and trabecular bone lamellae measured by annoindentation in the human femur. Journal of Biomechanics 32, pp. 1005-1012.

APPENDIX 1: DESCRIPTIVE DATA OF THE SUBJECTS

Group	Subject ID	Age (years)	Height (cm)	Weight (kg)	Body Fat %	Single leg jump maximum reaction force (N)
H-I	103	30.3	177.5	62.5	21.0	1690
	108	19.0	172.5	55.0	18.9	1587
	112	26.4	167.7	68.0	27.8	2696
	113	20.2	174.0	73.2	24.4	3636
	116	21.2	165.0	55.3	21.7	1688
	121	24.6	170.0	55.9	17.6	2739
	average (±SD)	23.6 (±4.29)	171.1 (±4.50)	61.6 (±7.64)	21.9 (±3.72)	2239 (±822.2)
O-I	213	23.3	156.5	56.5	26.0	1552
	215	35.3	168.5	58.2	26.5	1215
	216	22.9	177.2	79.8	34.4	2034
	217	33.3	162.2	61.2	23.0	1333
	218	19.0	161.0	59.8	26.1	1268
	221	22.9	188.5	76.4	28.9	1844
	average (±SD)	26.1 (±6.56)	168.9 (±11.9)	65.3 (±10.1)	27.5 (±3.87)	1541 (±334.4)
H-M	301	40.2	160.4	72.5	32.9	1738
	302	26.1	158.6	49.6	17.5	1297
	303	35.1	158.6	55.8	20.9	1407
	308	29.8	160.6	68.8	34.7	2260
	309	27.3	153.0	57.5	20.4	2216
	312	25.1	153.0	55.0	23.3	1487
	average (±SD)	30.6 (±5.91)	157.4 (±3.49)	59.9 (±8.84)	25.0 (±7.12)	1734 (±416.6)
R.L-I	401	25.4	173.0	55.6	11.1	1324
	402	32.2	167.0	56.0	17.6	1103
	404	33.5	159.6	52.0	10.5	1263
	411	21.6	172.5	58.3	11.0	1488
	412	19.9	172.0	55.6	11.9	1383
	414	25.0	162.2	44.0	13.3	1115
	average (±SD)	26.3 (±5.52)	167.7 (±5.76)	53.6 (±5.11)	12.6 (±2.65)	1279 (±151.4)
R.N-I	503	18.1	174.0	65.0	22.7	1614
	504	17.3	172.0	63.8	27.4	1481
	505	18.0	179.4	72.0	35.2	1467
	506	17.5	179.0	64.5	23.6	1740
	508	17.9	166.0	70.3	35.2	1566
	509	17.5	166.8	59.2	28.0	1465
	average (±SD)	17.7 (±0.32)	172.9 (±5.77)	65.8 (±4.66)	28.7 (±5.45)	1556 (±108.7)

Con-trol	604	21.6	168.0	54.1	25.0	1164
	605	27.7	164.5	65.0	21.6	1574
	606	29.0	167.5	70.4	33.8	1873
	607	19.9	174.0	61.5	27.3	1204
	608	20.9	166.6	67.3	39.9	1416
	609	21.5	167.0	50.5	28.9	1225
	average (±SD)	23.4 (±3.88)	167.9 (±3.21)	61.5 (±7.76)	29.4 (±6.55)	1409 (±275.1)

APPENDIX 2: SUBJECT SPECIFIC IMPACT FORCE

Group	Subject ID	Subject Specific Impact Force (N)
H-I	103	5252.1
	108	4857.1
	112	5325.0
	113	5627.7
	116	4763.2
	121	4861.0
	average (±SD)	5114.35 (±340.7)
O-I	213	4689.0
	215	4938.1
	216	5929.7
	217	4968.2
	218	4892.8
	221	5984.1
	average (±SD)	5233.65 (±568.9)
H-M	301	5377.4
	302	4422.7
	303	4691.0
	308	5241.6
	309	4677.1
	312	4574.3
	average (±SD)	4830.7 (±385.5)
R.L-I	401	4890.6
	402	4822.3
	404	4542.7
	411	5000.7
	412	4876.4
	414	4212.6
	average (±SD)	4724.2 (±293.8)
R.N-I	503	5303.1
	504	5223.6
	505	5667.3
	506	5358.0
	508	5386.8
	509	4955.1
	average (±SD)	5315.6 (±232.0)
Con-trol	604	4753.911
	605	5156.291
	606	5414.913
	607	5158.34
	608	5280.108

	609	4579.328
	average (±SD)	5057.1 (±321.9)
Overall average (±SD)		5046.0 (±404.8)

APPENDIX 3: DESCRIPTIVE DATA OF IMPORTED PROXIMAL FEMUR BONE GEOMETRIES

Group	Subject	Cortical bone volume (mm^3)	Trabecular bone volume (mm^3)	Total volume (mm^3)
H-I	103	2606400	9241600	11848000
	108	2342000	6468400	8810400
	112	2444960	6534240	8979200
	113	2857600	7151200	10008800
	116	2732480	4699920	7432400
	121	2183360	6779040	8962400
	average (±SD)	2527800 (±251739)	6812400 (±1461177)	9340200 (±1478481)
O-I	213	2704080	5609520	8313600
	215	2584480	6034720	8619200
	216	2590400	8860800	11451200
	217	2359760	5514480	7874240
	218	2239360	5493120	7732480
	221	2466400	8453600	10920000
	average (±SD)	2490747 (±170396)	6661040 (±1563894)	9151787 (±1615342)
H-M	301	2495760	6815440	9311200
	302	1883920	6852080	8736000
	303	2209600	5387520	7597120
	308	2773280	5713120	8486400
	309	2558880	5070880	7629760
	312	2287360	4499360	6786720
	average (±SD)	2368133 (±310785)	5723067 (±949047)	8091200 (±918592)
R.L-I	401	2467760	7232240	9700000
	402	1817120	6113920	7931040
	404	2359040	6093760	8452800
	411	2295040	7125760	9420800
	412	2326400	8874400	11200800
	414	2076720	5641120	7717840
	average (±SD)	2223680 (±236825)	6846867 (±1174342)	9070547 (±1308951)
R.N-I	503	2557600	8481600	11039200
	504	2264080	6502320	8766400
	505	2219280	6370320	8589600
	506	1949760	6241440	8191200
	508	2452640	5924160	8376800
	509	2023440	5852160	7875600
	average (±SD)	2244467 (±235844)	6562000 (±973513)	8806467 (±1136962)

Control	604	1989600	5895520	7885120
	605	1955920	5829520	7785440
	606	2515360	7583840	10099200
	607	2372960	6648640	9021600
	608	2130160	6131440	8261600
	609	2080160	6479840	8560000
	average (±SD)	2174027 (±222891)	6428133 (±650691)	8602160 (±862090)
Overall average (±SD)		2338142 (±262174)	6505584.444 (±1150109)	8843726.667 (±1231197)

APPENDIX 4: THE NUMBER OF NODES AND ELEMENTS IN THE FE MODELS

Group	Subject	Node	Element
H-I	103	141342	81196
	108	118053	67303
	112	126991	67277
	113	139339	72836
	116	121629	61983
	121	127394	69210
	average (±SD)	129125 (±9380)	69968 (±6526)
O-I	213	137898	67637
	215	124410	66746
	216	157175	83235
	217*	403842	271243
	218	137896	66794
	221	146143	80099
	average (±SD)	184561 (±107966)	105959 (±81295)
H-M	301	141529	72675
	302*	646118	435248
	303*	1192820	845533
	308*	1227667	873182
	309*	514523	351957
	312*	451570	311361
	average (±SD)	695705 (±431765)	481659 (±316525)
R.L-I	401	133875	74392
	402*	1257281	898085
	404	142632	70077
	411	129886	70777
	412	279425	105021
	414	139814	67293
	average (±SD)	347152 (±449540)	214274 (±335287)
R.N-I	503*	2347864	1665444
	504*	332843	220133
	505	134958	69994
	506*	305256	206649
	508	145878	70425
	509*	535156	376381
	average (±SD)	633659 (±852429)	434838 (±613496)
Control	604*	297136	198491
	605*	287499	194613
	606	144135	77565
	607	132277	71663
	608*	306077	206053
	609	120472	66052

	average (±SD)	214599 (±90661)	135740 (±70277)
Overall average (±SD)		367467 (±460787)	240406 (±335154)

* Mesh was performed by Patch Independent method

APPENDIX 5: MATLAB CODE

5-A: File format conversion code from .vtk to .mat

```
function V = readVTK(vtkfile)
%%%%%%%%%%%%%%%%%%%%%%%%%%%%%%%%%%%%%%%%%%%%%%%%%%%%%%%%%%%%%%%%%%%%%%%%%%%%
%  Usage: V = readVTK(vtkvile)
%
%   V:        The matrix to be stored
%   vtkfile:  The file name
%   notes:    Only reads binary STRUCTURED_POINTS
%
% Erik Vidholm 2006
%%%%%%%%%%%%%%%%%%%%%%%%%%%%%%%%%%%%%%%%%%%%%%%%%%%%%%%%%%%%%%%%%%%%%%%%%%%%

V = 0;

% open file (OBS! big endian format)
fid = fopen(vtkfile, 'r','b');

if(fid == -1)
    return
end

fgetl(fid); % # vtkDataFile Version x.x
fgetl(fid); % comments: e.g; VTK File Generated by Insight Segmenta-
tion and Registration Toolkit(ITK)
fgetl(fid); % BINARY
fgetl(fid); % DATASET STRUCTURED_POINTS

s = fgetl(fid);  % DIMENSIONS NX NY NZ (e.g; DIMENSIONS 384 288 120)

sz = sscanf(s,'%*s%d%d%d').' % This sscanf reads string s and converts
it into Matrix sz in format of removing first string in the line
                             % sz is a matrix; e.g; 284 288 120


a=fgetl(fid); % Origin OX OY OZ
b=fgetl(fid); % Spacing SX SY SZ
c=fgetl(fid); % total POINT_DATA NXNYNZ

s = fgetl(fid); % SCALARS/VECTORS name data_type (ex: SCALARS imageda-
ta unsigned_char)
svstr = sscanf(s,'%s',1)
dtstr = sscanf(s,'%*s%*s%s')

if(strcmp(svstr, 'SCALARS') > 0)
    fgetl(fid); % the lookup table
    if(strcmp(dtstr, 'unsigned_char')>0)
        %read data
        V = fread(fid, prod(sz),'*uint8');
        V = reshape(V,sz);
    elseif(strcmp(dtstr,'char') > 0)
        %read data
        V = fread(fid, prod(sz),'*int8');
```

```
        V = reshape(V,sz);
    elseif(strcmp(dtstr,'unsigned_short')>0)
        %read data
        V = fread(fid, prod(sz),'*uint16');
        V = reshape(V,sz);
    elseif(strcmp(dtstr,'short')>0)
        %read data
        V = fread(fid,prod(sz), '*int16');
        V = reshape(V,sz);
    elseif(strcmp(dtstr,'unsigned_int') > 0)
        %read data
        V = fread(fid, prod(sz), '*uint32');
        V = reshape(V,sz);
    elseif(strcmp(dtstr,'int')>0)
        %read data
        V = fread(fid, prod(sz),'*int32');
        V = reshape(V,sz);
    elseif(strcmp(dtstr,'float')>0)
        %read data
        V = fread(fid,prod(sz), '*single');
        V = reshape(V,sz);
    elseif(strcmp(dtstr,'double') > 0)
        %read data
        V = fread(fid, prod(sz), '*double');
        V = reshape(V,sz);
    end

elseif(strcmp(svstr,'VECTORS') >0)
    if(strcmp(dtstr, 'float') > 0)
        %read data
        V = fread(fid,3*prod(sz),'*single');
        V = reshape(V,[3 sz]);
        V = permute(V,[2 3 4 1]);
    end
end

fclose(fid);

% Save the created file in .mat format.
```

5-B: Code for the file conversion from mat.file to TetGen files

```
%%%%%%%%%%%%%%%%%%%%%%%%%%%%%%%%%%%%%%%%%%%%%%%%%%%%%%%%%%%%%%%%%%%%%%%%%%%%
% Author:   Shinya Abe
% Project:  Thesis
% Task:
%
%    Convert array.mat file created by appendix 5-A to TetGen file
%    format: a list of nodes (.node), a list of tetrahedran (.ele),
%            and a list of triangular faces (.face).
%
%
% Explanation of 'vol2mesh' function.
%
% [node, elem, bound] = vol2mesh(img, ix, iy, iz, opt, maxvol, dofix,
%                        method);
% input:
%    img: a volumetric binary image, which created from Appendix 5-A.
%    ix,iy,iz: Indices in x, y, z directions.
```

```
%    opt: It is the function parameter for the chosen meshing method
%         cgalsurf (CGAL).
%         This paramter specify the maximum radius of the Delaunay
%         sphere (element size) and needs to be bigger than 0 and
%         increasing this parameter makes the mesh geometry more
%         coarse.
%    maxvol: target maximum tetrahedral element volume determing the
%            density of the element in the volume.
%    dofix: 1: perform mesh validation&repair, 0: skip repairing
%    method: cgalsurf(CGAL) was chosen.
%
% output:
%    node: output, node coordinates of the tetrahedral mesh
%    elem: output, element list of the tetrahedral mesh
%    face: output, mesh surface element list of the tetrahedral mesh
%
%%%%%%%%%%%%%%%%%%%%%%%%%%%%%%%%%%%%%%%%%%%%%%%%%%%%%%%%%%%%%%%%%%%%%%%%%%%%%%%

clear all; clc; close all;

% Load the mat file created from 5-A and assign as a variable 'array'.
load('Raw201.mat','data');
array = data;

% Convert conrtical geometry
% Set 'array > 0 so that it concludes both 1 (cortical)
% and 2 trabecular bone geometry.
[node, elem, bound] = vol2mesh(array > 0, 1:size(array,1),
1:size(array,2), 1:size(array,3), 3, 100, 1, 'cgalsurf');
% visualize the meshed geometry.
trisurf(bound(:,1:3), node(:,1),node(:,2),node(:,3));
% 'Comment' three lines above if you want to convert trabecular bone
geometry.

% Convert trabecular geometry
% Set 'array > 1 so that it concludes only 2 trabecular bone geometry.
% [node, elem, bound] = vol2mesh(array > 1, 1:size(array,1),
1:size(array,2), 1:size(array,3), 3, 100, 1, 'cgalsurf');
% %visualize the meshed geometry.
% trisurf(bound(:,1:3), node(:,1),node(:,2),node(:,3));
% 'Uncomment' three lines above if you want to convert trabecular bone
geometry.

% Specificaion for opt and maxvol.
% 3 and 100 were chosen for opt and maxvol respectively
% in order to create fine mesh.

% Find Directory where 3 TedGen files are located.
% In case of the computer used in this thesis, they were saved in:
% C:\Users\XXX\AppData\Local\Temp\iso2mesh-XXX
% Information of directory can be found in 'Command Window' in MATLAB
% once this code is run.
```

5-C: Code for the smallest cross-section (slice) identification

```
%%%%%%%%%%%%%%%%%%%%%%%%%%%%%%%%%%%%%%%%%%%%%%%%%%%%%%%%%%%%%%%%%%%%%%%%%%%%
% Editor:   Shinya Abe
% Original Author: Daniel Oravec (Oravec, 2009)
% Project:  Thesis
% Task:
%
%    1) This reads output variable (e.g. vonMises stress) data
%       (in txt format) of both cortex and trabecular bone created
%       from ANSYS Workbench.
%
%    2) Calculate the slice # for the thinnest slice of
%       the femoral neck.
%
%    3) Then, calculate the averaged vonMises stress/output values
%       or each slice.
%
%  Prequisite:
%       Remove an unnecessary 1st text line from
%       both text files for the cortex and trabecular bones.
%       Otherwise, function 'load' woud not read txt file.
%  NOTE:
%       This code was originally made for vonMises stress values.
%       Variable names can be replaced by appropriate names if
%       necessary for other output variables such as total
%       displacement or strain.
%%%%%%%%%%%%%%%%%%%%%%%%%%%%%%%%%%%%%%%%%%%%%%%%%%%%%%%%%%%%%%%%%%%%%%%%%%%%

close all; clear all; clc;

% Open txt files
load 'vonMisesC.txt' % Change file name if necessary
load 'vonMisesT.txt' % Change file name if necessary

% Assign material number, 1 = cortex, 2 = trabecular bone
vonMisesC(:,6) = 1;
vonMisesT(:,6) = 2;

%%%%%%%%%%%%%%%%%%%%%%%%%%%%%%%%%%%%%%%%%%%%%%%%%%%%%%%%%%%%%%%%%%%%%%%%%%%%
% Explanation of this vonMisesC and vonMisesT array
% 1st column; node #
% 2nd column; x location of node
% 3rd column; y location of node
% 4th column; z location of node
% 5th column; equivalent vonMises Stress (MPa)/Output value
% 6th column; Material #, 1 = cortex, 2 = trabecular bone
%%%%%%%%%%%%%%%%%%%%%%%%%%%%%%%%%%%%%%%%%%%%%%%%%%%%%%%%%%%%%%%%%%%%%%%%%%%%

% Combine both cortex and trabecular bone valunes into one array
vonMises = [vonMisesC; vonMisesT];

% Assign xyz coordinate into varible I, I2, and I3.
I = vonMises(:,2:4);
I2 = round(I); % round x, y, and z coordinate to mm.
I3 = uint8(I2);% convert into unsigned 8-bit integers
I3(I3==0) = 1;

res = zeros(50,50, 50, 'uint8');
```

```
res2 = zeros(50,50,50);
regions = zeros(50,50,50);

%%%%%%%%%%%%%%%%%%%%%%%%%%%%%%%%%%%%%%%%%%%%%%%%%%%%%%%%%%%%%%%%%%%%%%%%%%%%
% Explanation of variables: res, res2, and regions
%
% res will contain 1 in the cell where vonMises values exist.
%
% res2 will contain vonMises values where each 1 exist in res.
%
% regions contains 1(=cortex) or 2(=trabecular) in cells where
% vonMises values exist.
%
%%%%%%%%%%%%%%%%%%%%%%%%%%%%%%%%%%%%%%%%%%%%%%%%%%%%%%%%%%%%%%%%%%%%%%%%%%%%

for i = 1:size(I3,1)
    res(I3(i,1),I3(i,2),I3(i,3)) = 1;
    res2(I3(i,1),I3(i,2),I3(i,3)) = vonMises(i,5)*1000000;
    regions(I3(i,1),I3(i,2),I3(i,3)) = vonMises(i,6);
end

% Next 22 lines are the algorism to find the thinnest slice in the
% neck region
for i = 1:size(res,3)-1
    [rows, cols] = find(res(:,:,i));
    if isempty(rows)
        continue
    end
    minx(1,i) = min(rows);
    maxx(1,i) = max(rows);
    miny(1,i) = min(cols);
    maxy(1,i) = max(cols);
end

xdiff = maxx-minx;
ydiff = maxy-miny;

avedim = (xdiff+ydiff)/2;

% Figure below will ask you to click two tops of two apexes.
figure;
plot(avedim)
title('Click the top of the two bumps')
[slicenumber,avedim2] = ginput(2);

minimum = min(avedim(uint8(slicenumber(1)):uint8(slicenumber(2))));

%smallest cross-section slice in neck area
min_slice = find(avedim == minimum)

%calculate and mean values along z-axis
values = vonMises(:,5)*1000000;
res3 = zeros(1,size(avedim,2));
for i = 1:size(avedim,2)
    I = (I3(:,3) == i);

    res3(1,i) = mean(values(I));
end
```

```
close all;

% Figure below will plot the average vonMises stress from both the
% cortical and trabecular bones for each slice.
figure;
plot(res3)
title('Averaged vonMises stress in MRI slice #')
xlabel({'Slice#';'Smaller#: toward femoral head';'Bigger#: toward the
distal end of femur'})
ylabel('vonMises stress, Pa')
hgsave('Averaged_vonMises_stress_in_MRI_slice')
```

5-D: Code for 8 region division

```
%%%%%%%%%%%%%%%%%%%%%%%%%%%%%%%%%%%%%%%%%%%%%%%%%%%%%%%%%%%%%%%%%%%%%%%%%%%%
% Editor:   Shinya Abe
% Original Author: Daniel Oravec (Oravec, 2009)
% Project:  Thesis
% Task:
%
%    1) Divide chosen thinnest regions of the femoral neck
%       into 8 equal pieces.
%    2) Calculate the mean values for each locations.
%
% NOTE:
%       Output result1 can be changed to
%         a) mean value only for cortical bone
%         b) mean value only for trabecular bone
%         c) mean value for combined of cortical and trabecular bone
%%%%%%%%%%%%%%%%%%%%%%%%%%%%%%%%%%%%%%%%%%%%%%%%%%%%%%%%%%%%%%%%%%%%%%%%%%%%

function result1 = createSectors8(orig,I2,regions)
% orig = res(:,:,i), I2 = res2(:,:,i), regions = regions.

% Center of mass calculation
I = bwmorph(orig, 'close');
I = imfill(uint8(I));
L = bwlabel(I);

% NOTE:
% 4 codes above may cause error finding centroid.
% However, this may be due to the mesh size.
% If more fined mesh size is used, 4 codes above may be correct.
% So use, finer mesh!

s = regionprops(uint8(I),'centroid');

% Figure below will show the selected slice
% to check if the chosen slice is correct.
figure
imshow(orig,[])

hold on;
plot(s(1).Centroid(1),s(1).Centroid(2),'r.')


centroids = cat(1, s.Centroid);
```

```
Mx = centroids(:,1);
My = centroids(:,2);
xmax = size(I,2);
ymax = size(I,1);

% Dividing image to sectors
x = 0;
y = -x + Mx + My;
if y < 0
    y = 0;
    x = -y + Mx + My;
elseif y > ymax
    y = ymax;
    x = -y + Mx + My;
end

hold on
plot(x,y,'r*')
hold off
a(1,1) = x;
a(1,2) = y;

x = xmax;
y = x - Mx + My;
if y < 0
    y = 0;
    x = y + Mx - My;
elseif y > ymax
    y = ymax;
     x = y + Mx - My;
end

hold on
plot (x, y, 'r*')
hold off
b(1,1) = x;
b(1,2) = y;

x = xmax;
y = -x + Mx + My;
if y < 0
    y = 0;
    x = -y + Mx + My;
elseif y > ymax
    y = ymax;
    x = -y + Mx + My;
end

hold on
plot(x,y,'r*')
hold off
a(2,1) = x;
a(2,2) = y;

x = 0;
y = x - Mx + My;
if y < 0
    y = 0;
    x = -y + Mx - My;
elseif y > ymax
```

```
    y = ymax;
    x = -y + Mx - My;
end

hold on
plot(x,y,'r*')
hold off
b(2,1) = x;
b(2,2) = y;

hold on;
plot(a(:,1),a(:,2),'y')
plot(b(:,1),b(:,2),'g')
hold off

c(1,1) = Mx;
c(1,2) = a(1,2);
c(2,1) = Mx;
c(2,2) = b(2,2);

d(1,1) = b(2,1);
d(1,2) = My;
d(2,1) = a(2,1);
d(2,2) = My;

hold on
plot(c(1,1),c(1,2),'r*')
plot(c(2,1),c(2,2),'r*')
plot(d(1,1),d(1,2),'r*')
plot(d(2,1),d(2,2),'r*')
plot(c(:,1),c(:,2),'y')
plot(d(:,1),d(:,2),'g')
hold off

% Create areas for sectors
e = [b(1,1) Mx d(2,1)];
r = [b(1,2) My d(2,2)];
Posterior1 = roipoly(I,e,r);

e = [d(2,1) Mx a(2,1)];
r = [d(2,2) My a(2,2)];
Posterior2 = roipoly(I,e,r);

e = [a(2,1) Mx c(2,1)];
r = [a(2,2) My c(2,2)];
Superior1 = roipoly(I,e,r);

e = [c(2,1) Mx b(2,1)];
r = [c(2,2) My b(2,2)];
Superior2 = roipoly(I,e,r);

e = [b(2,1) Mx d(1,1)];
r = [b(2,2) My d(1,2)];
Anterior1 = roipoly(I,e,r);

e = [d(1,1) Mx a(1,1)];
r = [d(1,2) My a(1,2)];
Anterior2 = roipoly(I,e,r);
```

```
e = [a(1,1) Mx c(1,1)];
r = [a(1,2) My c(1,2)];
Inferior1 = roipoly(I,e,r);

e = [c(1,1) Mx b(1,1)];
r = [c(1,2) My b(1,2)];
Inferior2 = roipoly(I,e,r);

% Calculate & output values for mean regional stress
Posterior1CT= round(mean(I2(Posterior1 & orig)));
Posterior2CT= round(mean(I2(Posterior2 & orig)));
Superior1CT = round(mean(I2(Superior1 & orig)));
Superior2CT = round(mean(I2(Superior2 & orig)));
Anterior1CT = round(mean(I2(Anterior1 & orig)));
Anterior2CT = round(mean(I2(Anterior2 & orig)));
Inferior1CT = round(mean(I2(Inferior1 & orig)));
Inferior2CT = round(mean(I2(Inferior2 & orig)));

% Calculate & output values for mean regional cortical stress

Posterior1C= round(mean(I2(Posterior1 & orig & regions == 1)));
Posterior2C= round(mean(I2(Posterior2 & orig & regions == 1)));
Superior1C = round(mean(I2(Superior1 & orig & regions == 1)));
Superior2C = round(mean(I2(Superior2 & orig & regions == 1)));
Anterior1C = round(mean(I2(Anterior1 & orig & regions == 1)));
Anterior2C = round(mean(I2(Anterior2 & orig & regions == 1)));
Inferior1C = round(mean(I2(Inferior1 & orig & regions == 1)));
Inferior2C = round(mean(I2(Inferior2 & orig & regions == 1)));

% Calculate & output values for mean regional trabecular stress
Posterior1T= round(mean(I2(Posterior1 & orig & regions == 2)));
Posterior2T= round(mean(I2(Posterior2 & orig & regions == 2)));
Superior1T = round(mean(I2(Superior1 & orig & regions == 2)));
Superior2T = round(mean(I2(Superior2 & orig & regions == 2)));
Anterior1T = round(mean(I2(Anterior1 & orig & regions == 2)));
Anterior2T = round(mean(I2(Anterior2 & orig & regions == 2)));
Inferior1T = round(mean(I2(Inferior1 & orig & regions == 2)));
Inferior2T = round(mean(I2(Inferior2 & orig & regions == 2)));

% make array by each location
% Output value for combined stress
result1 = [Inferior1CT;Inferior2CT;Anterior1CT;Anterior2CT;
Superior1CT;Superior2CT;Posterior1CT;Posterior2CT];

% make array for cortical bone by each location
% Output value only for cortical bone
%result1 = [Inferior1C;Inferior2C;Anterior1C;Anterior2C;
%Superior1C;Superior2C;Posterior1C;Posterior2C];


% make array for trabecular bone by each locatioin
% Output value only for trabecular bone
%result1 = [Inferior1T;Inferior2T;Anterior1T;Anterior2T;
%Superior1T;Superior2T;Posterior1T;Posterior2T];
```

5-E: Code for mean regional vonMises stress for each region

```
%%%%%%%%%%%%%%%%%%%%%%%%%%%%%%%%%%%%%%%%%%%%%%%%%%%%%%%%%%%%%%%%%%%%%%%%
% Editor: Shinya Abe
% Original Author: Daniel Oravec (Oravec, 2009)
% Project: Thesis
% Task:
%    This will calculate regional mean vonMises stress value
%    or output values for chosen regions.
%    In this thesis, total of 9 slices (+-4 slices from the thinnest
%    slice # calculated from the APPENDIX 5-C code.
%
%    1) Total number of slices are chosen.
%
%    2) regional mean stress are calculated.
%
% NOTE:
%    The function createSectors8 (APPENDIX 5-D code) will be used
%    inside of this code.
%%%%%%%%%%%%%%%%%%%%%%%%%%%%%%%%%%%%%%%%%%%%%%%%%%%%%%%%%%%%%%%%%%%%%%%%

result2 = zeros(9,8); % set array size 21 rows and 4 columns

k = 1;
for i=73:81 % change this range depending on where thinnest slice is
    % for example, in this code, the thinnest slice # is 77.
    result2(k,:) = createSectors8(res(:,:,i),res2(:,:,i), re-
gions(:,:,i));
    k = k+1;
end

averageInferior1 = mean(result2(:,1));
averageInferior2 = mean(result2(:,2));
averageAnterior1 = mean(result2(:,3));
averageAnterior2 = mean(result2(:,4));
averageSuperior1 = mean(result2(:,5));
averageSuperior2 = mean(result2(:,6));
averagePosterior1 = mean(result2(:,7));
averagePosterior2 = mean(result2(:,8));

result3 = [averageInferior1;averageInferior2;averageAngerior1;
    averageAnterior2;averageSuperior1;averageSuperior2;
    averagePosterior1;averagePosterior2];

% Figure below will plot the regional mean vonMises stress value
% /output values in bar chart figure.
figure
bar(result3,'r')
title({'Mean vonMises Stress';'calculated from 9 slices in each region
in the neck'})
xlabel('1-2: posterior,            3-4: superior,            5-6: an-
terior,           7-8: inferior')
ylabel('vonMises stress, Pa')
hgsave('Averaged_vonMises_stress_in_8SECTORS_WHOLE9slices')

save('9slicesAverageVonMises8sec.mat','result2')
save('meanVonMises8sec.mat','result3')
```

APPENDIX 6: WORKFLOW

1. Coversion of the MRI data to the importable file to ANSYS

1. Manual segmentation of MRI data of the proximal femur using the software ITK-SNAP, which is available from;
   http://www.itksnap.org/pmwiki/pmwiki.php
2. Save segmented date in .vtk format.
3. Import the segmented data in .vtk format into MATLAB and save them in .mat format. The MATLAB code used here is attached as Appendix 5-A.
4. Using the *vol2mesh* function from *iso2mesh*, perform meshing cortical bone geometry. The code for meshing this cortical geometry is shown in the Appendix 5-B. This iso2mesh is available from;
   http://iso2mesh.sourceforge.net/cgi-bin/index.cgi
5. Find the directory in the computer where post_vmesh.1.ele, post_vmesh.1.face, and post_vmesh.1.node are located. Then, move them to a suitable folder where you want to save.
6. Repeat steps 4 and 5 for meshing the trabecular bone geometry.
7. Next, the file is converted to *alias obj file* (.obj). Open the *winmeshview*, click *Load model*, open post_vmesh.1.ele for cortical bone. Then, click *Export model* and save the file as alias obj file (.obj). This winmeshview is available from;
   http://techhouse.brown.edu/~dmorris/projects/winmeshview/
8. Repeat step 7 for the trabecular bone.
9. Then, convert file in .obj into *Rhino 3D model* (.3dm). Open Rhinoceros CAD software, set the model size to be in *Small Objects* and units to be *Millimeters.* Open the .obj file and save it as the Rhino 3D model file format (.3dm) Do this for both cortical and trabecular bone.
10. Convert 3dm file to ACIS .sat format. Open Automesher, open 3dm file, and save them as ACIS .sat format. Do this step for both the cortical and trabecular bone geometry. Free trial of Automesher is available from;
    http://www.automapki.com/products/automesher-application.html

2. FE model creation

1. Open ANSYS Workbench, and choose *Static Structural* from *Analysis Systems* which is located in the left column. The small squarebox will appear in *Project Schematic* view, which box contains several programs such as *Engineering Data*, *Geometry, Model, Setup, Solution,* and *Results*.
2. Assign material properties. Open *Engineering Data*, and put the appropriate name for the cortical bone in the box under the *Contents of Engieering Data*. Then, choose *Isotropic Elasticity* from *Linear Elastic* in Toolbox in the left col-

umn and put values of Young's modulus and Poisson's ratio. Repeat this step for the trabecular bone. Then, click *Return to Project,* which makes going back to the main project screen.

3. Import geometries. Open *Geometry*, set *desired length unit* to be millimeter. Open *File* > Export Geometry File > choose cortical geometry file (.sat) > > click *Generate*. Repeat this step to import the trabecular bone geometry except for choosing *No* for *Clean Bodies* in *DesignModeler Geometry Options* before clicking *Generate.* Then close the DesignModeler to go back to main project screen.
4. Meshing. Open *Model* > open *Geometry* branch in the left column > assign materials to the cortical and trabecular bone geometry. Right click *Mesh* > click *Method* > select both cortical and trabecular geometries > choose *Tetrahedrons*. *Patch Conforming* algorithm is automatically selected by the program. If this setting fails to mesh the geometries, then choose *Patch Independent* algorithm. Specification with this algorithm is explained in the subchapter 3.5.3. Then, click *Generate Mesh*.
5. Apply the loading/boundary condition. Open *Static Structural* branch > right click *Static Structural* > *Insert* > *Fixed support*. Choose the distal end and the lateral side of the greater trochanter for this *Fixed support.* Right click *Static Structural* > *Insert* > *Force* > Choose Component > put calculated subject specific impact forces into X,Y,Z component so that it satisfy the desired loading condition. Choose *Bond* as the connection type.
6. Choose output from the FE models. Open *Solution* branch > *Insert* > *Stress* > *Equivalent (vonMises).* Do this for the cortical and trabecular bone separately. Open *Solution* branch > *Insert* > *Deformation* > *Total*. Do this for the cortical and trabecular bone separately.
7. Solve the problem. Click *Solve.*
8. Export the result stress/deformation and save in Text file (*.txt) format.

3. Post process of the vonMises stress values

1. Move the cortical and trabecular vonMises stress files (*.txt) into the appropriate folder. Using MATLAB code given in Appendix 5-C, find the smallest section slice of the femoral neck.
2. Choose the stress values from both cortical and trabecular, only cortical, or only trabecular bone in the MATLAB function code given in Appendix 5-D.
3. Specify the total number of slices you want the stress values be extracted from. The MATLAB code for this operation is given in Appendix 5-E. Running this code will save the regional vonMises values averaged from 9 slices as mean-VonMises8sec.mat.